HEAT TRANSFER AND PRESSURE DROP OF REGENERATIVE AIR PRE-HEATER ELEMENTS

Kristina Gruen

A dissertation submitted to the Faculty of Engineering, University of the Witwatersrand, Johannesburg, in fulfilment of the requirements for the degree of Master of Science in Engineering

Johannesburg, 1998

I declare that this dissertation is my own, unaided work. It is being submitted to the Degree of Master of Science in the University of the Witwatersrand, Johannesburg. It has not been submitted before for any degree or examination in any other University.

24th of November 1998

Abstract

In the present study the thermal and hydraulic performance of heating plates used in regenerative air pre-heater was investigated. Experimental results on new heating surfaces are presented as well as preliminary investigations into plates eroded by fly ash in the flue gas.

In the uneroded state, 12 different plate profile designs were tested. These new packs were tested in different configurations, i.e. with and without braces around the individual plates and with different numbers of plates per plate pack. For some designs the individuality of the packs (repeatability of manufacture) was investigated. In order to establish the accuracy of the test facility, a pack of flat plates was tested and compared with literature results.

It is shown that the profile designs with the smallest profile heights have the highest heat transfer coefficient, but also the highest pressure drop. Good performance in one parameter always means bad performance in another parameter.

Heat transfer coefficients and pressure drops of the various pack designs are in approximately inversely proportion to the hydraulic diameter. Profiles with a flat counterplate have a lower heat transfer coefficient than profiles with an undulated counterplate.

One eroded pack (with 20%, 30% and 40% mass loss) was tested and compared with an uneroded one in terms of heat transfer and pressure drop behaviour. Pressure drop was approximately 15% lower for the eroded plates (irrespective of the extent of erosion) and heat transfer coefficient was essentially unaffected.

Acknowledgement

This study was undertaken by myself far away from my home country (Germany) and it has enriched me both personally and professionally. I would like to acknowledge and thank the following people who have lent themselves to the successful completion of this study.

Firstly I would like to thank Doctor H.H. Jawurek and Professor T.J. Sheer of the University of the Witwatersrand for their supervision, advice and helpful comments. I would like to thank Walter Schmitz of ESKOM TRI, who initiated my study in South Africa. I wish to acknowledge my project leader at ESKOM TRI, Mike Lander, for numerous valuable discussions, his significant input into the study and also his endless enthusiasm for the project. I would like to express my appreciation to Deven Pillay, the manager of the Mechanical Engineering and Metrology Section, and the DAAD (Deutscher Akademischer Austauschdienst) for financially supporting this study. I would like to thank ESKOM TRI as a whole, where it was possible to use the various test facilities.

A number of students helped me with operating the test facilities. Without their help this study would not have been completed yet. Thank you very much guys.

Last but not least I would like to say, "Vielen, vielen Dank," to Linx Govender, who patiently corrected my English.

Contents

1. Introduction 1

2. Literature survey and specific objectives 9

- 2.1 Experimental methods 9
- 2.2 Performance of uneroded heating plates 17
- 2.3 Erosion 17
- 2.4 Specific objectives 21

3. Thermal Test Facility 22

- 3.1 Test section/test pack 26
- 3.2 Calculation of the heat transfer coefficient according to Mullisen and Loehrke [23] 27
- 3.3 MATLAB programs for the calculations of the results 29
- 3.4 Test procedure 31
- 3.5 Fluid properties 33
- 3.6 Difficulties encountered during the study 34
- 3.7 Presentation of the test results 34

4. Thermal tests of uneroded plates 36

- 4.1 Standard profile types 36
  - 4.1.1 Profile H8 38
    - 4.1.1.1 Influence of individual packs 43
    - 4.1.1.2 Influence of the braces 45
  - 4.1.2 Profile 278DU 47
    - 4.1.2.1 Influence of the braces 47
  - 4.1.3 Profile KH11 49
    - 4.1.3.1 Influence of the number of plates 49
    - 4.1.3.2 Influence of the braces 51
  - 4.1.4 Profile KH10 53
    - 4.1.4.1 Influence of the braces 53
  - 4.1.5 Profile V75 55
    - 4.1.5.1 Influence of the number of plates 55

4.1.5.2 Influence of the braces 57
4.1.6 Profile K4 57
4.1.6.1 Influence of the braces 57
4.1.7 Profile K5 59
4.1.7.1 Influence of the braces 59
4.1.8 Profile K6 61
4.1.8.1 Influence of the braces 61
4.1.9 Profile K8 63
4.1.9.1 Influence of the braces 63
4.1.10 Profile K6G 65
4.1.10.1 Influence of the braces 65
4.1.11 Profile K8G 67
4.1.11.1 Influence of the braces 67
4.2 Special profile "Cheese Grater" 69
4.3 Summary of the test results 73
4.4 Literature comparison 76
4.5 Regression of test results 81
4.6 Conclusions of testing uneroded plates 86

5. Erosion **89**
5.1 Appearance of erosion 89
5.2 Coal properties 90
5.3 Erosion in air pre-heaters 93

6. Erosion test facilities **102**
6.1 Modified Basket Test Facility (MBTF) 102
6.2 Cold Accelerated Erosion Rig (CAER) 104

7. Thermal tests of eroded plates **114**
7.1 Preparation of the eroded plates for the TTF 114
7.1.1 Image analysis system LECA 114
7.2 Pressure drop across the pack for eroded packs 116

7.3 Heat transfer coefficient uncertainties of eroded packs 118
7.3.1 Flat plates with holes 122
7.3.2 Steps approaching to solve the problem 123
7.3.3 Fundamental heat balances 126
7.4 Heat transfer coefficients of eroded plates 137

8. Summary and conclusions **140**

9. Recommendations for future work **142**

APPENDIX A	Difficulties encountered during the progress of work	145
APPENDIX B	MATLAB programs	165
APPENDIX C	Table of test runs at the TTF	178
APPENDIX D	Table of results	189
APPENDIX E	Uncertainty analysis	190
APPENDIX F	Error between the experimental and the calculated temperatures	201
APPENDIX G	Numerical scheme according to Mullisen and Loehrke [2]	204
APPENDIX H	Fluid Properties	210
APPENDIX I	Sample calculation of additional pressure loss caused by the presence of braces	214

REFERENCES 218

List of figures

Figure		page
1.1	Rothemuehle design of a regenerative heat exchanger (after [1])	2
1.2	Ljungstroem design of a regenerative heat exchanger (after [1])	2
1.3	Position of the air pre-heater in the power station (after [1])	3
1.4	Pair of plates with direction of flow (after [1])	4
1.5	Performance of heating plates	5
3.1	Schematic diagram of the Thermal Test Facility	23
3.2	Screen of the Labview Program	25
3.3	Test pack with braces	26
3.4	Half-flow passage and half plate	28
3.5	Division into finite-difference nodes	28
4.1	Different heating profiles direction of flow is perpendicular to the page	37
4.2	Results for the H8 pack from Apparatebau Rothemuehle, tested in Germany and South Africa	39
4.3	Results for the H8 pack from Apparatebau Rothemuehle, tested in Germany and South Africa, dimensionless values	40
4.4	Results for two different H8 packs (RM and Howden Power), heat transfer coefficient vs. mass flow	42
4.5	Results for two different H8 packs (RM and Howden Power), pressure drop across pack vs. mass flow	42
4.6	Results for three different H8 packs from Howden Power, heat transfer coefficient vs. mass flow	44
4.7	Results for three different H8 packs from Howden Power, pressure drop across pack vs. mass flow	44
4.8	Results for a H8 pack with and without braces, heat transfer coefficient vs. mass flow	46
4.9	Results for a H8 pack with and without braces, pressure drop across pack vs. mass flow	46
4.10	Results for different 278DU packs with and without braces, heat transfer coefficient vs. mass flow	48
4.11	Results for different 278DU packs with and without braces, pressure drop across pack vs. mass flow	48
4.12	Results for the KH11 pack with a different number of plates, heat transfer coefficient vs. mass flow	50
4.13	Results for the KH11 pack with a different number of plates, pressure drop across pack vs. mass flow	50
4.14	Results for the KH11 pack, influence of the braces, heat transfer coefficient vs. mass flow	52

4.15	Results for the KH11 pack, influence of the braces, pressure drop across pack vs. mass flow drop vs. mass flow	52
4.16	Results for a KH10 pack with and without braces, heat transfer coefficient vs. mass flow	54
4.17	Results for a KH10 pack with and without braces, pressure drop across pack vs. mass flow	54
4.18	Results for a V75 pack, heat transfer coefficient vs. mass flow	56
4.19	Results for a V75 pack, pressure drop across pack vs. mass flow	56
4.20	Results for a K4 pack with and without braces, heat transfer coefficient vs. mass flow	58
4.21	Results for a K4 pack with and without braces, pressure drop across pack vs. mass flow	58
4.22	Results for a K5 pack with and without braces, heat transfer coefficient vs. mass flow	60
4.23	Results for a K5 pack with and without braces, pressure drop across pack vs. mass flow	60
4.24	Results for a K6 pack with and without braces, heat transfer coefficient vs. mass flow	62
4.25	Results for a K6 pack with and without braces, pressure drop across pack vs. mass flow	62
4.26	Results for a K8 pack with and without braces, heat transfer coefficient vs. mass flow	64
4.27	Results for a K8 pack with and without braces, pressure drop across pack vs. mass flow	64
4.28	Results for a K6G pack with and without braces, heat transfer coefficient vs. mass flow	66
4.29	Results for a K6G pack with and without braces, pressure drop across pack vs. mass flow	66
4.30	Results for a K8G pack with and without braces, heat transfer coefficient vs. mass flow	68
4.31	Results for a K8G pack with and without braces, pressure drop across pack vs. mass flow	68
4.32	"Cheese Grater" profile, photograph in flow direction	69
4.33	"Cheese Grater" profile, photograph from the side	70
4.34	"Cheese Grater" profile, photograph of two plates	70
4.35	"Cheese Grater" profile, detail photograph of the punchings	71
4.36	Results for the "Cheese Grater" pack, heat transfer coefficient vs. mass flow	72
4.37	Results for the "Cheese Grater" pack, pressure drop across pack vs. mass flow	72
4.38	Results for different profiles of air heater packs, heat transfer coefficient vs. mass flow	73
4.39	Results for different profiles of air heater packs, pressure drop across pack vs. mass flow	74

4.40	Colburn- and Friction-factor v. Reynolds-number, ESKOM and Kays and London data	76
4.41	Colburn- and Friction-factor v. Reynolds-number, ESKOM data and Migay calculation	78
4.42	Nusselt-number vs. Reynolds-number for flat plates, experimental and calculated values [29]	80
4.43	Friction-factor vs. Reynolds-number for flat plates, experimental and calculated values [29]	80
4.44	Colburn- and Friction-factor vs. Reynolds-number, H8 profile	82
4.45	Colburn- and Friction-factor vs. Reynolds-number, KH11 profile	82
4.46	Colburn- and Friction-factor vs. Reynolds-number, 278DU profile	83
4.47	Colburn- and Friction-factor vs. Reynolds-number, K6 profile	83
4.48	Colburn- and Friction-factor vs. Reynolds-number, K8 profile	84
4.49	Colburn- and Friction-factor vs. Reynolds-number, V75 profile	84
4.50	Colburn- and Friction-factor vs. Reynolds-number, KH10 profile	85
5.1	Flue-gas and air streams in the Ljungstroem air-heater type (Rothemuehle trade literature)	95
5.2	Flue-gas and air streams in the Rothemuehle air-heater type (Rothemuehle trade literature)	95
5.3	Leading edge erosion investigations at the Kendal air heater, unit 1, right hand side	97
5.4	Leading edge erosion investigations at the Kendal air heater, unit 1, left hand side	98
5.5	Leading edge erosion investigations at the Matimba air heater, unit 6	99
5.6	Blockage investigations at the Matimba air heater, unit 6	101
6.1	Single Modified Basket	102
6.2	Half section of an air heater, with a Modified Basket in the 2nd outer ring	103
6.3	Layout of the CAER	105
6.4	Plate 2 and 3, KH11, 20% eroded	107
6.5	Plate 10 and 11, KH11, 20% eroded	107
6.6	Plate 16 and 17, KH11, 20% eroded	108
6.7	Plate 24 and 25, KH11, 20% eroded	108
6.8	Plate 2 and 3, KH11, 30% eroded	109
6.9	Plate 10 and 11, KH11, 30% eroded	109
6.10	Plate 16 and 17, KH11, 30% eroded	110
6.11	Plate 24 and 25, KH11, 30% eroded	110
6.12	Plate 2 and 3, KH11, 40% eroded	111

6.13	Plate 8 and 9, KH11, 40% eroded	111
6.14	Plate 16 and 17, KH11, 40% eroded	112
6.15	Plate 24 and 25, KH11, 40% eroded	112
7.1	Pressure drop across the pack vs. mass flow, KH11, uneroded and eroded plates	117
7.2	Inlet and outlet temperatures histories of an uneroded pack	119
7.3	Heat transfer coefficient vs. mass flow, KH11 profile, uneroded and eroded (original calculations without any adaptions)	120
7.4	Inlet and outlet temperatures histories for an eroded pack	121
7.5	Heat transfer coefficient vs. mass flow, flat plates with and without holes	122
7.6	Pressure drop vs. mass flow, flat plates with and without holes	123
7.7	Schematic representation of an eroded plate with holes	126
7.8	Schematic representation of the thicker part of the plate	127
7.9	Schematic representation of the thinner part of the plate	128
7.10	Schematic view of an eroded plate with thicker and thinner regions and holes	131
7.11	Schematic view of an eroded plate with an average plate thickness	132
7.12	Iteratively optimised additional mass at different stages of erosion	136
7.13	Heat transfer coefficient vs. mass flow, uneroded and eroded pack, KH11 profile	137
7.14	Colburn- and Friction-factor vs. Reynolds-number, KH11, 20% erosion, experimental and calculated results	138
7.15	Colburn- and Friction-factor vs. Reynolds-number, KH11, 30% erosion, experimental and calculated results	138
7.16	Colburn- and Friction-factor vs. Reynolds-number, KH11, 40% erosion, experimental and calculated results	139
A1	Arrangement of the thermocouples at the inlet an the outlet of the test section, flow into the picture	150
A2	Temperature readings without flow at ambient conditions (after calibration)	151
A3	a) correct installation of the turbulator (wings down), b) incorrect installation of the turbulator (wings up), angle for both installations between turbulator and flow direction is 30° (original according to Caby [26]	154
A4	Heat transfer coefficient vs. mass flow, H8 profile, different installations of the turbulator at 30°	163
A5	Pressure drop vs. mass flow, H8 profile, different installations of the turbulator at 30°	163
G1	Multiple in-line plates	204
G2	Single pair of plates	204

G3	Half-flow passage and half plate	205
G4	Division into finite-difference nodes	205
I1	Flow through a pack without and with braces, definition of the different cross sections	214

List of Tables

Table		Page
2.1	Life expectancy of air heaters in abrasive-ash-laden flue gas [19]	18
2.2	Erosion rate and chemical composition of different fly ashes [23]	20
4.1	Numbering system of the H8 packs	41
4.2	Geometry data of the standard H8 pack (300 mm x 300 mm x 500 mm)	41
4.3	Geometry data of the standard 278DU pack (300 mm x 300 mm x 500 mm)	47
4.4	Geometry data of the standard KH11 pack (300 mm x 300 mm x 500 mm)	49
4.5	Geometry data of the standard KH10 pack (300 mm x 300 mm x 500 mm)	53
4.6	Geometry data of the standard V75 pack (300 mm x 300 mm x 500 mm)	55
4.7	Geometry data of the standard K4 pack (300 mm x 300 mm x 500 mm)	57
4.8	Geometry data of the standard K5 pack (300 mm x 300 mm x 500 mm)	59
4.9	Geometry data of the standard K6 pack (2 plates less than the standard number of plates, 300 mm x 300 mm x 500 mm)	61
4.10	Geometry data of the standard K8 pack (300 mm x 300 mm x 500 mm)	63
4.11	Geometry data of the standard K6G pack (300 mm x 300 mm x 500 mm)	65
4.12	Geometry data of the standard K8G pack (300 mm x 300 mm x 500 mm)	67
4.13	Geometry data of the standard "Cheese Grater" pack (300 mm x 300 mm x 500 mm, plate thickness 0.7 mm)	71
4.14	Influence of braces on the pressure drop of different profiles	87
4.15	Influence of the number of plates for different profile types	88
5.1	Coal and ash properties of several South African power stations	91
5.2	Coal features, particle size, solids burden, flow velocity and impaction rates [19]	92
5.3	Recommended velocities in air pre-heaters for different coal types	93
7.1	Geometry of the test pack at different stages of erosion	116
7.2	Results of the mass optimisation for the eroded KH11 pack	135
A1	Influences of incorrect temperature readings on the heat transfer coefficient	147
A2	Heat transfer coefficients for different temperatures calibrations	149
F1	Influences of the error on the temperature difference and the heat transfer coefficient	203

Nomenclature

symbol	*unit*	*expression*
a	m	half plate thickness
A	m^2	area
d	m	diameter
c	J/(kg K)	specific heat
h	W/(m^2 K)	heat transfer coefficient
k	W/(m K)	thermal conductivity
L	m	length of pack
$\dot{m}$	kg/s	mass flow rate
P	W	pumping power
Δp	Pa	pressure drop
$\dot{q}$	kW/kg	heat flow rate per unit mass
$\dot{Q}$	W	heat flow rate
R	kJ/(kg K)	gas constant
Δt	K	temperature difference
t	s	time
t	°C	temperature
T	K	temperature
v	m/s	velocity
$\dot{V}$	m^3/s	volume flow rate
W	m	width of the pack
x		flow - direction
ρ	kg/m^3	density
ν	m^2/s	kinematic viscosity
μ	Pa s	dynamic viscosity

Subscripts

1	any kind of profile
2	smooth profile
calc	calculated
cross	cross sectional
cond	conductive
conv	convective
d	dry
exp	experimental
f	fluid
fg	flue gas
free	free flow
h	hydraulic
heat	heat transfer
in	inlet
n	normalised
lab	laboratory
out	outlet
s	solid
s	saturation
st	storage material
v	vapor
w	wall
w	wet

dimensionless groups

A	coefficients
B	coefficients
C	coefficient of discharge
Co	Colburn-factor
e	expansion factor (see Appendix A)
E	velocity approach factor (see Appendix A)
F	Friction-factor
Nu	Nusselt-number
NTU	number of transfer units
Pr	Prandtl-number
Re	Reynolds-number
S	Shape factor [43]
α	flow coefficient (see ISO 5167)
η_{gas}	gas temperature efficiency [3]
η_{air}	air temperature efficiency [3]
ε	dimensionless error between experimental and calculated fluid temperature
κ	isentropic exponent
τ	pressure ratio (see ISO 5167)
β	diameter ratio (see ISO 5167)

1. Introduction

In the power generation industry the heat exchange between flue-gas/air and flue-gas/flue-gas through continuous operation of regenerative heat exchangers has been accepted, because of their:

- compactness,
- relatively low capital investment costs,
- good cleaning possibilities and
- high reliability.

These heat exchangers are characterised by simultaneously heating up and cooling down the gas streams without interruption. The heat storage material (usually corrugated plates) runs continuously through the hot and cold periods. The hot fluid gives its energy content first to the storage material. After turning into the cold section the material transmits its stored energy to the incoming air. The gas streams are of the counter-flow type. There are two different principles for rotary air pre-heaters (see Figure 1.1 and Figure 1.2):

- the Ljungstroem design, where the matrix rotates between stationary ducts,
- the Rothemuehle design, where the matrix is stationary and the rotating hood distributes the two streams through it.

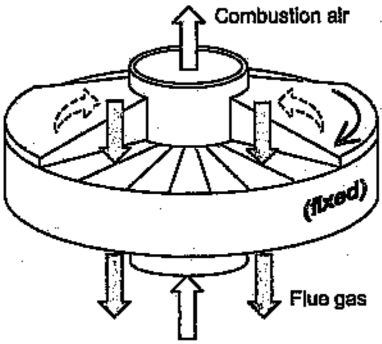

Figure 1.1: Rothemuehle design of a regenerative heat exchanger
(after [1])

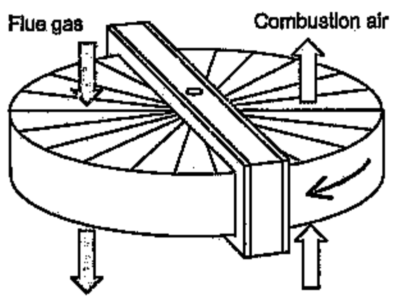

Figure 1.2: Ljungstroem design of a regenerative heat exchanger
(after [1])

The one design is the kinematic reverse of the other design. The two designs are essentially similar with respect to their structure and operating conditions. Their main applications are in the power generation and pollution control industry:

- as an air pre-heater for heating up the combustion air before the boiler,
- as a gas/gas heat exchanger to cool down and heat up flue gases in wet de-sulphurization plants and DENOX (NO_x scrubbing) plants.

The position of an air pre-heater in a power station is shown in Figure 1.3.

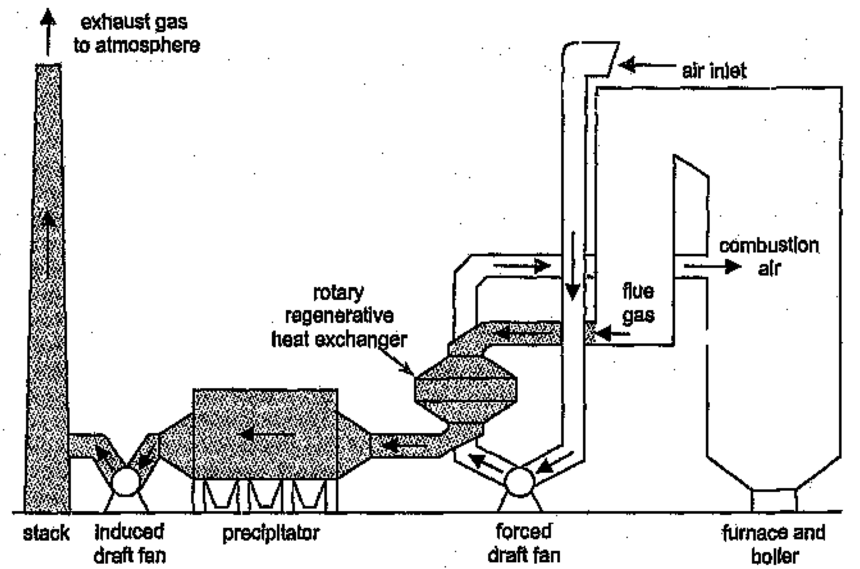

Figure 1.3: Position of the air pre-heater in the power station (after [1])

One disadvantage of regenerative heat exchangers is the systematic leakage:

- leakage by means of mixing of the streams as the matrix passes from one section to the other,
- leakage by means of fluid passing through the radial seals.

However, these leakages are within economic and technical limits. Firstly, there is a relatively small amount of leakage and secondly, since there is a higher pressure in the air side, only clean air can enter into the flue gas stream and not vice versa.

Regenerative heat exchangers can be designed with diameters from 1 m to 20 m. A 20 m diameter heat exchanger weighs 1,700 tons and contains about 200,000 m^2 heat transfer area. The speed of rotation for a Ljungstroem design is between 0.75 and 1.5 rpm. The Rothemuehle design is half as fast because of the two winged hoods.

Different plates (element) profiles are available to optimise the operation of a heat exchanger operating under specific conditions. The various profile types are characterised by different heat transfer coefficients, friction factors and heat transfer areas. A typical pair of plates is shown in Figure 1.4.

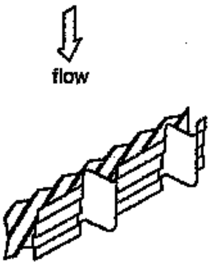

Figure 1.4: Pair of plates with direction of flow (after [1])

The type of element utilised depends on the design criteria required for the application. Air heater elements can generally be evaluated according to their thermal, pressure drop, erosion and corrosion performance as well as their performance in respect to blockage. All five criteria are linked to design features of elements (material, geometry and plate thickness). A high performance in one aspect can result in poor performance in other aspects. The choice of elements depends on the desired performance which is influenced by coal characteristics and the desired system efficiency.

Capital cost of packing, the number of re-packings required, boiler efficiency and fan power consumption determine the life cycle cost of the system. Prediction of the above mentioned parameters will lead to an improvement in cost effectiveness of the entire air heater.

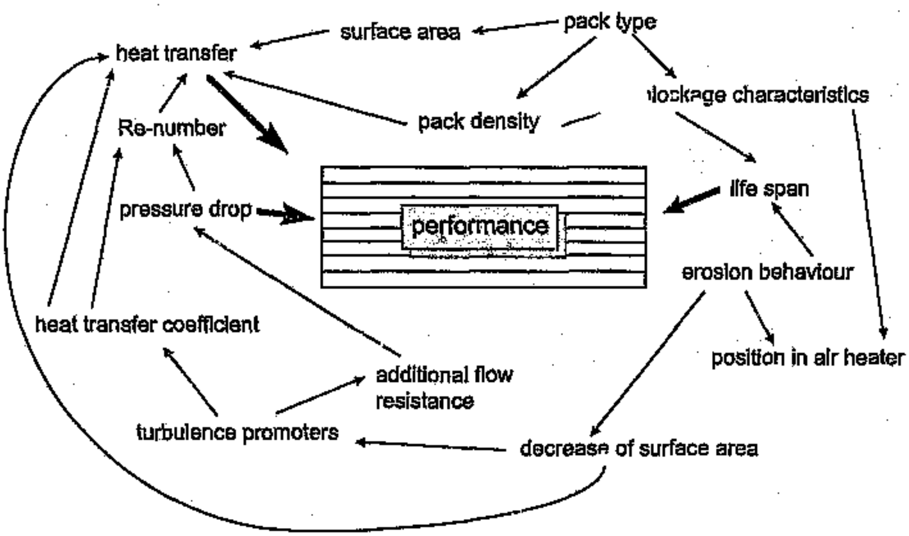

Figure 1.5: Performance of heating plates

From the above schematic it can be seen, that there are many criteria which influence the performance of an air-heater pack, and thus the entire air-heater.

The present study deals mainly with the thermal and hydraulic performance of new heating plates. It also includes first steps of investigations into plates eroded by fly ash in the flue gas.

Erosion influences the heat transfer and the pressure drop of regenerative air pre-heater elements. For this reason it is not sufficient to use only the heat transfer coefficients and friction factors relating to new packs to calculate the expected heat transfer and pressure loss of a regenerative air pre-heater. For heat transfer and pressure drop investigations on air heater packs which have been in operation for a period of time it would be necessary to use pressure loss and heat transfer coefficients which relate to the state of the pack.

ESKOM TRI (Technology, Research and Investigation; part of ESKOM and situated in the South of Johannesburg) in conjunction with the School of Mechanical Engineering of this University has initiated an air heater research project to investigate the effect of erosion on the characteristics of regenerative air pre-heaters. Air pre-heaters, as used in ESKOM, were originally designed for European operating conditions, for coals with lower ash contents. However, South African coal fired power stations suffer from considerably higher ash burden in their flue gas which results in different problems being experienced from those in Europe. High ash contents in the flue gas lead to increased erosion rates on air heater elements.

ESKOM has developed three different test facilities to investigate the characteristics of heating plates, which are used in regenerative air pre-heaters.

The Thermal Test Facility (TTF), located at TRI, is designed to measure the heat transfer coefficient and pressure drop of air heater elements. It runs according to the single-blow method and has been in operation since 1995. A direct curve matching model for transient heat exchange tests according to Mullisen and Loehrke [2] is used to determine the heat transfer coefficient from the measured temperature jumps at the inlet and the outlet of the test pack.

The Cold Accelerated Erosion Rig (CAER), located at Matimba Power Station (near Ellisras, in the Northern Province, ca. 350 km from Johannesburg), simulates erosion behaviour of air heater packs. Pack erosion is accelerated to the extent that test packs show the same degree of erosion in a few days which would under normal operating conditions take years to achieve.

The third test facility, the Modified Baskets Erosion Facility (MBEF) located at Matimba and Kendal Power Station (near Witbank, in the Mpumalanga Province, ca. 120 km from Johannesburg), was built to investigate the erosion characteristics of heating packs in situ. The packs are located in an air heater where they undergo an accelerated erosion under realistic air pre-heater conditions.

In order to compare the thermal and flow performance of new and eroded elements, the different types of packs can be tested as received from the manufacturer and at different stages of erosion. Since all three test facilities i.e. the TTF, CAER and MBEF, accommodate the same specimen size, the test packs need not be altered for the sequence of tests proposed.

In the uneroded state, 12 different profile designs were tested. These new packs were tested in different configurations, i.e. with and without braces around the separate plates and with different numbers of plates. For some designs the individuality of the packs will be shown. In order to establish the accuracy of the TTF, a pack of flat plates was tested and compared with literature results. After presenting the results for new packs, results for one eroded pack will be given.

In order to investigate the thermal and hydraulic performance of eroded plates the packs were eroded in the Cold Accelerated Erosion Rig at Matimba to three different stages of erosion i.e. 20%, 30% and 40% mass loss. After each stage these packs were brought back to the TRI laboratory (350 km) in order to test their thermal and flow performance. In the present study only one pack design has be considered under erosion conditions.

During the work on this project special attention was given to check the test rig, the data acquisition system and the data reduction scheme for accura everal mistakes were identified and corrected.

2. Literature survey and specific objectives

This literature survey covers three topics, related to the present study: Firstly, the experimental methods of determining the heat transfer coefficient, secondly, the performance of new (uneroded) heating plates, and thirdly, erosion as relevant to the present work.

From this follow the specific objectives of this study.

2.1 Experimental methods

The two main testing methods for measuring an average heat transfer coefficient of a heat exchanger plate are the steady state and the transient technique (single-blow method). The steady-state technique employs a cross-flow test core for which two separate fluid streams are used. There are two known possibilities, either two identical fluid streams, i.e. air, with equal mass flow rates are used, or condensing steam on one side of the test core and air on the other side is used. The disadvantages of the steady state method are:

- a complicated ducting system is necessary for the two fluid streams,
- every test point is very time consuming,
- the test apparatus with the steam generator is very costly,
- if two streams of air are used a mixer is necessary to ensure that there is no temperature variation over the flow cross section.

The steam-to-air-test system was used by Kays and London [3].

The transient method consists of establishing a steady flow (usually of air) through the heat exchange matrix, bringing about a sudden change in inlet temperature, and extracting, by means of a mathematical model, an average heat transfer coefficient from the measured inlet and outlet temperature-time records. Older models required the inlet temperature profile to be a step change; this could in practise be only imperfectly realised.

The transient technique is preferred to the steady-state method because of several reasons:

- single test points are less time consuming,
- less complex experimental test rig,
- only one fluid stream is required and
- no wall temperatures have to be measured.

The transient technique will be explained in detail in Chapter 3.

Both these techniques give global heat transfer coefficients. Over the years, results on local heat transfer coefficients have also become available. Local heat transfer distribution over the surface is based on applying thermochromic liquid crystal and true-colour image processing. The average heat transfer coefficients can be calculated from local heat transfer values. Since in the present case the overall performance of an air pre-heater should be improved, it is not worthwhile measuring the local heat transfer coefficients. In the following pages the transient method to measure the heat transfer coefficient, which is used in the present study, is presented.

Over the years several researchers improved and increased the accuracy of the model first developed by Anzelius [4]. The following passages give a historic overview concerning the single-blow method.

The single blow method was first presented in 1926 by Anzelius [4]. The method is the most frequently used mathematical model for the single blow measuring method. He assumed that the sole mechanism of transfer is forced convection between the fluid and the solid. In 1929 Schumann [5] described his method, which is similar to the aforementioned one, ie. to calculate the heat transfer coefficient based on the inlet and outlet temperature histories. He proposed a graphical direct curve matching method based on flow through porous media. Schumann presented diagrams showing dimensionless fluid exit temperature curves as a function of NTU (number of transfer units).

With the help of these graphs for each exit temperature history the adequate NTU, which represents the correct heat transfer coefficient, could be determined. For the temperature inlet history he used a step function.

In 1950 Locke [6] presented the maximum slope technique, which is an indirect curve matching method. It is based on the explicit relation between the NTU and the maximum slope of the exit temperature curve. Since this technique only compares one value, the maximum slope, with the NTU, this method reduces the computational effect in the analysis. The inlet temperature rise is limited to a step function. The maximum slope technique is restricted to NTU < 3, because of two reasons: the first is due to the inflection points from the analytic solution of NTU versus maximum slope, and the second is due to the response of the physical system (maximum slope at time zero).

Howard (1964) [7] extended Locke's maximum slope model by including the effects of longitudinal conduction in the solid storage material.

Pucci et al. (1967) [8] were the first to investigate on perforated plates for NTU values ranging from 2.47 to 15.9. They also used the maximum slope technique including longitudinal conduction in the storage material and a step function as inlet temperature history. They presented as well experimental data of a profile type which is similar to one tested in the present study. Unfortunately the results can not be compared because Pucci et al. examined a lower Reynolds-number range (Re < 800) than the present study (700 > Re > 6000). The authors gave the following uncertainties concerning their experimental data: Colburn-factor = ± 7.5% - 15%, Friction-factor = ±5% and Reynolds-number = ±3%.

Liang and Yang [9] in 1975 developed a model in which they used an exponential inlet temperature rise, which is more realistic than a step change. A step rise as a inlet temperature function is in practise almost impossible to realise. They did not consider longitudinal conduction in the solid. To match the experimental and the predicted outlet temperatures they developed a five-point curve matching scheme. A value of the heat transfer coefficient was obtained at each of the 5 points on the breakthrough curve and the arithmetic average was used to represent the complete curve. They also extended the valid range for values NTU > 3 and NTU < 0.2. For their temperature measurements they used 20 thermocouples at the inlet and 20 thermocouples at the outlet. For measuring uncertainties they gave following values: Friction-factor = ± 3% and Colburn-factor = ± 6%.

In Mullisen and Loehrke's [2] publication of 1986 the temperature rise is not any longer restricted to a step function or an exponential function as it was before. The temperature inlet function can be arbitrary because the temperature outlet profile is solved by a numerical finite-difference scheme. The authors also consider longitudinal conduction of the solid storage material in their model. They employed an algorithm to match the entire measured and predicted exit temperature curves, and not only 5 points like proposed by Liang and Yang. The difference between the experimental and the calculated temperature is minimised by means of the least squares condition. This data reduction model was chosen for the present study, because it offers the advantage of using any kind of temperature inlet function and it considers the longitudinal conduction of the storage material. They also presented experimental data of interrupted flat plates in the range of 0.1 < NTU < 20. At the inlet and at the outlet of the test section they measured the temperature histories using 6 thermocouples. They considered their overall measuring uncertainties at about ± 2%. In Chapter 3 this method will be described completely including the assumptions, boundary conditions and limits. The numerical scheme is presented in Appendix G.

Cheng and Huang [10] in 1994 extended the theoretical model for the maximum slope single-blow transient testing method. They considered additionally the longitudinal diffusion and the thermal capacity of the fluid. These assumptions become important only if liquids are used as the heat transfer medium. Since in the present case only air is used, this model is not required.

In 1996 Chen and Chang [11] presented a study describing the measurements of thermal performance of cyrocooler regenerators. The regenerator matrix was made of oversized wire-screens packed into a circular tube They considered the heat flux from the fluid flow into the tube wall, axial conduction of the tube wall and the Joule-Thomson expansion for the fluid flowing through the rig. In the present case these refinements do not lead to any improvements. The values of the Joule-Thomson coefficient (function of pressure drop, dynamic viscosity and temperature rise during heating) is in the present case two orders of magnitude smaller (1/100) than for the cryocooler regenerators. This explains why it is not necessary to consider the Joule-Thomson effect in the present study. To measure the inlet and outlet histories they used 2 thermocouples each which were calibrated with an uncertainty of 0.04 °C. For measuring uncertainties in total they gave the following values: Nusselt-number = ± 5.66%, Friction-factor = ± 6.63% and Reynolds-number = ± 4.32%.

Heggs and Burns [12] compared four commonly used data reduction techniques to calculate the heat transfer coefficient using the same measured inlet and outlet temperature histories obtained from a single-blow test facility. They tested spherical steel balls experimentally and applied four different techniques on this raw test data to evaluate the NTU. The four different techniques are the direct curve matching technique, firstly used by Schumann, the maximum slope method, firstly used by Locke, the shape factor method (Darabi [13]) and the fluid differential area method (or differential fluid enthalpy method, Bacic et al. [14]). The first two methods have been described earlier. The shape factor method is an alternative to the Locke approach. It measures the time interval between the 20 and 80% breakthrough points and relates this to the shape-factor/NTU relationship. The shape-factor is defined as follows:

$$S = \frac{m \cdot c_f \cdot \Delta t_{20-80}}{\rho_{st}(1-\in)c_{st} L\, A_{free}} \tag{2.1}$$

with: $\in$ = bed voidage, dimensionless

Bacic et al. proposed an explicit multipoint technique, where the time constant of the inlet forcing function has to be measured and also the temperature difference between the inlet and the outlet temperatures up to a specified time. From these values they evaluated the differential fluid enthalpy change (dimensionless, see [12]), which is related to NTU.

For any single flow rate, the four analysis techniques yielded different NTU values. The differential fluid enthalpy method predicted always the highest value, followed by the curve matching, the maximum slope. The shape factor results produced the lowest values. It resulted in up to 20% less in NTU values than the curve matching method. Since the differential fluid enthalpy and the curve matching are both multipoint matching methods it is understandable that their results show better agreement than the other methods. The results of the multipoint matching methods are considered as the most reliable. Additionally they found that the heat transfer coefficient is higher for cooling test runs than for heating test runs; these results were not explained.

Heggs and Burns [12] stated that the results gained from all the four data reduction methods are not within the bounds of the experimental error, which they assumed to be ± 4%. Results of the curve matching method and the fluid enthalpy method lay close to these bounds. They recommended the least square method for their investigations with spheres in the Reynolds-number range 290 - 1140 because the differential fluid enthalpy methods results in an overprediction of the heat transfer performance.

2.2 Performance of uneroded heating plates

The flow through irregular formed channels is an important issue for several types of heat exchangers (e.g. all forms of recuperative plate heat exchangers). The literature offers a considerable body of heat transfer coefficient and pressure drop data, mostly based on tests under laboratory conditions. This means that the heating plates were tested as new, without any fouling or erosion features. Due to the large amount of published data concerning corrugated passages only that literature, which relates best to the profile types used in ESKOM air pre-heaters, is mentioned below.

One of the earliest studies concerning heat transfer and pressure drop of heating plates is described by Kays and London [2]. They experimentally examined various heating surfaces, e.g. flat plates, wavy channels and corrugated plates with regard to their thermal and hydraulic performance. Contrary to most authors they used the steady-state method. Some of their profile configurations can be taken into consideration for comparison with profile types used today, e.g. profiles with a flat counter plate like the KH10, K6G and K8G profile. (Commonly used profiles are shown in Figure 4.1.) Chapter 4 contains a comparison between the literature data and the results of the present study.

Results, using a higher range of the Reynolds-number than in the present study, have been published by Migay [15]. The shapes of the applied profiles are similar to those known as KH and DU. He examined mainly the influence of the corrugation height of the profiles in the Reynolds-range of 2000 - 15000. He did not investigate the transition and the laminar region of the flow. The paper does not specify the experimental method used. The results are shown in graphs indicating Nusselt-number vs. Reynolds-number and hydraulic resistance vs. Reynolds-number, in which the definition of the hydraulic resistance is not given. Migay also described empirical equations to calculate the Nusselt-number in relation to Reynolds-, Prandtl-number and geometry (height and pitch of the profiles).

These equations can be used to check the results from the ESKOM Thermal Test Facility. Finally he presents some theoretical approaches to determine the heat transfer based on energy and stress equation. A comparison between his results and the TRI results can be found in Chapter 4.

A paper which deals with in-service heaters of plate profile designs like the KH11 or the K-profile combined with a smooth plate, is presented by Karlsson and Holm [16]. Unfortunately the presentation of their results is unusual. The comparison of these results with other experimental data is difficult, because of the following reasons.

Firstly they used the temperature efficiency, mean value between gas temperature efficiency and air temperature efficiency (see below), to express the heat recovery of the air heater by measuring several inlet and outlet temperatures of an actual air heater. The efficiencies are defined as follows:

gas temperature efficiency:

$$\eta_{gas} = \frac{t_{gas,in} - t_{gas}}{t_{gas,in} - t_{air,in}} \tag{2.2}$$

air temperature efficiency:

$$\eta_{air} = \frac{t_{air} - t_{air,in}}{t_{gas,in} - t_{air,in}} \tag{2.3}$$

Secondly they do not mention the velocity-dependency directly, rather they show curves, in which the temperature efficiency is plotted against the ratio of heat-capacity air ($\dot{m}_{air} \cdot c_{p,air}$) and heat capacity flue gas ($\dot{m}_{fg} \cdot c_{p,fg}$). This paper also includes some results of laboratory tests. These results, however, are either given in a normalised representation or with insufficiently defined values. This precludes comparison with other data.

From the measurements on actual air heaters with different types of heating surfaces the authors show that the notched undulated profile (comparable with the KH11 profile) is the most suitable profile in terms of temperature efficiency and friction loss on the gas and on the air side of the air pre-heater.

Stasiek et al. [17, 18] investigated the dependence of the Nusselt-number and the Friction-factor on the corrugation angle of the heating plates by using the thermochromic liquid crystals method. They experimentally examined only cross corrugated geometry in order to restrict the range of parameters. The considered Reynolds-number range between 500 - 4000. The presentation of their results are given in graphs showing the local and the average Nusselt-number vs. Reynolds-number and the Friction-factor vs. Reynolds-number. The presented geometry is quite different from those which will be examined in this study. The results are therefore not considered for comparison with the experimental data from the current study. However, this publication could be interesting for further studies because in the second part [18] a numerical investigation (CFD) of heat and flow characteristics of the same cross corrugated geometry is given.

2.3 Erosion

The publications [19, 20, 21, 22, 23] concerning erosion of heat transfer surfaces deal only with the erosion features and do not mention anything about the thermal and the flow performance of eroded surfaces. The investigations deal with general aspects of erosion like aerodynamic flow field variables, eroding particle variables and heat exchanger variables. These issues are of major importance for developing new profile types, but do not help in classifying eroded profiles according to their thermal and hydraulic performance.

The most detailed publications concerning erosion in coal-fired power plants are those of Raask [19, 20]. In [19] he gives a wide overview of the nature of erosion, its mechanism and the factors that influence the erosion rate.

He also describes the special features of different types of coals. He emphasises the South African coal as a very abrasive coal and the coal of Matimba power station as the one with the highest SiO_2 and quartz contents. Raask has reported that only if highly abrasive fuels such as high ash-bituminous coal, quartz-rich brown coals and lignites are used in the power plant then significant erosion wear may occur in air pre-heaters. The reason erosion in air heaters is less than in other parts of a power plant is due to the relatively low velocity of the flue gas and the combustion air. This relative low velocity is required for a longer residence time for the heat transfer in the air heater. It is recommended that the velocity should not be higher than 10 m/s. The following table indicates the life expectancy of air heaters in abrasive-ash-laden flue gas:

Table 2.1: Life expectancy of air heaters in abrasive-ash-laden flue gas [19]

Type of a air heater	Flue gas velocity [m/s]	life expectancy [years]
tubular	12	15 to 20
tubular	15	8 to 12
tubular	20	2 to 3
regenerative	8	12 to 15
regenerative	10	5 to 8
regenerative	12	3 to 5

Numerous publications can be found concerning the fundamental mechanisms of erosion. The authors give different theories of how erosion occurs and how the erosion rate can be theoretically determined. A variety of opinions exists on the mechanism of material removal in erosion. Erosion can be seen as a two stage mechanism in which particles produce some erosion and then fragment to produce additional damage. It was also suggested that local melting during impact and attachment of surface material to the impacting particles produce erosion. Another model consists of an energy balance between the kinetic energy of the particle and the work expended during indentation.

One publication about the fundamental mechanisms of erosion is given by Finnie et al. [21]. They describe detailed forms of erosion mechanism involving the effect on different materials. Finnie et al. describe the erosive removal of material by mechanical theories. They assume a constant normal to tangential force of the particles and hence a force vector constant direction.

Hutchings [22] has defined three different types of deformation:

- plowing, caused by spherical projectiles,
- cutting, caused by angular particles with forward rotation,
- cutting, caused by angular particles with backward rotation.

The mechanical mechanism of erosion is stated to be more important because it affects the weight loss rather than the thermal effects. This paper differs from Finnie's only in one point. Hutchings assumes a constant yield pressure in the area where the particles plastically deform the substrate. That means the force vector changes direction continually during impact.

Suckling and Allen [23] have investigated features of eight different coals used in ESKOM power stations. They examined the erosion rate and the morphology and mineralogy of the ash particles. The morphology was determined by examining of ash specimens under a scanning electron microscope. The mineralogy of each coal is represented by the quartz and mullite content of the ash. The erosion rate was investigated in a test rig with an impact angle of 40 degrees, a velocity of about 40 m/s and a particle feed rate of 0.47 g/s. The results of the erosion rate and the corresponding quartz and mullite content as a %age of total mass of fly ash are listed in the following table.

Table 2.2: Erosion rate and chemical composition of different fly ashes [23]

Power station	Erosion rate [$mm^3/g_{erodent} \cdot 1000$]	Quartz content % of total	Mullite content % of total
Kendal	5.1	13.8	60.4
Matimba	5.43	18.0	49.1
Duhva	5.91	17.1	59.2
Hendrina	7.21	41.2	39.0
Tutuka	7.31	28.2	44.2
Arnot	7.89	17.7	52.2
Matla	10.5	14.7	36.7
Lethabo	11.0	21.2	64.6

These results show no visible relationship between the erosion rate and the mineralogy, contrary to what would have been expected. The authors admit that further tests are necessary to establish more positive and definitive results.

More useful and more detailed information can be found in internal ESKOM information [24, 25]. This information contains a complete coal and ash analysis for the coal used in the Hendrina and in the Matimba Power Station. Boshoff [25] published an analysis of coal product samples of different South African collieries. Since these sources contain the basic information of the erosion behaviour on heating plates, which are investigated in the present study, they will be discussed in detail in Chapter 5.

As it can be seen from the above survey none of the authors investigated the interrelation between erosion and heat and flow performance of heating plates. All the aforementioned experiments concerning the heat transfer and pressure drop only considered unused heating plates. It is not possible to relate the heat transfer coefficient and the pressure drop of new plates to that of eroded plates. There is a need to examine experimentally the influence of erosion on the heat transfer and pressure drop across packs of different types of corrugated heating plates. It is especially important since in South Africa the coal is more erosive that heating plates erode much faster than in other countries, as the above erosion study shows.

2.4 Specific objectives

In view of the foregoing, the specific objectives of this study were defined as follows:

- To verify the correctness of the Thermal Test Facility at TRI firstly by comparatively testing a Rothemuehle pack of heating elements which has been tested before in the Rothemuehle test facility and secondly by testing flat plates and comparing these results with literature data.
- To test all different, new heating profiles, as supplied by Howden Power in the Thermal Test Facility at TRI.
- To compare the hydraulic and thermal performance of the different heating elements.
- To establish the possibility of testing eroded packs using the same procedure as for new plates.
- To test one eroded profile type to determine its thermal and hydraulic performance.

3. Thermal Test Facility

The Thermal Test Facility (TTF) has been operating at TRI, ESKOM, Johannesburg since 1996. It was built by Caby, an MSc Student of the School of Mechanical Engineering, University of Witwatersrand, Johannesburg [26]. The working principle of the test facility is based on the transient single-blow method (see Chapter 2) to measure the heat transfer coefficient of heating plates. Additionally, the pressure drop across the test pack is measured.

Figure 3.1 shows a schematic diagram of the test rig.

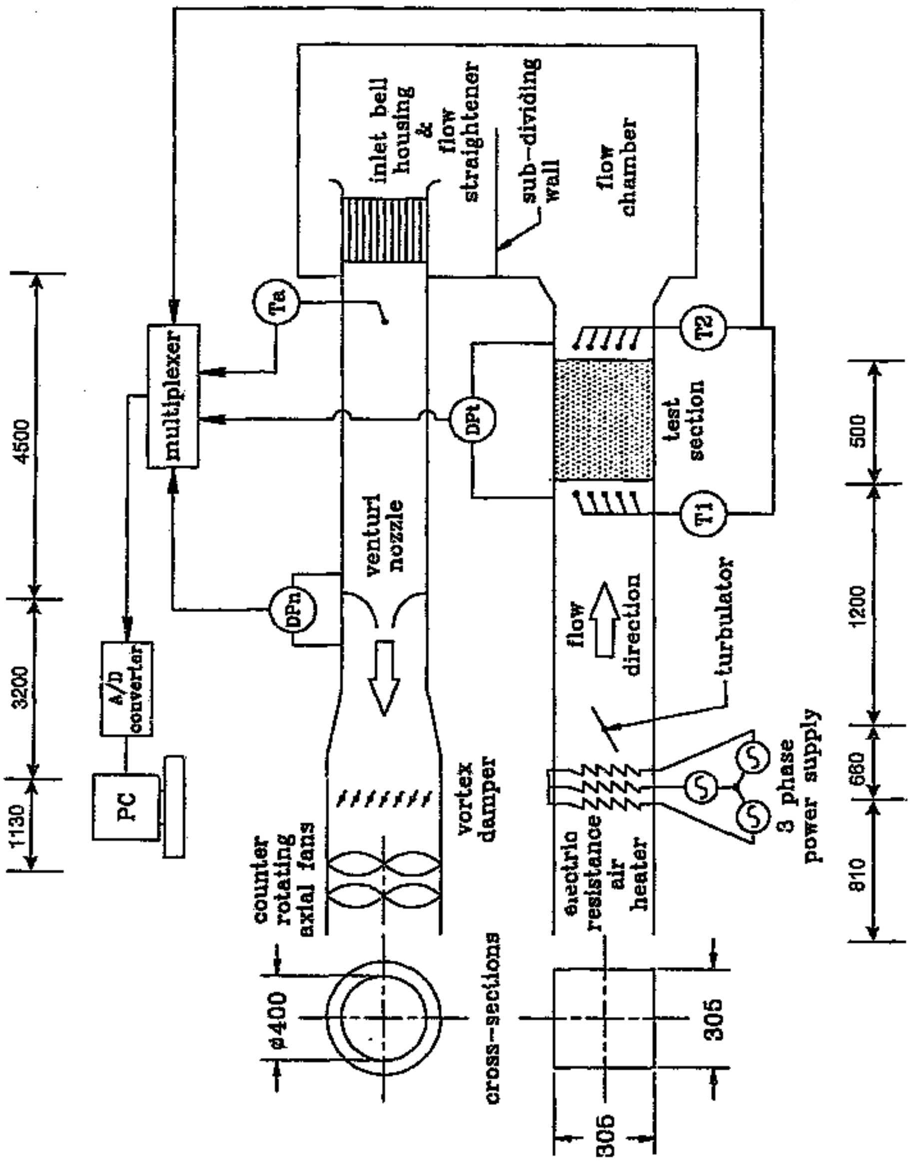

Figure 3.1: Schematic diagram of the Thermal Test Facility

It can be seen from Figure 3.1 that the test rig operates in the suction mode. The air is sucked by either one or two fans, depending on the required mass-flow, from the inside of the laboratory. After passing through the test rig the air is blown outside through the roof. The 35 kW heating device is situated 1 m behind the air inlet. It consists of three identical banks of electric resistance heater coils. The heater has a 3-phase, 60 A power supply and is controlled by a 45 kW, 3-phase thyristor controller. Behind the heaters, a turbulator is built-in to mix up the heated air and so avoid temperature stratification in the flow area. The best results were found if the turbulator is installed in the flow channel with an angle of 30° (see Appendix A). After a flow length of 1.5 m behind the turbulator the test section of 500 mm is situated. In front of the test section a mesh of 8 thermocouples and behind it another 8 thermocouples are installed so that both the inlet and the outlet temperature histories are measured (details of positioning are given in Appendix A). Both these temperature histories are recorded by the data acquisition system. Also the pressure drop across the pack is measured by a piezometric ring of each 4 pressure tappings upstream and 4 tappings downstream of the test section. These pressures are also recorded. Behind the test section there is a flow chamber to change the direction of the flow (laboratory constraints). In the second part of the ducting the nozzle for measuring the mass-flow is situated. To ensure that the flow is straight and uniform at the inlet of the second duct a flow straightener is installed. At the venturi nozzle the pressure drop and the temperature are measured. A damper is located behind the nozzle to adjust the air mass-flow rate. The mass flow can be adjusted from 0.1 - 1.1 kg/s. At the end of the duct two counter rotating axial fans are situated.

The 17 thermocouples used in the test facility are precision fine wire thermocouples manufactured by Omega Engineering, Inc.. They are copper-constantan thermocouples with a diameter of 0.254 mm. They have a teflon insulation. The cold junction compensation is built into the National Instrument Signal Conditioning Unit.

The data of the 16 thermocouples at the entrance and the exit of the test section, the data of the pressure readings across the test section, the pressure drop across the nozzle and the nozzle temperature data are all sampled by a National Instrument SCXI data acquisition system. The readings then go through a National Instrument A/D converter and are recorded in a PC (Pentium 150 Hz.). The data acquisition system is controlled by a program written using Labview software. Labview is a graphical programming development for data acquisition and control, data analysis and data presentation.

The Labview program for the Thermal Test Facility, written by Uys [27], displays all the measured temperature and pressure readings on-line on the screen (see Figure 3.2)

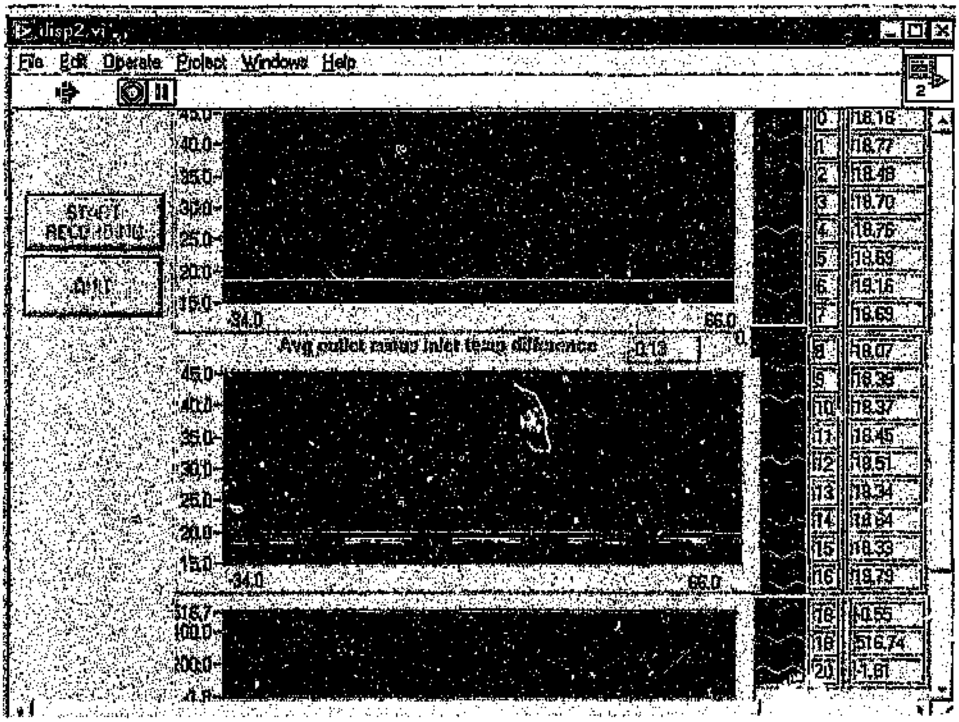

Figure 3.2: Screen of the Labview Program

The first graph shows the 8 inlet temperature readings and the second graph shows the 8 outlet temperature readings. The pressure readings are displayed in the bottom graph. Each graph has a colour coding key displayed on the right hand side. Next to each colour identification and the channel number is a numeric readout of the current value of each channel. This allows easy observation of instantaneous values, while the graphs allow viewing of the overall test progress. They also make it easy to see if any of the inputs are drifting out of the line from the others. The horizontal axis of the graph displays time in seconds. Between the two temperature graphs is a readout of the difference between the average inlet and the average outlet temperature of the test pack. This allows observation of the progress of the pack cooling down. It is important that the residual differential temperature across the pack is as small as possible before a new test point is started.

3.1. Test section/test pack

The cross sectional area of the test section is 305 x 305 mm²; the length is 500 mm. All the test packs manufactured by Howden Power fit exactly into the test section. Insulation at the top and bottom of the pack minimises the heat loss. The packs can be put into the section either with or without braces.

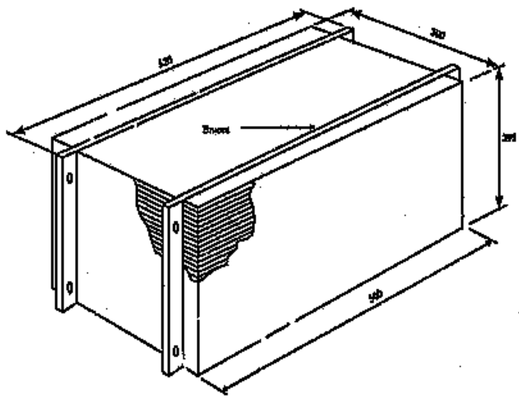

Figure 3.3: Test pack with braces

3.2. Calculation of the heat transfer coefficient according to Mullisen and Loehrke [2]

To determine the heat transfer coefficient from the temperature-time histories at the inlet and the outlet of the test pack a direct curve matching model developed by Mullisen and Loehrke [2] is used. Contrary to previous models, this model is not restricted to an ideal step change in temperature or a periodic temperature function at the pack inlet. Finite-difference equations make it possible to use any temperature history.

The model is based on the following assumptions:

- the fluid velocity profile is uniform across the cross sectional flow area over the testing time;
- the fluid temperature profile is uniform across the cross sectional flow area;
- the properties of the test pack surface remain constant throughout the whole test pack (see [26]);
- thermal conductivity of the air is zero;
- thermal conductivity of the steel plates perpendicular to the flow direction is infinite;
- only the thermal conductivity of the steel plate in the longitudinal direction is considered;
- the side walls of the test section are adiabatic;
- the thermal capacity of the fluid is zero.

The basis of the model are the two heat balances, one for the metal, the other for the fluid (equation 3.1 and equation 3.2). The numerical scheme is fully described in Appendix G.

$$\frac{\partial T_s}{\partial t} = \frac{k}{\rho c_s}\frac{\partial^2 T_s}{\partial x^2} + \frac{h}{\rho a c_s}\left(T_f - T_s\right) \qquad (3.1)$$

$$\frac{\partial T_f}{\partial x}+\frac{W\,h}{\dot{m}\,c_{p,f}}\left(T_f-T_s\right)=0 \tag{3.2}$$

Considering the symmetry of the flow channel, the heat balances are applied to half of the material and half of the flow channel (between centre-line storage material and centre-line flow channel, see Figure 3.4)

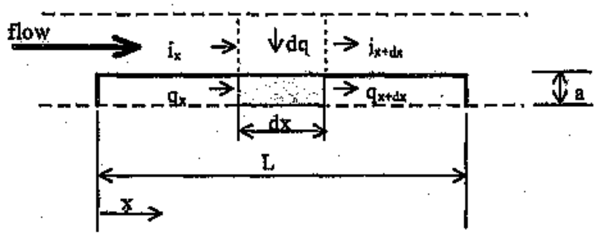

Figure 3.4: Half-flow passage and half plate

Figure 3.5 shows the division of the half-flow passage and the half plate into finite-difference nodes.

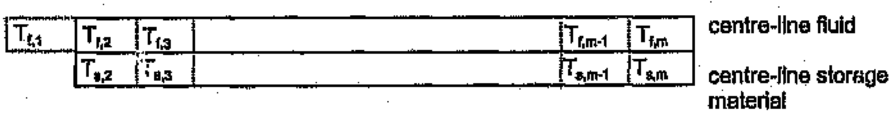

Figure 3.5: Division into finite-difference nodes

Additionally, the boundary conditions are known because of the measured inlet temperatures. Equations 3.1 and 3.2 are converted to finite-difference equations and solved numerically. The objective is to calculate the heat transfer coefficient, which is embodied in both equations. An approximate value for the heat transfer coefficient and the appropriate boundary conditions are used in these equations to calculate a theoretical exit fluid temperature history. This is then compared with the measured fluid exit temperature history. If the histories match within specified limits, the assumed value of the heat transfer coefficient is the correct average heat transfer coefficient of the core. If the history does not match, the heat transfer coefficient is changed iteratively until the specified agreement is achieved. For the convergence criterion an average absolute difference value ε is used (see also Appendix F).

$$\varepsilon = \sqrt{\sum_{i=0}^{n}\left(T^*_{out,i,calc} - T^*_{out,i,exp}\right)^2} \tag{3.3}$$

where: i = 0...n, time steps of 0.33 sec. (test duration is approx. 50 sec.)

$T^*_{out,i,calc}$ = dimensionless, calculated outlet temperature for each time step i

$T^*_{out,i,exp}$ = dimensionless, experimental outlet temperature for each time step i

The dimensionless temperatures are defined as follows (see also Appendix F):

- dimensionless inlet temperature:

$$T^*_{in,i} = \frac{T_{in,i} - T_{in,1}}{T_{in,max} - T_{in,1}} \tag{3.4}$$

- dimensionless outlet temperature:

$$T^*_{out,i} = \frac{T_{out,i} - T_{out,1}}{T_{out,max} - T_{out,1}} \tag{3.5}$$

The authors give an overall accuracy value of ± 2% of their model compared with test results. For further information about the calculation method see Appendix G.

3.3. MATLAB programs for the calculation of results

Two separate MATLAB programs were used to calculate the results from of the raw test data. The MATLAB program *prepdat2.m*, which had to be run first, used as input a data matrix for each test point (mass flow point) recorded by the LABVIEW program. This matrix contained 3 readings per second for each of the 22 input channels (8 channels for inlet temperatures, 8 channels for outlet temperatures, 1 for nozzle temperature, 1 for pressure drop across the nozzle, 1 for nozzle static pressure, 1 for time, 2 for pressure drop across the pack). *Prepdat2.m* calculated the average inlet and outlet temperatures of each set eight thermocouples. Secondly this program determined the mass flow using the pressure drop across the nozzle and the temperature. The air viscosity and density was calculated using the average temperature at the nozzle and the barometric pressure. For these calculations the humidity of the air was not considered, because its effect is negligible.

The purpose of the second program *htcoefa.m* in combination with the function *findcoef.m* was to calculate the heat transfer coefficient for each mass flow point. The average inlet and outlet temperatures histories were used as an input. The values of the mass, heat transfer area and cross sectional area of the pack had to be input by the user. The program contained a finite difference model according to Mullisen and Loehrke [23]. Starting with an initial value for the heat transfer coefficient of 50 W/(m²K) the function *findcoef.m* calculated an outlet temperature history and compared this with the one measured. The solution, which means the heat transfer coefficient which gives the best fitting calculated outlet temperature history was found by iteration. This program used a special MATLAB function *(fmins)* which found the local minimum of a function within a given tolerance. The convergence criterion was the average absolute difference between the calculated and the experimental outlet temperature called error (see also 3.2). *Fmins* stopped calculating when the heat transfer coefficient did not change within the specified tolerance which was 0.01 W/(m²K). *Fmins* used a Simplex search method as an instrument to find the minimum. Usually the error laid between 0.05 and 0.2, depending on the Reynolds-number of the test point. With increasing Reynolds-number the error also increased. An error of 0.2 would mean in absolute temperature a difference of 0.15 °C, which could be considered as the limit of accuracy of the thermocouples. The print-outs of these programs can be found in Appendix B.

3.4. Test Procedure

Determination of basic geometry data and mass

For determining the geometry of the test pack firstly the average height, width and length of the pack had to be measured. These values were needed for put the actual heat flow area and the volume of the pack.

Secondly the mass of the pack (with/without braces) was needed. For the calculation of the heat transfer coefficient only the mass of the pack without braces was considered, because the braces do not take part in the heat transfer. The time duration is too short for this compact mass lump to heat up significantly. Also the number of plates had to be counted, the notched and undulated ones. To make sure that the pack stays always in the same order each plate had to numbered. The whole pack got a number to avoid confusions (e.g. H8_00, H8_01......KH11_00, KH11_01).

Determining the expanded length ratio

To calculate the heat transfer area of a test pack the expanded (stretched) length ratio of profile plates had to be determined. The expanded length ratio is the ratio between the curved length and the straight length of the profile. To get an average, 4 notched and 4 undulated plates were taken as reference plates. There were two possibilities to measure the expanded length ratio.

- 1st possibility, using the digitalizing board: Therefore a picture of the profile curve was needed. This was gained by rubbing with a pen on a piece of paper on top of the profile. On the digitalizing board the profile curve was driven by a special pen. This gives immediately the value of the expanded length of the undulated and the notched plates.
- 2nd possibility, using of masking tape to put in the profiles (at least 10 notches or undulations), take it off, glue it on a piece of paper and measure the expanded length of the undulations or notches

After measuring the straight length of the profile plates with a ruler, the expanded length ratio of expanded length to actual length of the plate could be calculated. With the help of the expanded length ratio the heat transfer area and the cross sectional area could be calculated.

Air properties

As air properties the actual barometric pressure and the dry and wet bulb temperature were needed. The temperatures were measured several times during the test run. The air properties like density, humidity, air viscosity and Prandtl-number were calculated in an excel-spreadsheet according to the formulas in Appendix H.

Test data sheet

For each test run a test data sheet was filled in with all the geometry data and air properties. Additionally to the data recorded by the PC, in the test data-sheet the pressures (nozzle and pack) and the heating position was recorded by hand.

Preparing the test run

Firstly the pack had to be put into the test section, either with or without braces. Then it had to be made sure that there was no gap between the pack and the test section. Above and below the test pack insulation was put to minimise heat loss. The pressure measuring devices had to be switched on to warm up. To ensure steady state conditions the fans are switched on 10 minutes before the start of the test run.

Actual test run

The LABVIEW program for recording the test data (temperatures and pressures) was started. The mass-flow range between 0.1 kg/s and 1.1 kg/s was covered with 16 to 18 measuring points. For these points the damper had to be adjusted to the required position. Also the heater was adjusted so that the inlet temperature jump for each mass flow was approximately the same (approximately 20°C). All the test runs were started with the lowest mass flow. To check whether the flow was stable the data was already recorded 10 sec. before the heating. Then the heater was switched on for 40 sec (total record time was 50 sec). After stopping the recording of data the heater was switched off. Now the whole system had to cool down (approx. 5 min.), the next test point could be adjusted and then the next test point could be started. But before starting the next test point it had to be ensured that the average temperature difference between inlet and outlet was small, i.e. the system had cooled down properly

Calculating results

Firstly the excel program *matrix.xls* was run, which converted the data into a matrix for further calculations in MATLAB. Secondly the MATLAB program *prepdat2.m* calculated the average outlet and inlet temperatures of the 16 thermocouples and the mass flow from the nozzle data for each test point. Thirdly the main MATLAB program *htcoefa.m* was run. It calculated the heat transfer coefficient according to Mullisen and Loehrke [2] using a finite difference model. The temperature histories of the inlet and outlet temperature were used as input data from a file. The mass, the heat transfer area and the cross sectional area of the pack had to be given in by h. The output of this last program is a matrix which contains all the data from one test n, i.e. each mass-flow point with appropriate Reynolds-number, heat transfer coefficient and pressure drop across the pack. The calculation time of this program was 1.5 hours for 16 measuring points on a Pentium 150 MHz.

3.5. Fluid properties

The following fluid properties of air were needed in the present study:

- barometric pressure
- humidity
- gas constant
- kinematic viscosity

The barometric pressure required to be corrected for temperature and for gravity. The gravity correction considers of the influence of altitude and the influence of latitude.

The appropriate calculation methods are detailed in Appendix H.

3.6. Difficulties encountered during the study

Several experimental and computational difficulties, and sources of inaccuracy were encountered or discovered in the sourse of this study. These problems and the methods of overcoming them are described in Appendix A.

3.7. Presentation of test results

Firstly the Matlab program calculated the heat transfer coefficient for a particular mass flow. One possibilty of presenting the test data were graphs where the heat transfer coefficient and the pressure drop was shown vs. the mass flow. A disadvantage of this sort of presentation was that the mass flow did not represent the velocity in the pack because of different hydraulic diameters for different packs. Another possibility was to present graphs where the heat transfer coefficient and pressure drop vs. velocity were shown. To eliminate the influence of fluid properties either curves showing heat transfer coefficient and pressure drop vs. velocity at normal conditions (101.3 kPa and 0 °C) or curves showing dimensionless numbers like the Colburn- and Friction-factor vs. Re-number could be used. The definition of the dimensionless numbers are as follows.

- the Colburn-factor is defined as follows

$$Co = \frac{Nu}{Re \cdot Pr^{1/3}} = \frac{h \cdot d_h}{k \cdot Re \cdot Pr^{1/3}} = \frac{h}{\frac{\dot{m}}{A_{free}} \cdot c_p} \cdot \left(\frac{\mu \cdot c_p}{k}\right)^{2/3} \tag{3.6}$$

with: Nu = Nusselt-number $Nu = \frac{h \cdot d_h}{k}$ (3.7)

Re = Reynolds-number (see below)

Pr = Prandtl-number $Pr = \frac{\eta \cdot c_p}{k}$ (3.8)

h = heat transfer coefficient [W/(m² K)]

d_h = hydraulic diameter [m]

k = heat conductivity of air [W/(m K)]

$\dot{m}$ = mass flow rate [kg/s]

A_{free} = free cross section of pack [m²]

c_p = specific heat of air [J/(kg K)]

μ = dynamic viscosity of air [Pa·s] $(\mu = \nu \cdot \rho)$

- the Friction-factor is defined as follows

$$F = \frac{\Delta p}{2 \cdot v^2 \cdot \rho} \cdot \frac{d_h}{L} \tag{3.9}$$

with:

v = velocity in the pack [m/s]

d_h = hydraulic diameter [m]

L = length of the pack [m]

ρ = density of air [kg/m³]

Δp = pressure drop across the pack [Pa]

- the Reynol -number is defined as follows

$$Re = \frac{v \cdot d_h}{\upsilon} = \frac{d_h \cdot \frac{\dot{m}}{A_{free}}}{\mu} \tag{3.10}$$

with: υ = kinematic viscosity of air [m²/s]

4 Thermal tests of uneroded plates

This chapter details progress made since the beginning of 1997 concerning thermal and pressure drop performance testing of regenerative air heater test packs on the thermal test facility situated at TRI. More than 160 test runs have been performed during this time (until March 1998) on a number of different air heater pack types commonly used in ESKOM. The geometry of these profiles is shown in Figure 4.1. Most of the profiles were tested in various configurations. For example, the performance of the same pack type with different numbers of plates was tested. Packs were tested with and without braces. Some of the packs were tested with different types of braces. The majority of the packs which are used in the thermal test facility are supplied by Howden Power. The test results have been checked by carrying out at least two test runs for every configuration.

4.1 Standard profile types

The following picture (Figure 4.1) shows all the profiles, which are commonly used in ESKOM air heater.

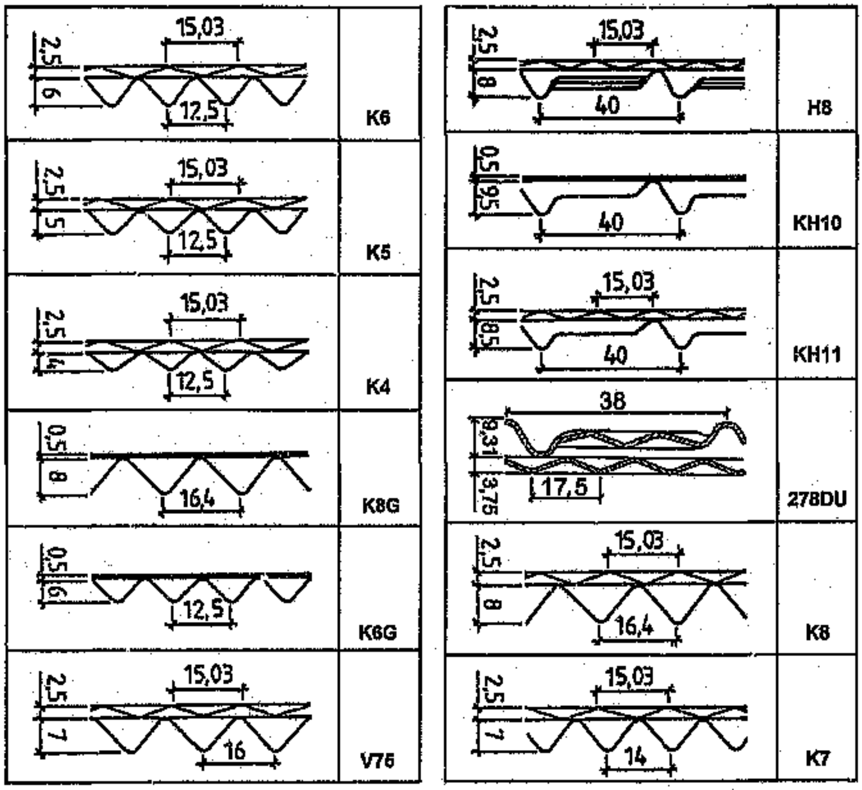

Figure 4.1: Different heating profiles (direction of flow is perpendicular to the page)

4.1.1 Profile H8

The H8 profile shape is shown in Figure 4.1. The notched plate is characterised by steps, up and down in the flow direction, to disturb the flow additionally to what is done by the undulated plate. The undulated plate is characterised by W-shaped wavy structures, which means the directions of these waves are at an angle of 30° to the flow direction and this direction changes twice on the length of 500 mm. The rolling height is 2.5 mm.

This has been the first pack type to be tested since it had previously been used to establish the validation of the test rig. One pack of this type had been obtained from Apparatebau Rothemuehle (RM) in Germany, where it had also been tested. Caby [26] had tested this same pack in ESKOM's newly commissioned test facility and results confirmed that the TRI test facility was working properly. Figure 4.2 shows the pressure drop across the pack and the heat transfer coefficient of the same RM test pack containing 55 plates, as tested in Germany and South Africa normalised to standard conditions (0°C, 101.3 kPa). The graph shows three different test runs from South Africa (_1, _2, _41) and one test run from Germany (_RM)

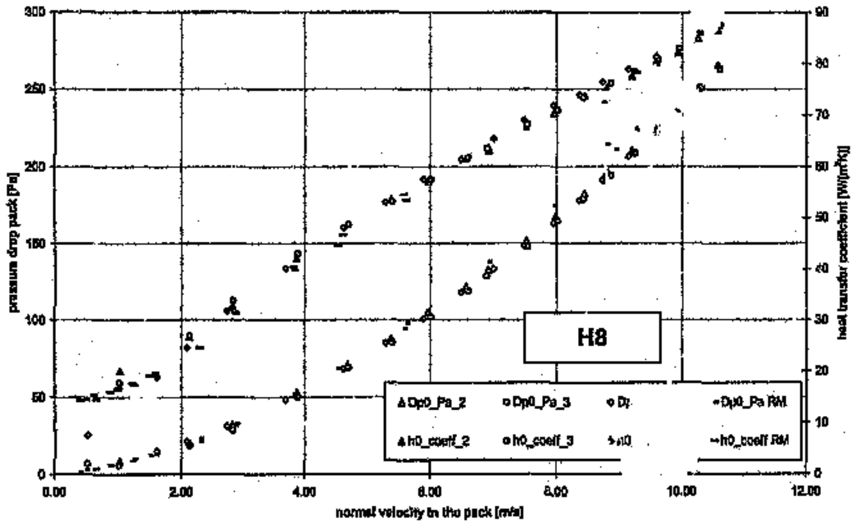

Figure 4.2: Results for the H8 pack from Apparatebau Rothemuehle, tested in Germany and South Africa

To compare the RM results (heat transfer coefficient and pressure drop) with the results obtained from the Thermal Test Facility (TTF) at TRI, values have been calculated for normal conditions (0 °C, 101.3 kPa). Another possibility for comparison is to calculate dimensionless numbers such as the Colburn-factor, the Fanning Friction-factor and Reynolds-number, which are defined in Chapter 3.

Figure 4.3 shows a diagram Colburn- and Friction-factor vs. Reynolds-number of the Rothemuehle and the present results.

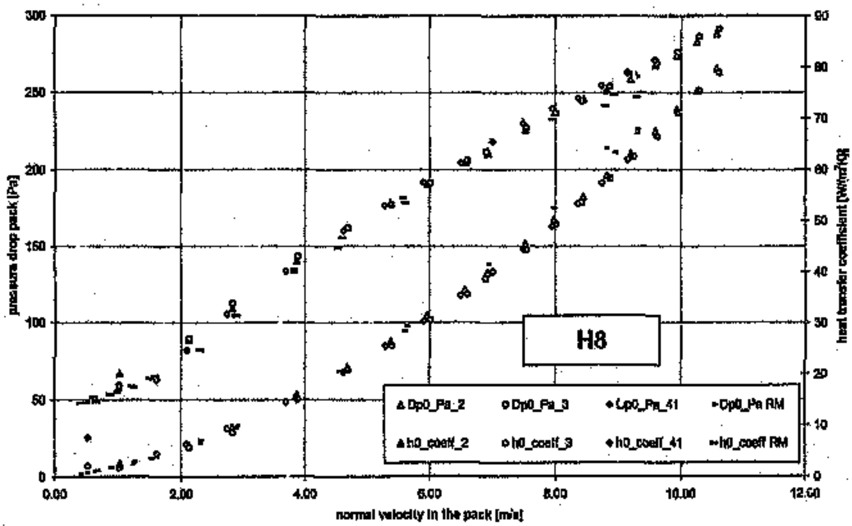

Figure 4.2: Results for the H8 pack from Apparatebau Rothemuehle, tested in Germany and South Africa

To compare the RM results (heat transfer coefficient and pressure drop) with the results obtained from the Thermal Test Facility (TTF) at TRI, values have been calculated for normal conditions (0 °C, 101.3 kPa). Another possibility for comparison is to calculate dimensionless numbers such as the Colburn-factor, the Fanning Friction-factor and Reynolds-number, which are defined in Chapter 3.

Figure 4.3 shows a diagram Colburn- and Friction-factor vs. Reynolds-number of the Rothemuehle and the present results.

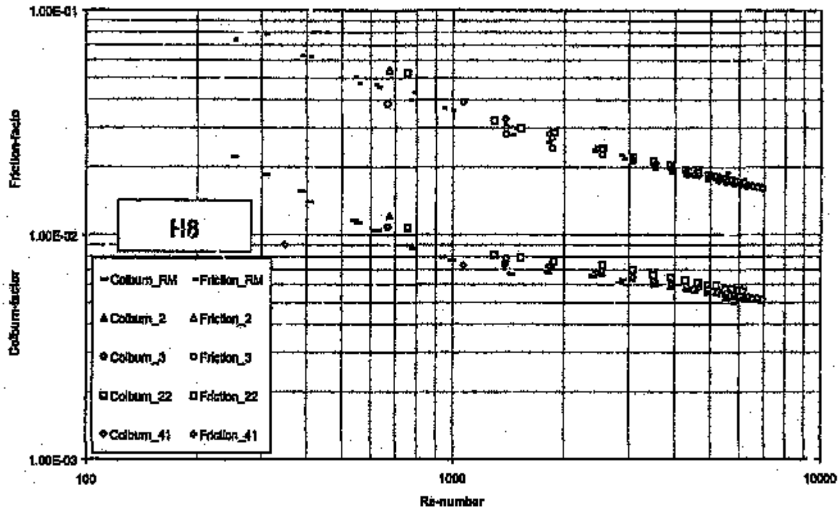

Figure 4.3: Results for the H8 pack from Rothemuehle, tested in Germany and South Africa, dimensionless values

From Figure 4.2 and Figure 4.3 it can be seen that for both the ESKOM and RM tests the pressure drops are well matched. However, the RM heat transfer coefficient is slightly lower than the TRI one over the whole velocity range. The reason for this could be due to the difference in the data reduction systems. RM uses a step-temperature function and a calculation method according to Locke [6]. At TRI the data reduction method according to Mullisen and Loehrke [2] is used. However, the deviations of the heat transfer coefficients are less than 10 %, which is within the measuring uncertainties of the test facilities (see Appendix E).

For the H8 profile the following numbering system is used to differentiate between the different test packs:

Table 4.1: Numbering system of the H8 packs

manufacturer	pack number
Rothemuehle (RM)	H8_00(a)
Howden Power	H8_02(a), H8_03(a), H8_04(a), ...

After verifying that the TRI Thermal Test Facility is reliable, packs supplied by Howden Power could be tested and results compared with those from the RM pack.

The geometry of the RM H8 pack and a H8 pack supplied by Howden Power with 0.5 mm plate thickness and 0.5 m in length was compared. The cross sectional area, the heat transfer area and the mass is related to packs for the test section (300 mm x 300 mm x 500 mm) and is not related to the standard unit of 1 m^3. The mass is taken without braces. These values refer to the standard number of plates. This is valid for all following profile types, unless otherwise stated.

Table 4.2: Geometry data of the standard H8 pack
(300 mm x 300 mm x 500 mm)

Profile type	hydr. Ø [mm]	A_{cross} [m^2]	A_{heat} [m^2]	mass [kg]	no of plates	undul. form
H8	8.71	9.11E-03	18.22	36.2	55	W-shape
H8 (RM)	8.65	9.17E-03	18.34	35.89	55	W-shape

The results are shown in the following figures (Figure 4.4 and Figure 4.5).

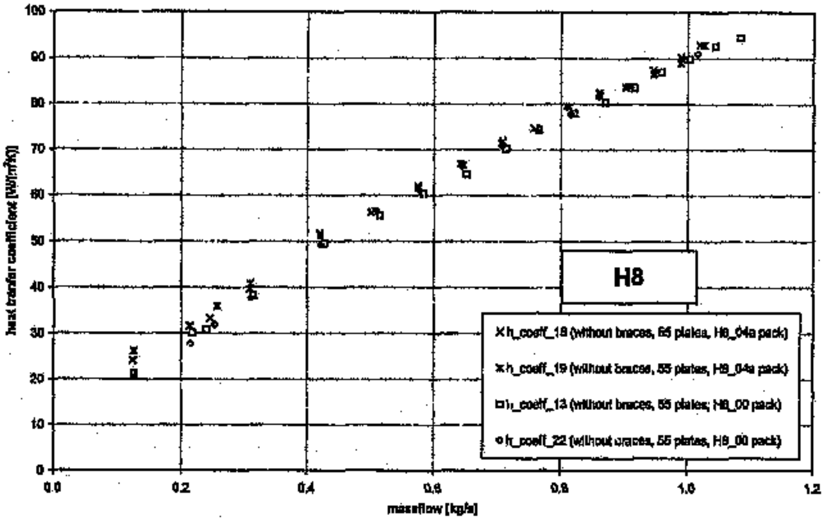

Figure 4.4: Results for two different H8 packs (RM and Howden Power), heat transfer coefficient vs. mass flow

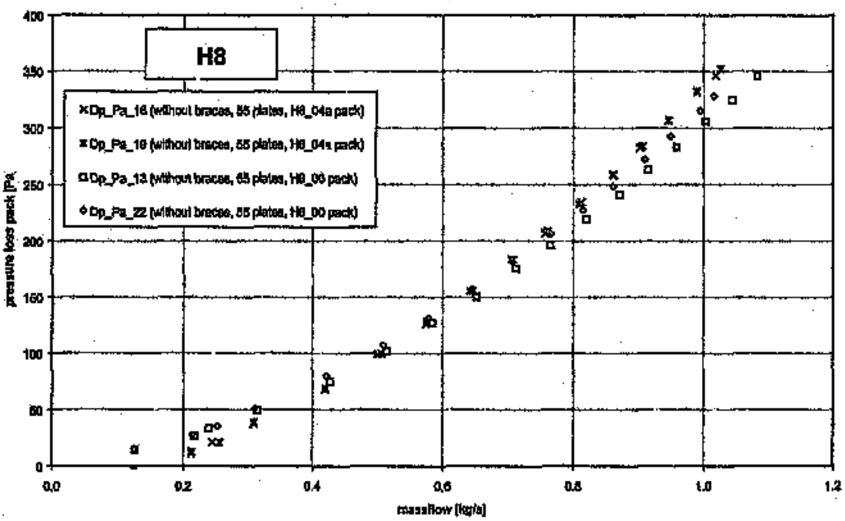

Figure 4.5: Results for two different H8 packs (RM and Howden Power), pressure drop across pack vs. mass flow

These graphs show that there are only small deviations in the pressure drop and the heat transfer coefficient. It can be concluded that the Howden Power and the RM pack show similar performance characteristics.

4.1.1.1 Influence of individual packs

Three different H8 packs manufactured by Howden Power were tested to determine the influence of the individuality (repeatability of manufacture) of the different air heater packs. Figure 4.6 shows the results of the heat transfer coefficient vs. mass flow and Figure 4.7 shows the pressure drop across the pack. The graphs show two test runs for each test pack.

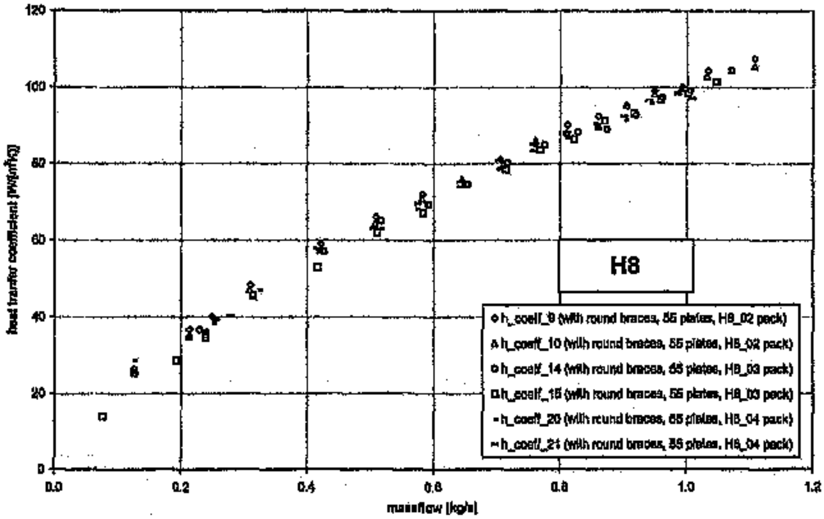

Figure 4.6: Results for three different H8 packs from Howden Power, heat transfer coefficient vs. mass flow

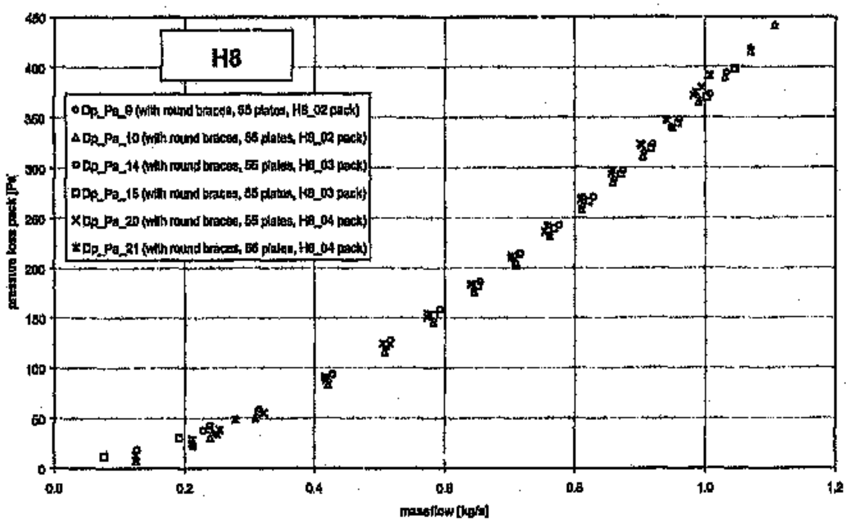

Figure 4.7: Results for three different H8 packs from Howden Power, pressure drop across pack vs. mass flow

As it can be seen from these figures, all test runs from three different H8 packs with braces show that there is little variation in the heat transfer coefficient as well as in the pressure drop. This leads to the conclusion that there is a negligible difference in thermal performance between individual test packs of the H8 type.

4.1.1.2 Influence of the braces

One Howden Power test pack has been tested with and without braces. These braces are of mild steel round bar (diameter = 10 mm, $mass_{Braces}$ = 2 kg). Two of them hold the pack together.

The following graphs (Figure 4.8 and Figure 4.9) show the results of each of the two test runs.

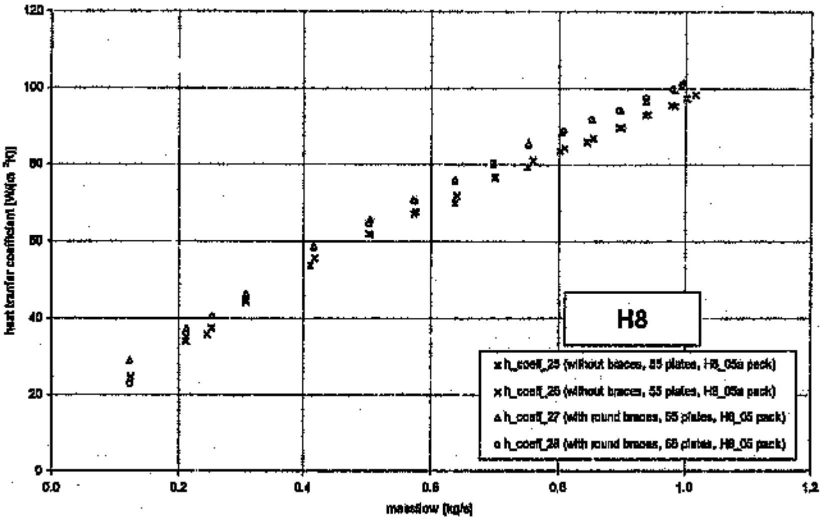

Figure 4.8: Results for a H8 pack with and without braces, heat transfer coefficient vs. mass flow

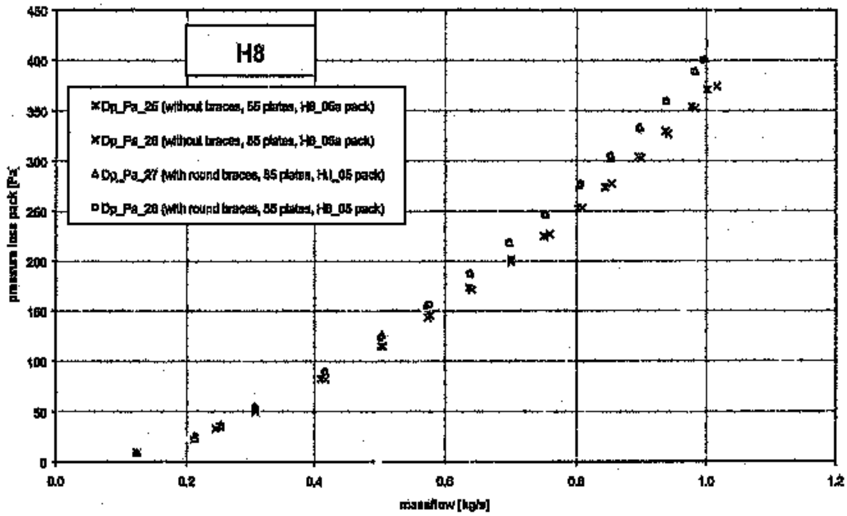

Figure 4.9: Results for a H8 pack with and without braces, pressure drop across pack vs. mass flow

These figures show that the influence of the braces is not negligible. This is contrary to what was earlier reported by Caby [21]. Both the heat transfer coefficient and the pressure drop are higher with braces than without braces. The presence of the braces increases the pressure drop because of higher entrance and exit losses. These higher entrance and exit losses are due to the increased material area which causes contraction and expansion of the flow. The increase of pressure drop is about 10 % and the heat transfer coefficient with braces is also about 10 % higher than without braces at the highest mass flow rate. Due to the higher pressure drop, greater turbulence can be expected in the pack so that the heat transfer must also be higher.

4.1.2 Profile 278DU

The 278DU profile is the other profile type for which the notched plate has a flow disturbance in the flow direction. The basic form of this profile is similar to that of the KH11 (see Figure 4.1), except that on the flat part of the notched plate between the hill and the valley there are rolled wavy indents with an angle of 30 degrees to the flow direction.

Table 4.3: Geometry data of the standard 278DU pack
300 mm x 300 mm x 500 mm)

Profile type	hydr. Ø [mm]	A_{cross} [m²]	A_{heat} [m²]	mass [kg]	no of plates	undul. Form
278DU	10.4	7.79E-03	15.58	34.22	45	diagonal

This profile type has been tested with and without braces, but always with the same number of plates.

4.1.2.1 Influence of the braces

Figure 4.10 and Figure 4.11 show the results of the test runs with and without braces.

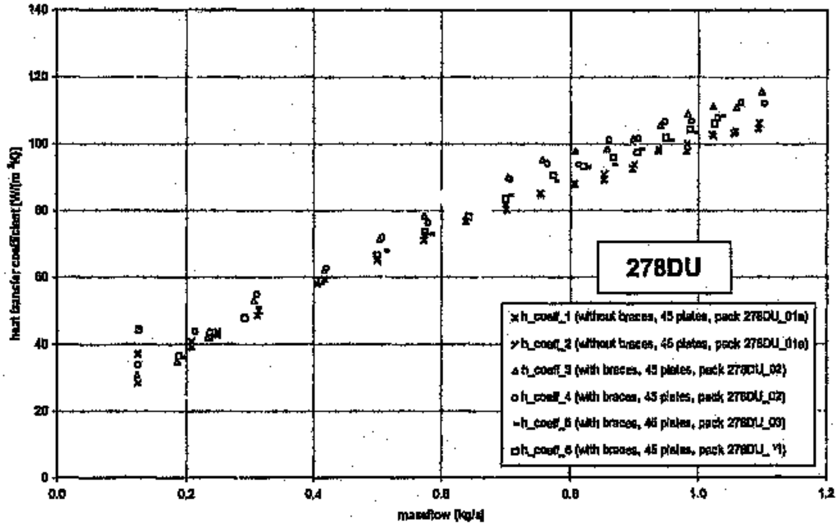

Figure 4.10: Results for different 278DU packs with and without braces, heat transfer coefficient vs. mass flow

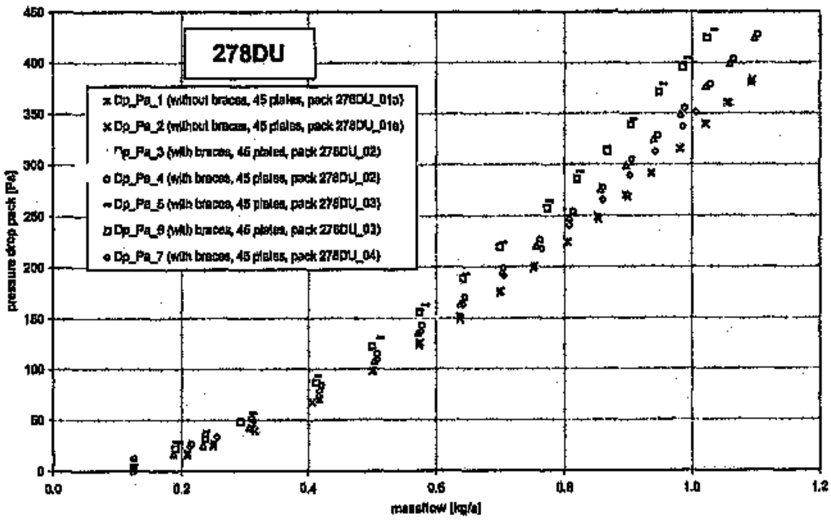

Figure 4.11: Results for different 278DU packs with and without braces, pressure drop across pack vs. mass flow

These results lead to the following conclusions concerning the influence of braces on the 278DU profile type: On the heat transfer coefficient the effect is unclear because of the scatter of the results, although there is evidence that the coefficient is lower for the pack without braces. The pressure drop at 1 kg/s is also 35 Pa higher with braces than without braces.

4.1.3 Profile KH11

The KH11 profile is similar to the H8 and the 278DU profile. The only difference is that the notched plate of the KH11 has no steps in the flow direction. The undulated plate is exactly the same for both profile types (Figure 4.1).

Table 4.4: Geometry data of the standard KH11 pack
(300 mm x 300 mm x 500 mm)

Profile type	hydr. Ø [mm]	A_{cross} [m²]	A_{heat} [m²]	mass [kg]	no of plates	undul. form
KH11	8.86	8.98E-03	17.96	34.92	53	W-shape

All KH11 packs used in the following test runs were manufactured by Howden Power. The following discussion deals with the influence of the number of plates, the kind of braces (round or flat) and the presence or absence of braces.

4.1.3.1 Influence of the number of plates

For a 300 mm wide pack the standard number of plates (packing density) is 53 plates [28]. However, to test the influence of the number of plates on the thermal performance this profile was also tested with 51 plates. The following figures show the results (Figure 4.12 and Figure 4.13).

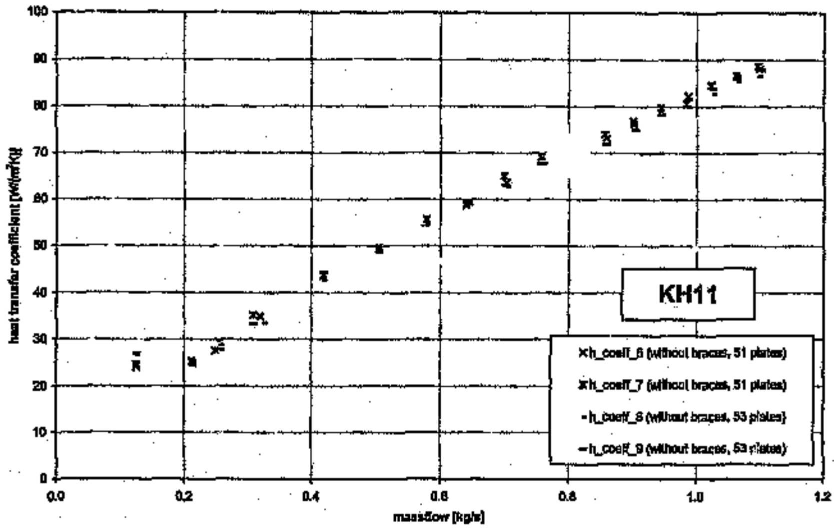

Figure 4.12: Results for the KH11pack with a different number of plates, heat transfer coefficient vs. mass flow

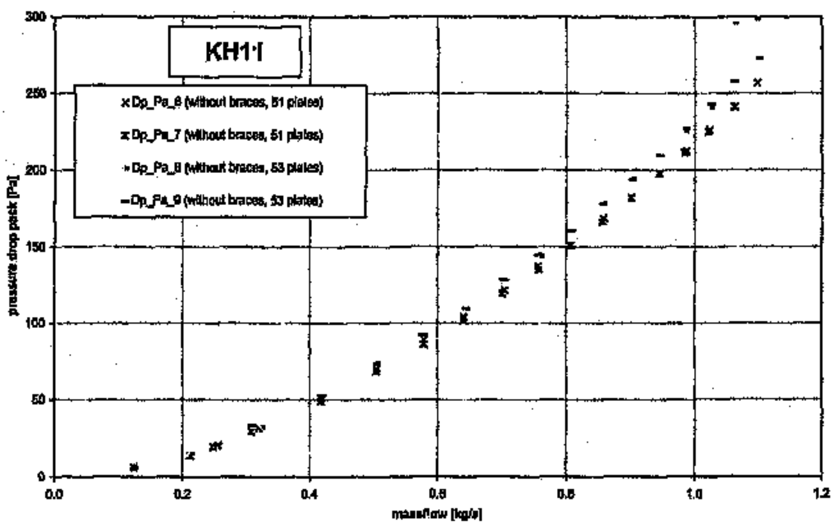

Figure 4.13: Results for the KH11 pack with a different number of plates, pressure drop across pack vs. mass flow

As these graphs show, a variation of two plates has a very small influence on the heat transfer coefficient and on the pressure drop. The pressure drop is slightly higher (5 %) as can be expected due to the increased material area but this difference is within the measuring uncertainties. Similarly, the difference in the heat transfer coefficient is within measurement uncertainties.

4.1.3.2 Influence of the braces

The KH11 pack has been tested with flat-bar braces, with round-bar braces and without braces. The flat bar is oriented parallel to the fluid flow so that the frontal area influencing flow is the same as that for the round braces. Figure 4.14 and Figure 4.15 show the results.

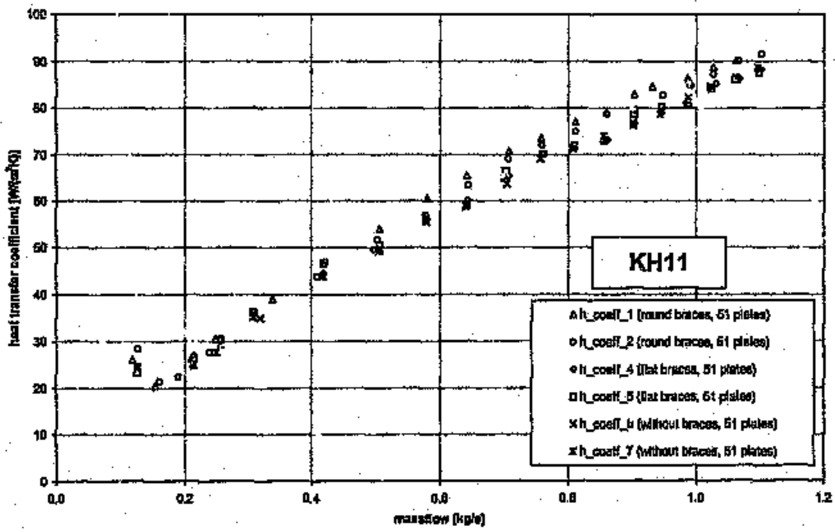

Figure 4.14: Results for the KH11 pack, influence of the braces, heat transfer coefficient vs. mass flow

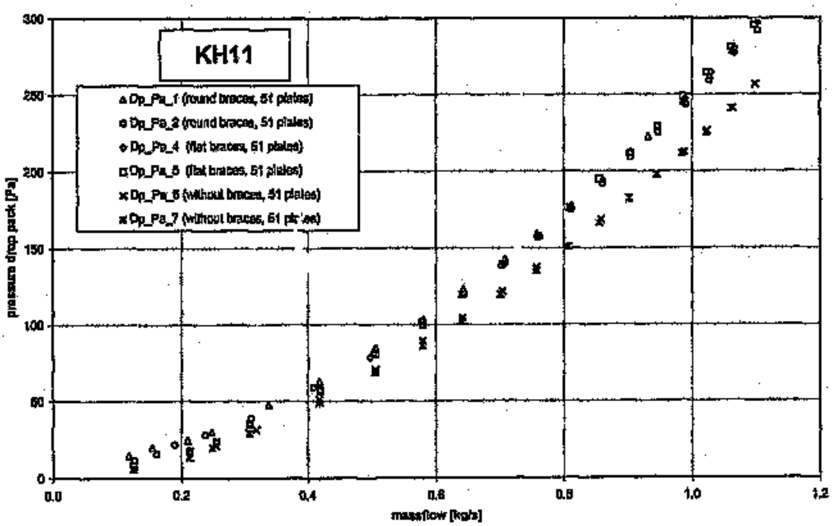

Figure 4.15: Results for the KH11 pack, influence of the braces, pressure drop across pack vs. mass flow

Figure 4.15 shows clearly that the kind of brace has little influence (within the limits of uncertainty) on the pressure drop across the KH11 pack. However, there is a marked difference in the results of the packs with and without braces. At a mass flow of 1 kg/s the difference is 30 Pa, which is 12%.

The curve for the heat transfer coefficient does not show the expected trend. Relating to the pressure drop, it would be expected that the heat transfer is also positively influenced by the presence of the braces, irrespective of the form of the braces. However, Figure 4.14 shows that only the pack with the round bar braces has a slightly higher heat transfer coefficient. The heat transfer coefficients for the packs with flat and without braces are the same. These results are not explicable. However, there is evidence that there may be an influence on the heat transfer coefficient due to the pack braces (also see previous discussion for H8 pack in 4.1.1.2). In future tests all packs will be tested without braces to isolate any possible effects of the braces on thermal and pressure drop performance.

4.1.4 Profile KH10

The KH10 profile is characterised by the same notched plate as the KH11 profile (Figure 4.1). However, the profile height is 1 mm higher and instead of an undulated plate, this profile has an adjacent flat plate.

Table 4.5: Geometry data of the standard KH10 pack (300 mm x 300 mm x 500 mm)

Profile type	hydr. Ø [mm]	A_{cross} [m²]	A_{heat} [m²]	mass [kg]	no of plates	undul. form
KH10	7.99	9.84E-03	19.68	39.27	59	flat

4.1.4.1 Influence of the braces

Figure 4.16 and Figure 4.17 show the results of the KH10 profile with and without braces. All tests were done with the same number of plates.

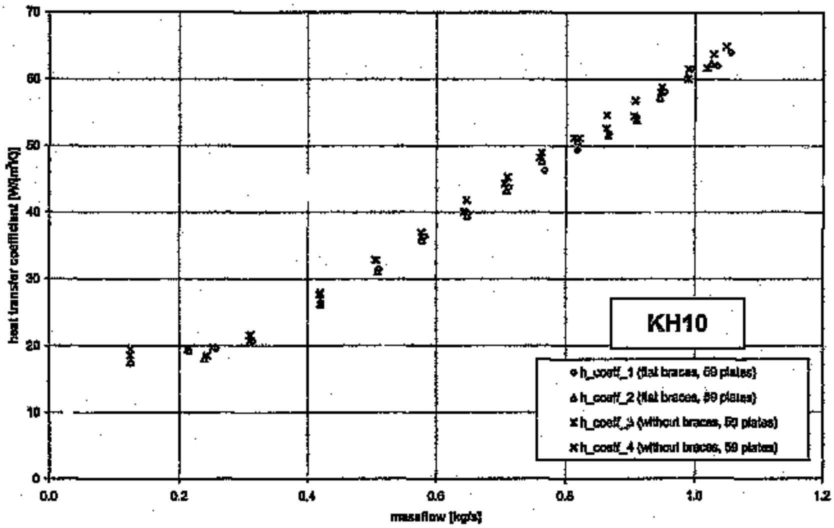

Figure 4.16: Results for a KH10 pack with and without braces, heat transfer coefficient vs. mass flow

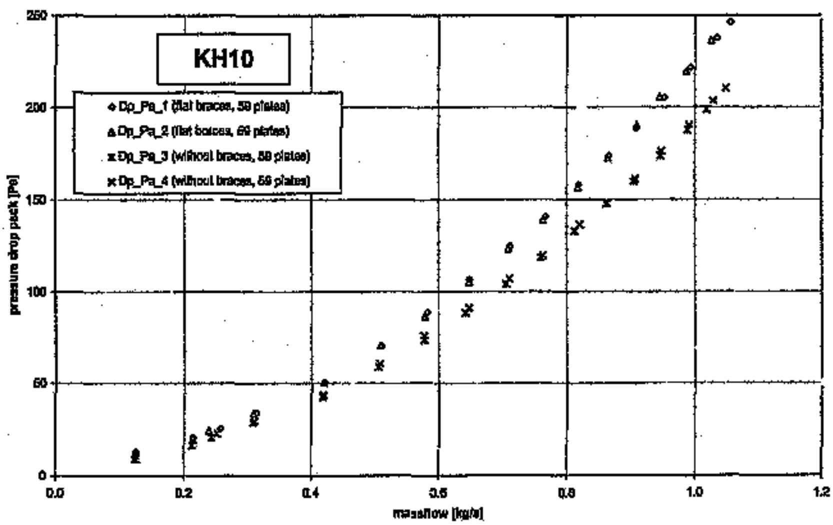

Figure 4.17: Results for a KH10 pack with and without braces, pressure drop across pack vs. mass flow

Both graphs show the same tendencies as those of the profile types mentioned previously. The influence of the braces on the pressure drop is again significant, i.e. 30 Pa at a mass flow of 1 kg/s. However, the influence on the heat transfer is within measurement uncertainties. The different test runs indicate some scatter.

4.1.5 Profile V75

The V75 profile belongs to the group of profiles where the notched plate is characterised by a wavy curve (Figure 4.1). The peaks of this profile are quite pointed. The undulated plate is the same as at the H8 pack. The height of the notched plate is, including the plate thickness of 0.5 mm, 7.5 mm.

Table 4.6: Geometry data of the standard V75 pack
(300 mm x 300 mm x 500 mm)

Profile type	hydr. Ø [mm]	A_{cross} [m²]	A_{heat} [m²]	mass [kg]	no of plates	undul. form
V75	7.16	1.08E-02	21.68	41.95	61	W-shape

For this profile type two different packs were tested to investigate the influence of the braces and the influence of the number of plates on thermal and pressure drop results. Figure 4.18 and Figure 4.19 show these results.

4.1.5.1 Influence of the number of plates

Figure 4.18 shows that the heat transfer coefficient of a V75 pack with either 59 or 61 plates is similar. Also the pressure drop remains the same for either 59 or 61 plates. Both packs were tested with braces.

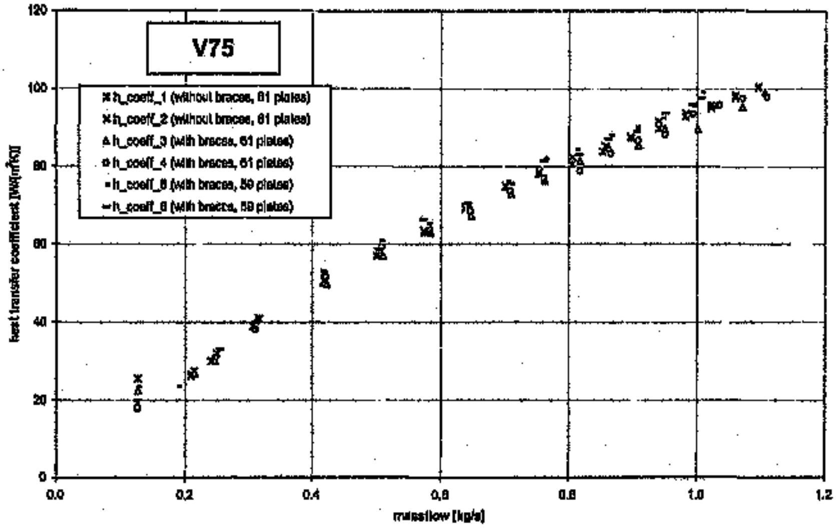

Figure 4.18: Results for the V75 pack,
heat transfer coefficient vs. mass flow

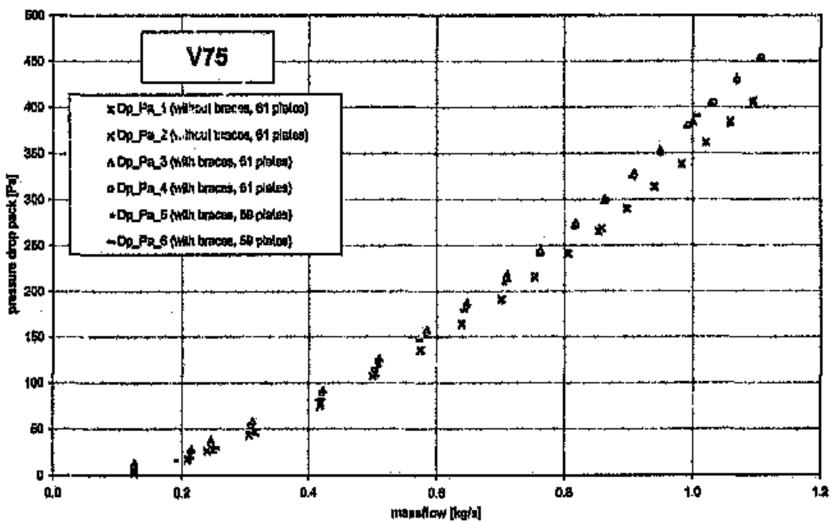

Figure 4.19: Results for the V75 pack,
pressure drop across pack vs. mass flow

4.1.5.2 Influence of the braces

Figure 4.18 and Figure 4.19 also show the influence of braces. Again a comparison of the heat transfer coefficients shows that there is no visible difference. However, the pressure drop shows an influence of the braces. At a mass flow of 1 kg/s the pack with braces has a 35 Pa greater pressure drop than the pack without braces.

4.1.6 Profile K4

The notched plate of the K4 profile is very similar to that of the V75 profile (Figure 4.1). The difference is the profile height, which for the K4 is 4 mm, and the peaks are not that pointed. The undulated plate is the same as those for the previously mentioned packs.
The small rolling height of the notched plate makes this profile a very closed and compact profile with a high heat transfer area but also a high tendency for blockage.

Table 4.7: Geometry data of the standard K4 pack
(300 mm x 300 mm x 500 mm)

Profile type	hydr. Ø [mm]	A_{cross} [m²]	A_{heat} [m²]	mass [kg]	no of plates	undul. Form
K4	4.9	1.44E-02	28.89	57.08	89	W-shape

4.1.6.1 Influence of the braces

The heat transfer coefficient and the pressure drop across the pack with and without braces are shown in the following figures (Figure 4.20 and Figure 4.21).

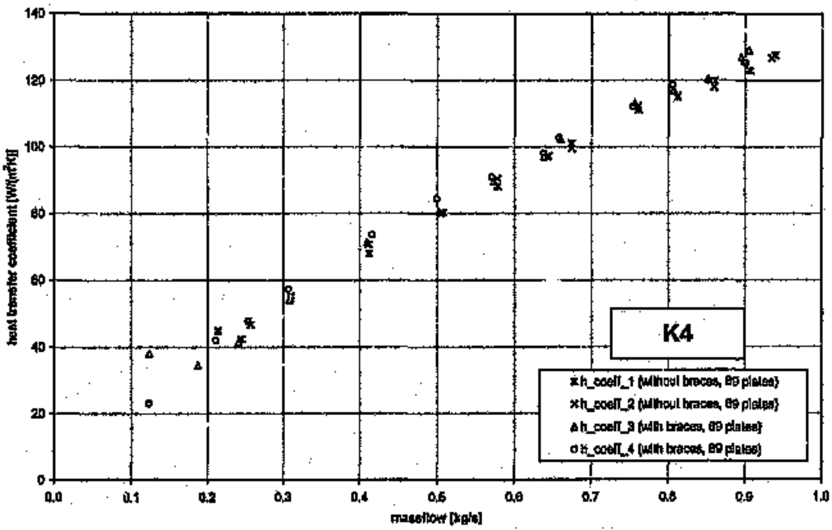

Figure 4.20: Results for a K4 pack with and without braces,
heat transfer coeffic·-nt vs. mass flow

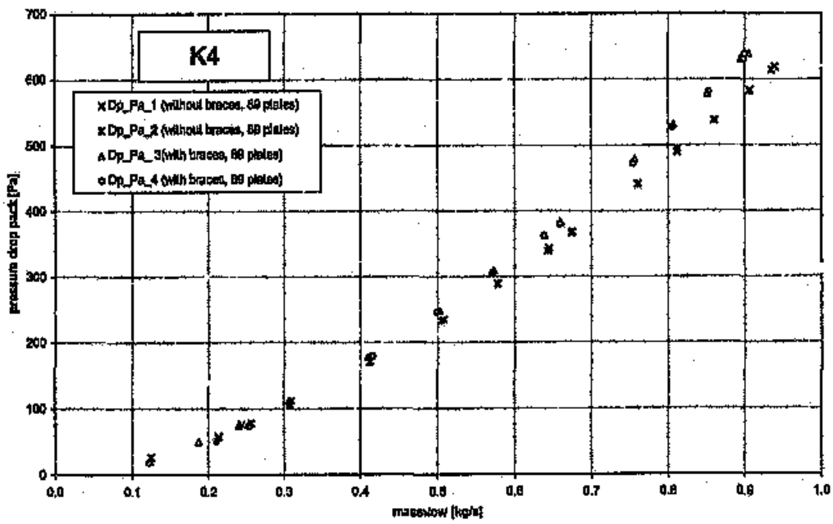

Figure 4.21: Results for a K4 pack with and without braces,
pressure drop across pack vs. mass flow

As expected this profile has a relatively high heat transfer coefficient and also a high pressure drop. The difference between a pack with and without braces is visible in both graphs. The heat transfer coefficient is slightly higher (5 %) and the pressure loss is 40 Pa (10 %) higher for the pack with braces.

4.1.7 Profile K5

The K5 profile is similar to the K4 profile (Figure 4.1). The only difference between these profiles is the amplitude of the notched profile. The K5 profile has an amplitude of 5 mm (including the plate thickness of 0.5 mm) and the K4 of 4 mm.

Table 4.8: Geometry data of the standard K5 pack
(300 mm x 300 mm x 500 mm)

Profile type	hydr. Ø [mm]	A_{cross} [m^2]	A_{heat} [m^2]	mass [kg]	no of plates	undul. form
K5	5.63	1.3E-02	25.91	51.13	77	W-shape

4.1.7.1 Influence of the braces

This pack has been tested with and without braces. The following graphs (Figure 4.22 and Figure 4.23) show the results of each of the two test runs.

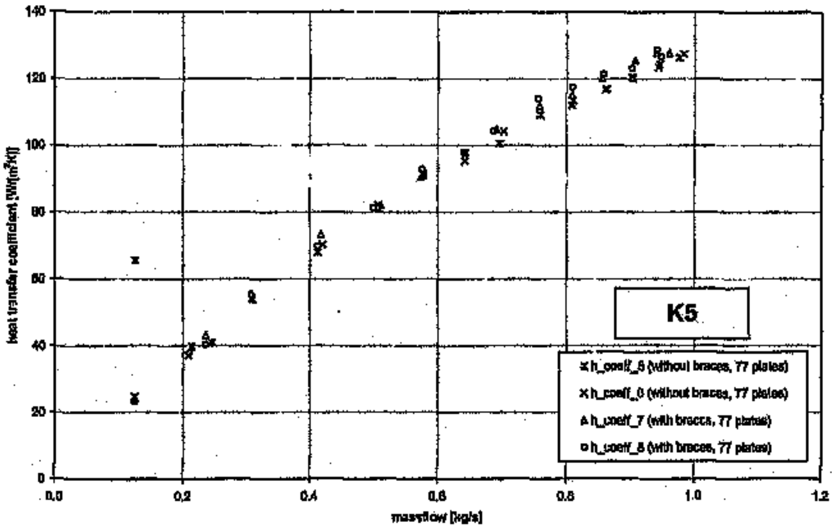

Figure 4.22: Results for the K5 pack with and without braces, heat transfer coefficient vs. mass flow

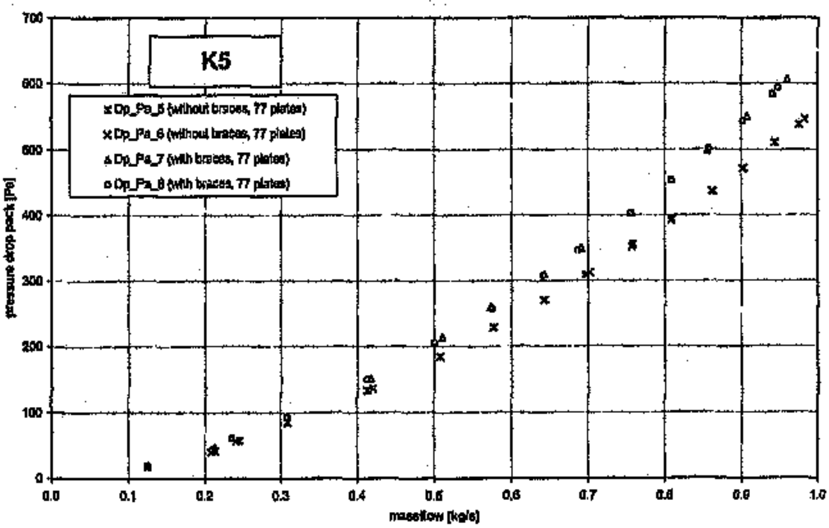

Figure 4.23: Results for the K5 pack with and without braces, pressure drop across pack vs. mass flow

Figure 4.22 shows some scatter of test data. It is not clear if there is an influence on the heat transfer because of the braces or not. However, the results with braces seem slightly higher than without braces.

The influence on the pressure drop across the pack is obvious from the graphs. At 1.0 kg/s the pressure drop with braces is 55 Pa higher than without braces.

4.1.8 Profile K6

The K6 profile also belongs to the family of the K-profiles. The height of the notched plate is 6 mm, including the plate thickness of 0.5 mm. The undulated plate is the same as those for the previously discussed packs.

Table 4.9: Geometry data of the K6 pack (2 plates less than the standard number of plates, 300 mm x 300 mm x 500 mm)

Profile type	hydr. Ø [mm]	A_{cross} [m^2]	A_{heat} [m^2]	mass [kg]	no of plates	undul. form
K6	6.13	1.24E-02	24.81	45.7	67	W-shape

4.1.8.1 Influence of the braces

For the K6 profile type one pack has been tested in the thermal test section, six times with flat braces and twice without braces. The following graph shows that the heat transfer results have a relatively wide spread for the 6 different test runs. This spread is wider than that for any of the other profiles. However, the pressure drop does not show this behaviour. The test runs show lower pressure drops for the pack without braces than for packs with braces, as expected.

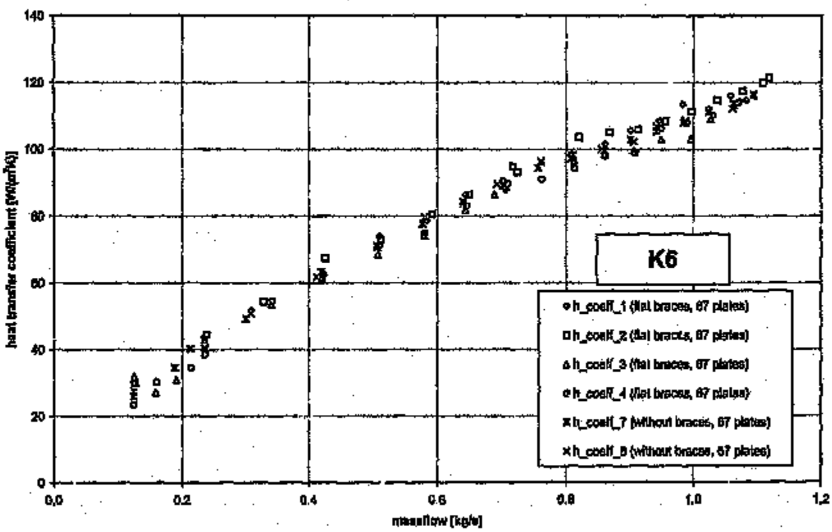

Figure 4.24: Results for the K6 pack with and without braces, heat transfer coefficient vs. mass flow

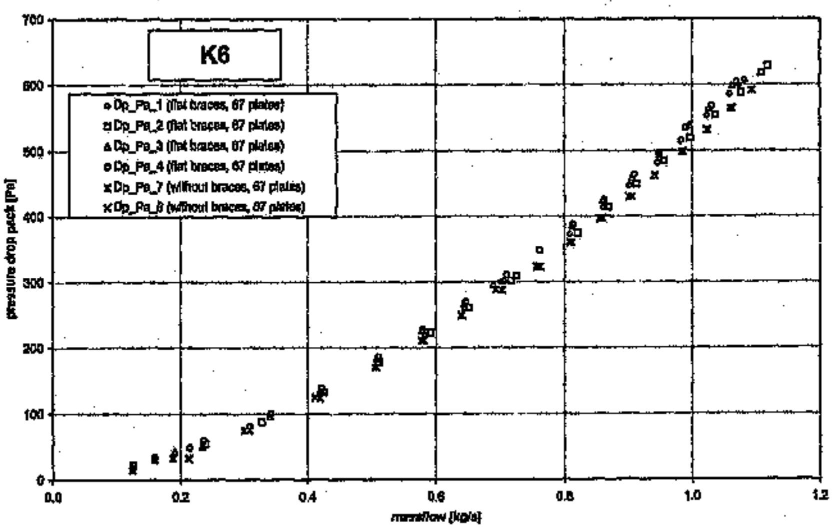

Figure 4.25: Results for the K6 pack with and without braces, pressure drop across pack vs. mass flow

Figure 4.24 and Figure 4.25 present the thermal and hydraulic results of the K6 test pack. As mentioned earlier there is some scatter of the heat transfer coefficients. This explains why there is no clearly defined influence due to the presence of braces. The results of the pressure drop show however a difference of 30 Pa at a mass flow rates of 1 kg/s.

4.1.9 Profile K8

The K8 profile is characterised by the largest rolling height of all K-profiles. This is 8 mm including 0.5 mm plate thickness (Figure 4.1). The undulated plate is again the same as in the previously discussed sections.

Table 4.10: Geometry data of the standard K8 pack
(300 mm x 300 mm x 500 mm)

Profile type	hydr. Ø [mm]	A_{cross} [m²]	A_{heat} [m²]	mass [kg]	no of plates	undul. form
K8	7.95	9.75E-03	19.5	37.92	55	W-shape

4.1.9.1 Influence of the braces

The test pack has been tested twice with braces and twice without braces. The graph (Figure 4.26) indicates that the K8 profile does not show any influence of the braces on the heat transfer coefficient. All four test runs coincide.

However, Figure 4.27 shows the same pressure drop behaviour as profile types mentioned before. The pressure drop across the pack is 30 Pa higher with braces than without braces at a mass flow rate of 1.0 kg/s.

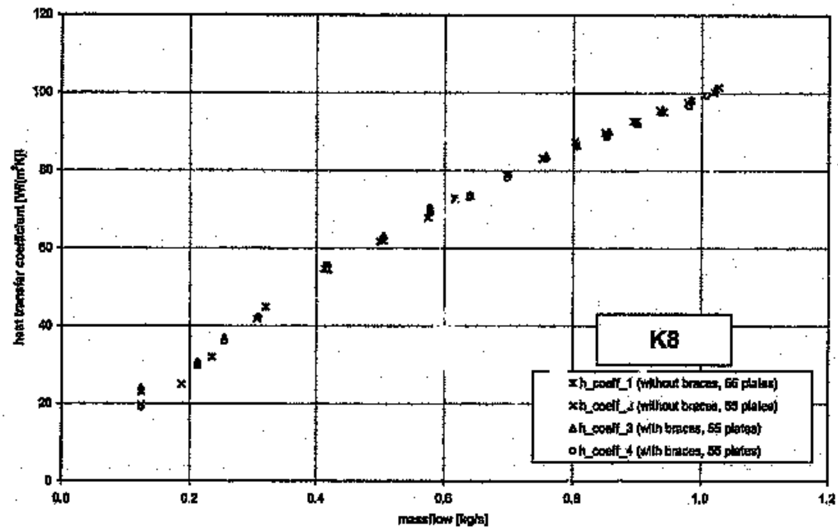

Figure 4.26: Results for the K8 pack with and without braces,
heat transfer coefficient vs. mass flow

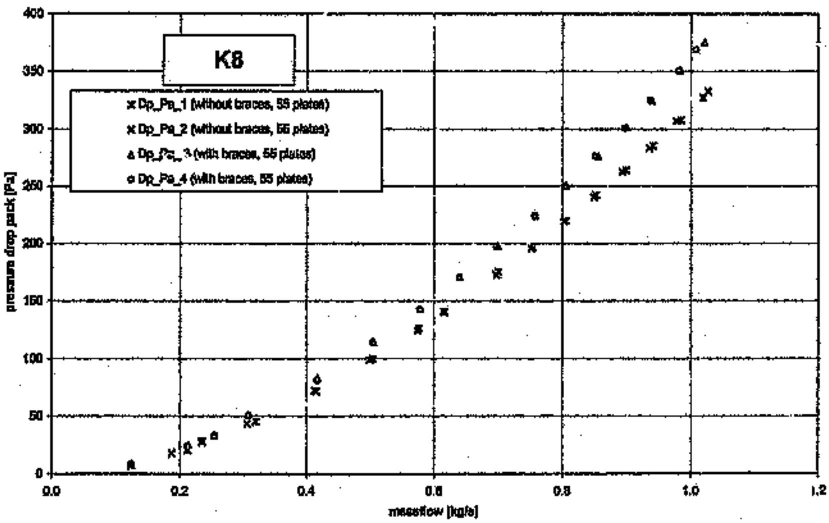

Figure 4.27: Results for the K8 pack with and without braces,
pressure drop across pack vs. mass flow

4.1.10 Profile K6G

The K6G profile consists of the K6 notched plate and a flat counter plate instead of an undulated one (Figure 4.1). The flat counter plate makes this profile type less susceptible to fouling and blockage. On the other hand this profile type has a low heat transfer performance due to the lack of turbulences caused by an undulated plate.

Table 4.11: Geometry data of the standard K6G pack (300 mm x 300 mm x 500 mm)

Profile type	hydr. Ø [mm]	A_{cross} [m^2]	A_{heat} [m^2]	mass [kg]	no of plates	undul. form
K6G	4.34	1.59E-02	31.73	60.47	89	flat

4.1.10.1 Influence of the braces

The following graphs (Figure 4.28 and Figure 4.29) show the test results of the K6G profile. The heat transfer results do not conform with the results from the previous mentioned profiles where the heat transfer coefficient with braces was either higher or equal to profile types without braces. This profile has a slightly higher heat transfer coefficient without braces even when the pressure drop with braces is higher than without braces. To prove the validity of these results all the test runs were repeated for two packs of this type of profile. All test runs show the same results, i.e. the heat transfer coefficient for the K6G profile without braces is higher than with braces.

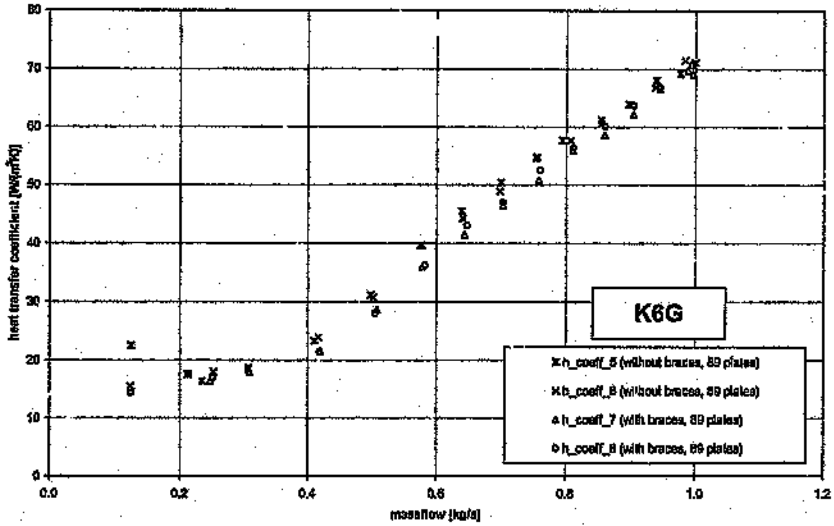

Figure 4.28: Results for the K6G pack with and without braces, heat transfer coefficient vs. mass flow

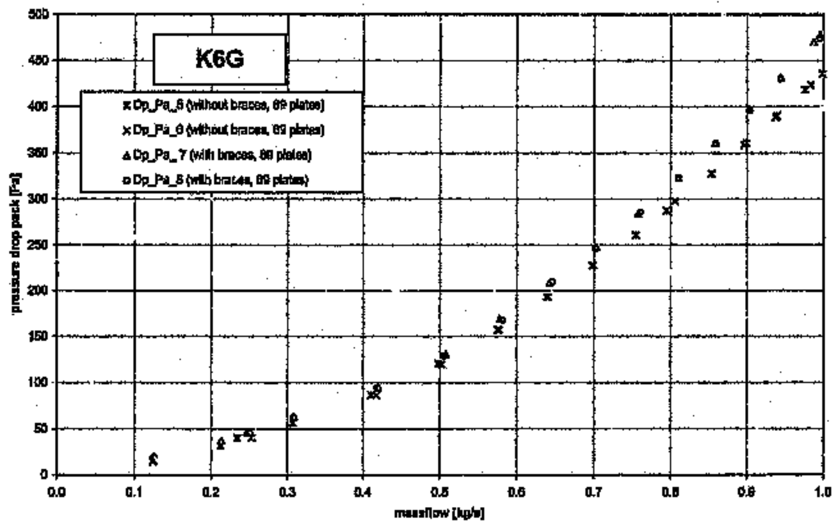

Figure 4.29: Results for the K6G pack with and without braces, pressure drop across pack vs. mass flow

4.1.11 Profile K8G

The K8G profile type consists of a 8 mm high notched K-profile and a flat counter plate, similar to the K6G profile. The purpose of testing this pack was to check whether this profile also has inconsistent heat transfer behaviour with the braces similar to the K6G profile. The K8G profile is the closest profile to the K6G profile. Both types have a flat counter plate.

Table 4.12: Geometry data of the standard K8G pack
(300 mm x 300 mm x 500 mm)

Profile type	hydr. Ø [mm]	A_{cross} [m²]	A_{heat} [m²]	mass [kg]	no of plates	undul. form
K8G	6.17	1.23E-03	24.6	46.67	69	flat

4.1.11.1 Influence of the braces

The same pack of the K8G profile was tested twice with braces and twice without braces. The results are shown in Figure 4.30 and Figure 4.31.

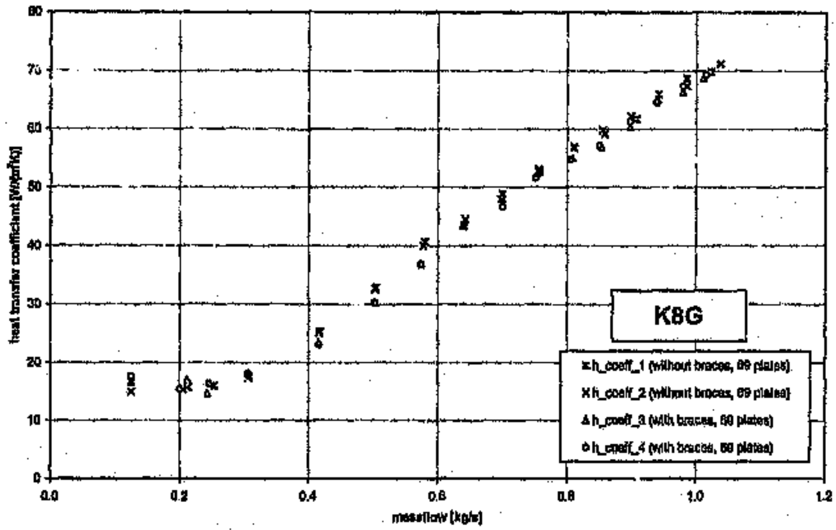

Figure 4.30: Results for the K8G pack with and without braces, heat transfer coefficient vs. mass flow

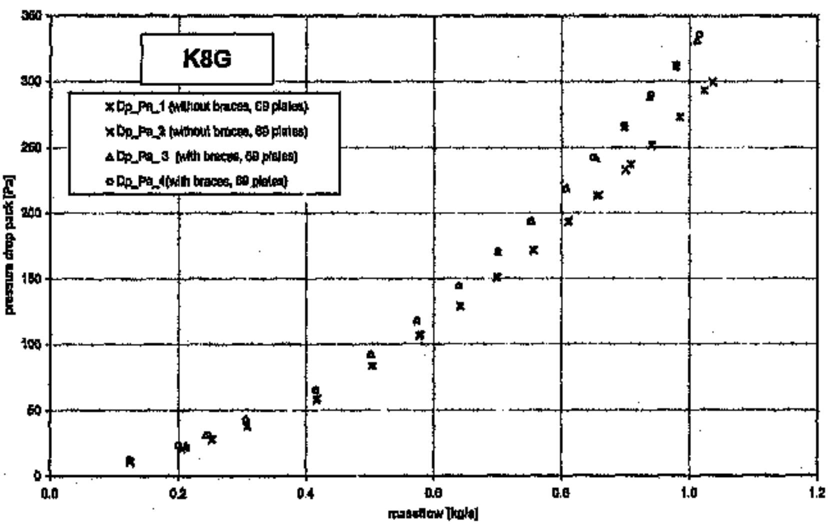

Figure 4.31: Results for the K8G pack with and without braces, pressure drop across pack vs. mass flow

As can be seen the K8G does not show the same behaviour concerning the heat transfer coefficient as the K6G profile. The heat transfer coefficient of the K8G profile is the same for a pack with and one without braces. The results of the pressure drop are like expected. The pack with braces has a higher pressure drop than the pack without braces. The difference at 1 kg/s is 40 Pa.

4.2 Special profile: "Cheese Grater"

The "Cheese Grater" profile is a special profile, which is not used in ESKOM air pre-heaters. The name of this profile describes the plates. There are no undulated and notched plates, all plates look the same. Semi-circular tapered notches are punched into all plates in two different sizes. The holes are punched out towards both sides of the plates (up and down). The photographs in Figure 4.32 - Figure 4.35 show the "Cheese Grater" profile.

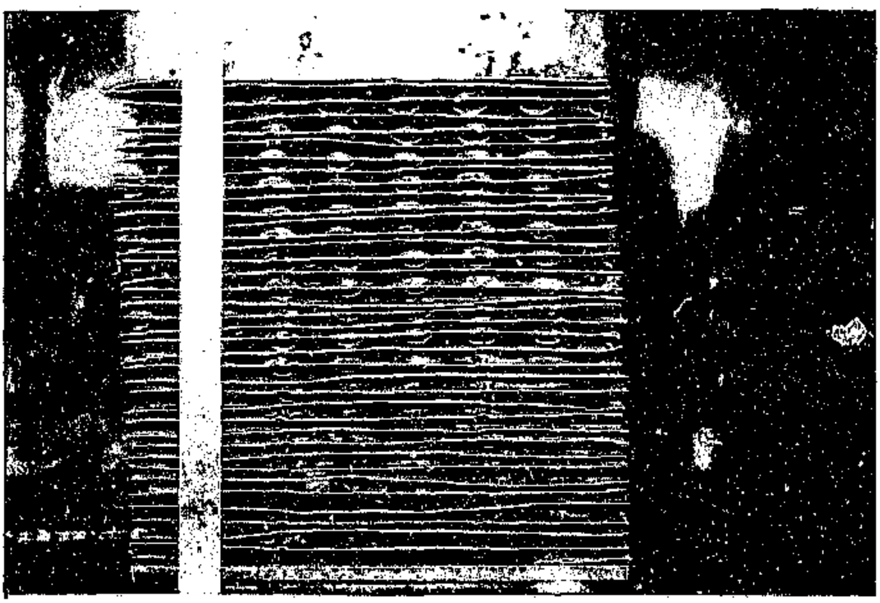

Figure 4.32: "Cheese Grater" profile, photograph in flow direction

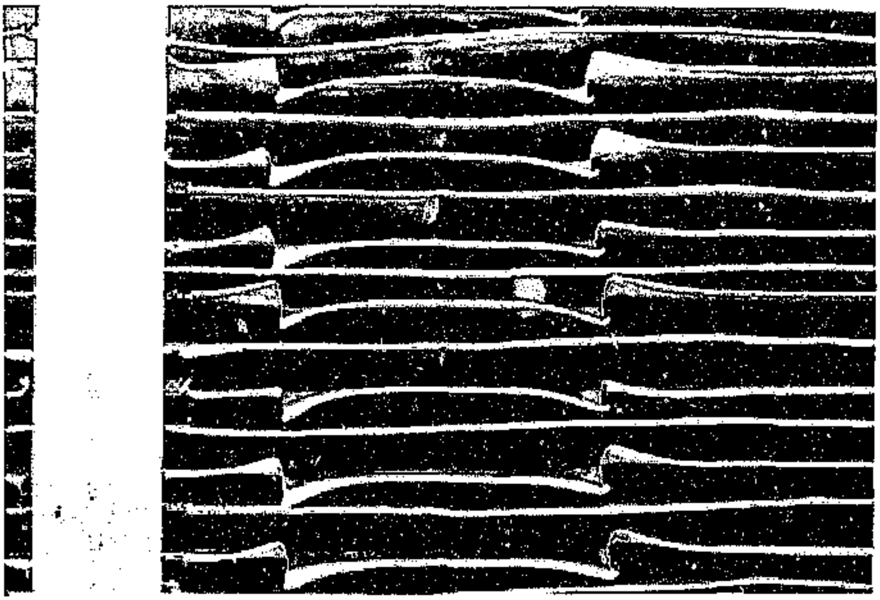

Figure 4.33: "Cheese Grater", photograph from the side

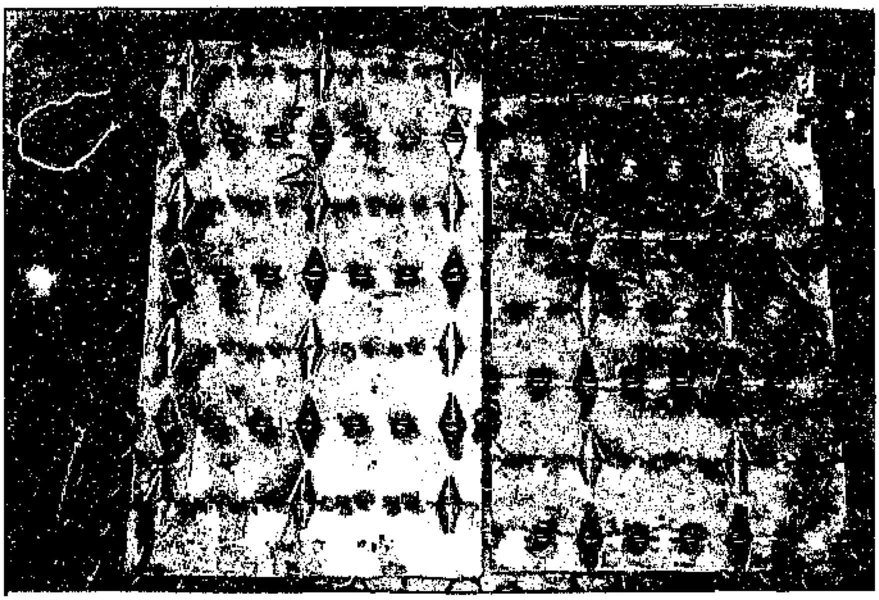

Figure 4.34: "Cheese Grater", photographs of 2 plates

Figure 4.35: "Cheese Grater", detail photograph of the punchings

Table 4.13: Geometry data of the standard "Cheese Grater" pack
(300 mm x 300 mm x 500 mm, plate thickness 0.7 mm)

Profile type	hydr. Ø [mm]	A_{cross} [m²]	A_{heat} [m²]	mass [kg]	no of plates	undul. form
Chgr	13.9	7.98E-03	11.44	32.5	37	-

The following figures (Figure 4.36 and Figure 4.37) show the results from the TTF.

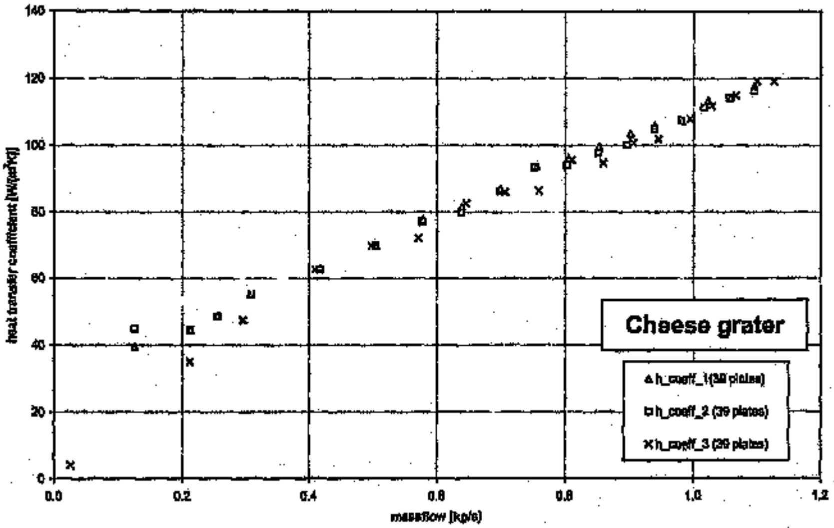

Figure 4.36: Results for the "Cheese Grater" pack, heat transfer coefficient vs. mass flow

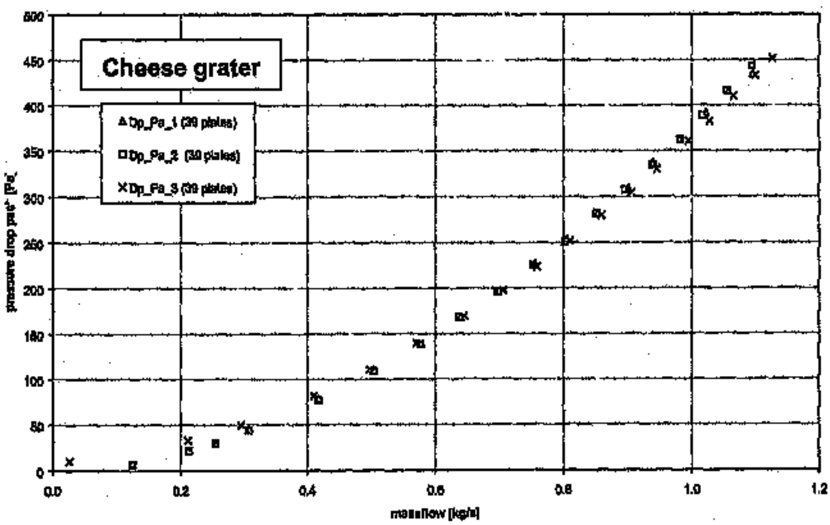

Figure 4.37: Results for the "Cheese Grater" pack, pressure drop across pack vs. mass flow

It is immediately apparent that this profile has a high heat transfer coefficient and a relatively low pressure drop. The following section shows comparisons with commonly used profile types.

4.3 Summary of the test results

The following figures (Figure 4.38 and Figure 4.39) show a comparison of the thermal and hydraulic test results of all previously discussed packs (without braces).

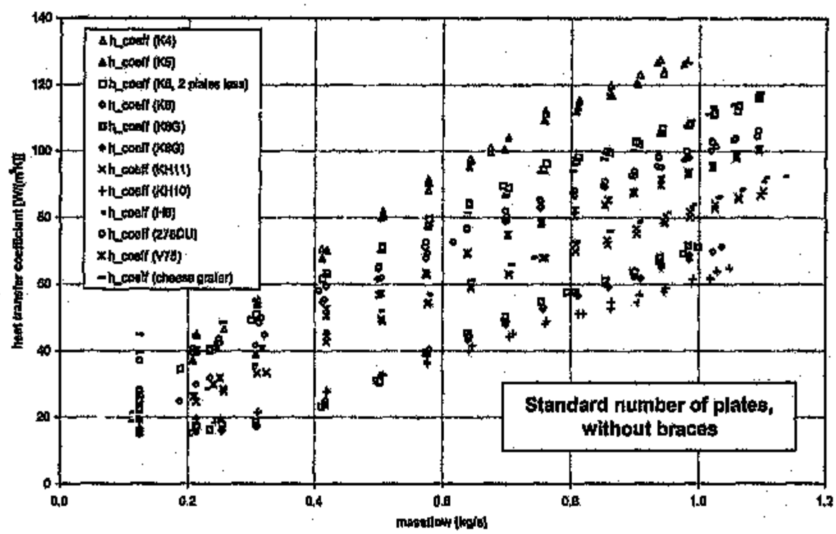

Figure 4.38: Results for different profiles of air heater packs,
heat transfer coefficient vs. mass flow

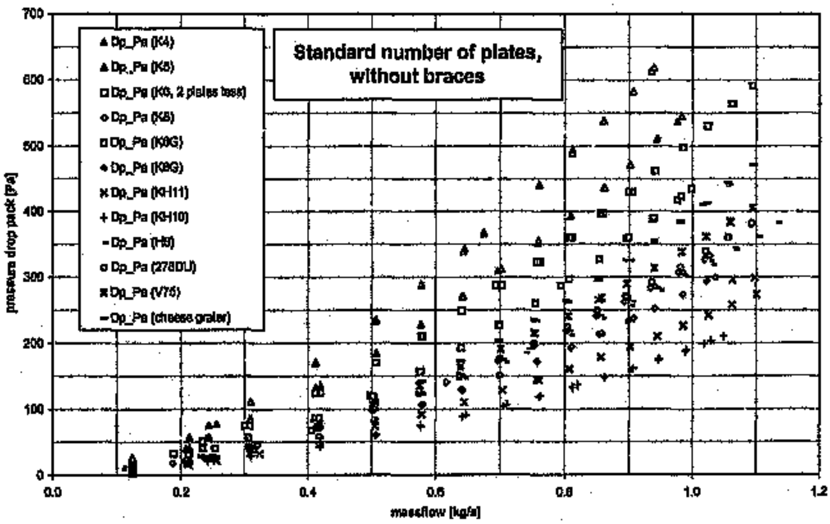

Figure 4.39: Results for different profiles of air heater packs, pressure drop across pack vs. mass flow

As expected, the K4 and the K5 profiles have the highest heat transfer coefficients because they are the smallest profiles (highest plate packing densities). The "Cheese Grater" profile and the K6 profile are also characterised by a high heat transfer value. The rest of the profiles are arranged approximately in order of their hydraulic diameters. The profiles with a flat counter plate have a significantly lower heat transfer coefficient than profiles with an undulated counter plate. The undulations produce additional turbulence which increase the heat transfer.

It is of interest that the 278DU profile has a notably higher heat transfer coefficient than the KH11. The difference between these two plates is that the 278DU profile has additional undulations on the flat part of the notched plate.

The graph presenting the pressure drop across the packs (Figure 4.39) shows the sequence of the plate types in reverse order to that of the heat transfer coefficients (Figure 4.38). This is to be expected since the profiles with a high heat transfer performance caused by additional turbulence have a higher pressure drop.

Another point of interest is that the "Cheese Grater" profile, which has nearly the same heat transfer coefficient as the K6 profile, has a much lower pressure drop. Although this would seem encouraging, it should be noted that this new profile has less than half of the specific heat transfer area of the K6 ("Cheese Grater" = 254.22 m^2/m^3, K6 = 551.33 m^2/m^3). A heat exchanger designed with the "Cheese Grater" profile would therefore have to be twice the size of one containing the K6 profile to transfer the same amount of heat energy.

The 278DU profile also shows some interesting results. This profile has a relatively high heat transfer coefficient and a relatively low pressure drop although the heat transfer area is relatively high (278DU = 346.22 m^2/m^3). This profile is the only one of which the height of the undulated plate is 3.5 mm instead of 2.5 mm. It is possible that this positively influences the overall performance.

Looking at the pressure drop it is interesting that the K4 profile has a higher pressure drop than the K5, since their heat transfer coefficients are the same.

From the graphs with and without braces as discussed previously it can be seen that all profiles show a higher pressure drop with braces than without braces. Due to the increased material area at the entrance and the exit of the pack there is a higher contraction and expansion of the flow. This causes additional turbulence. The influence of the braces on the heat transfer coefficient is not clear. It would be expected that due to the higher pressure drop the heat transfer also increases. However, the heat transfer results of the other profiles vary only within the measurement uncertainty. It is therefore difficult to make any conclusions.

4.4 Literature comparison

There are not many literature references which can be used to compare the present results with others. Kays and London [3] tested many different geometries like tubes, grids, perforated plates and corrugated channels. They plotted their results in Colburn- and Friction-factor vs. Reynolds-number diagrams. The Kays and London profiles, which are most similar to ESKOM profiles have a wavy notched plate and a flat counter plate. ESKOM profiles which can be compared with these Kays and London profiles are the K6G, K8G and KH10. These three profile types have a flat counter plate. Figure 4.40 shows a comparison of three Kays and London and three ESKOM profiles, where the geometry matches best. The Kays and London (K&L) profile types are characterised by their hydraulic diameter (d_h) and the profile height (h). The geometry of the ESKOM profiles can be seen in Table 4.5, Table 4.11 and Table 4.12.

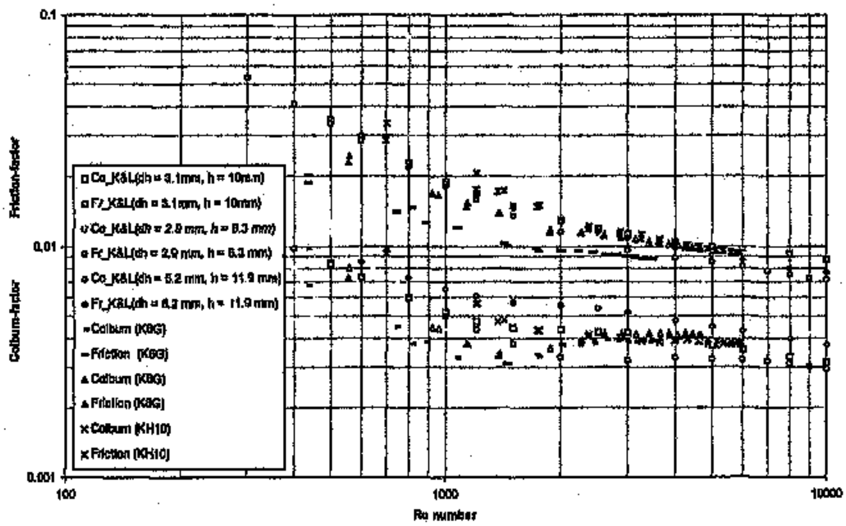

Figure 4.40: Colburn- and Friction-factor vs. Reynolds-number, ESKOM and Kays and London data

The shape of these particular undulated K&L plates is wavy like the K-profiles. The difference is the pitch of the waves. K&L profiles have narrower waves, so the flow channels are smaller (hydraulic diameter smaller). Figure 4.40 shows that the heat transfer performance shows good agreement. Especially the K8G results match excellently with the K&L data (except of the transition region, 1000 < Re < 2000). The geometry of this profile is the closest to the geometry of the K&L profiles.

Migay [15] also examined profiles, which are similar to the ESKOM profiles and can be taken for comparison. He investigated the thermal and hydraulic performance of plates which are similar to the ESKOM KH11 and 278DU profiles. In his publication there are only graphs (some double logarithmic) containing experimental data like hydraulic resistance and Nusselt-number, without values in a table. This makes it impossible to obtain the experimental data for a comparison with present results. As mentioned in the literature survey, Migay gives additionally empirical equations to calculate the Nusselt-number. He gives a Nusselt-number equation which represents the thermal performance of KH11 related profiles, based on the experimental results, fluid properties and geometry (height and pitch of the profiles). According to Migay this equation is valid for Re > 2700. Figure 4.41 shows that it is also valid for smaller Reynolds-numbers. In Figure 4.41 this approximation is used to check the KH11-results from the ESKOM Thermal Test Facility. It can be seen that both the calculated curve and the experimental ESKOM-data coincide well.

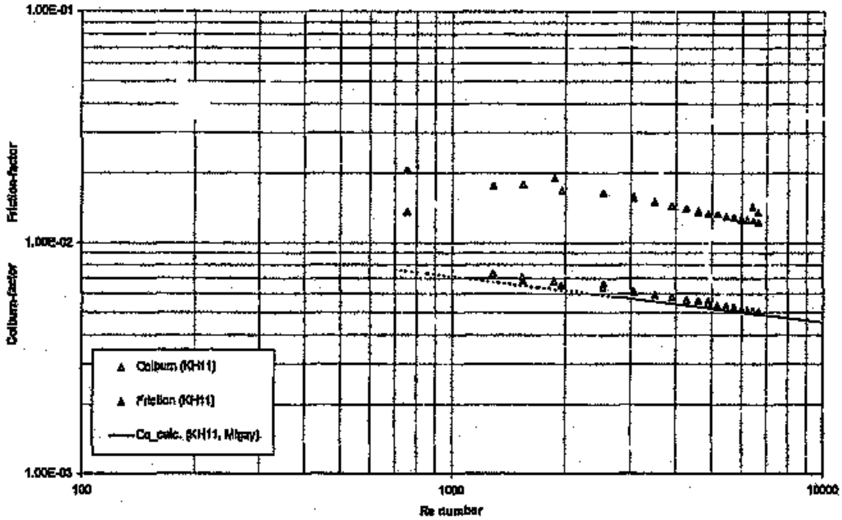

Figure 4.41: Colburn- and Friction-factor vs. Reynolds-number, ESKOM data and Migay calculation

Another possibility to check the results of the TTF is to test flat plates and compare these results with theoretical values which can be found in the literature [29]. The test pack of flat plates used for this study consisted of 30 galvanised, smooth, 0.6 mm thick plates, which are installed vertically in the test section, without any additional disturbance. Figure 4.42 and Figure 4.43 show the experimental and the theoretical results. The calculated Nusselt-numbers and Friction-factors are obtained from the equations:

- Nusselt-number according to Dittus-Boelter:

$$Nu = 0.023 \cdot Re^{0.8} \cdot Pr^{0.4}, \tag{4.1}$$

- Nusselt-number according to Gnielinski, including the Friction-factor of smooth tubes:

$$Nu = \frac{\left[F_{smooth} / 8\right]\left(Re - 1000\right) Pr}{1 + 12.7\left[\left(F_{smooth}\right) / 8\right]^{1/2}\left(Pr^{2/3} - 1\right)} \tag{4.2}$$

- Nusselt-number according to Gnielinski, including the Friction-factor of the actual measurements

$$Nu = \frac{\left[F_{flat\ plates} / 8\right]\left(Re - 1000\right) Pr}{1 + 12.7\left[\left(F_{flat\ plates}\right) / 8\right]^{1/2}\left(Pr^{2/3} - 1\right)} \tag{4.3}$$

- Friction-factor for laminar flow according to Hagen-Poiseuille

$$F = \frac{64}{Re} \tag{4.4}$$

- Friction-factor for turbulent flow according to Blasius

$$F = 0.316 \cdot Re^{-1/4} \tag{4.5}$$

All the above mentioned equations were found in Incropera and DeWitt [29].

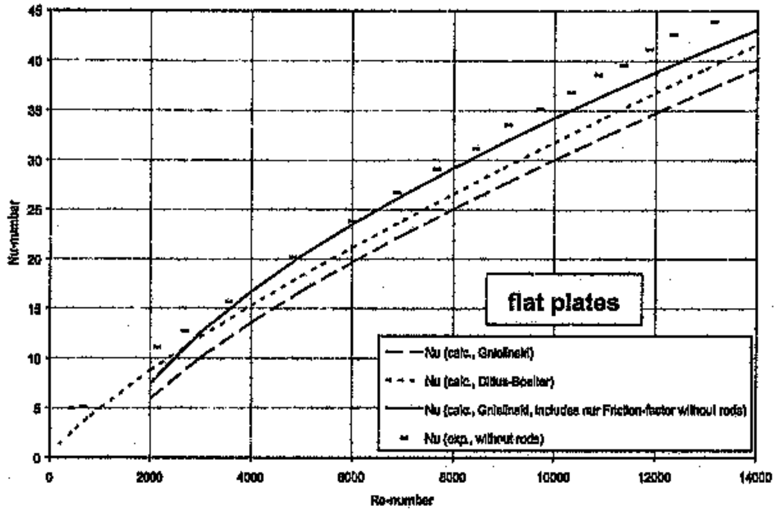

Figure 4.42: Nusselt-number vs. Reynolds-number for flat plates, experimental and calculated values [29]

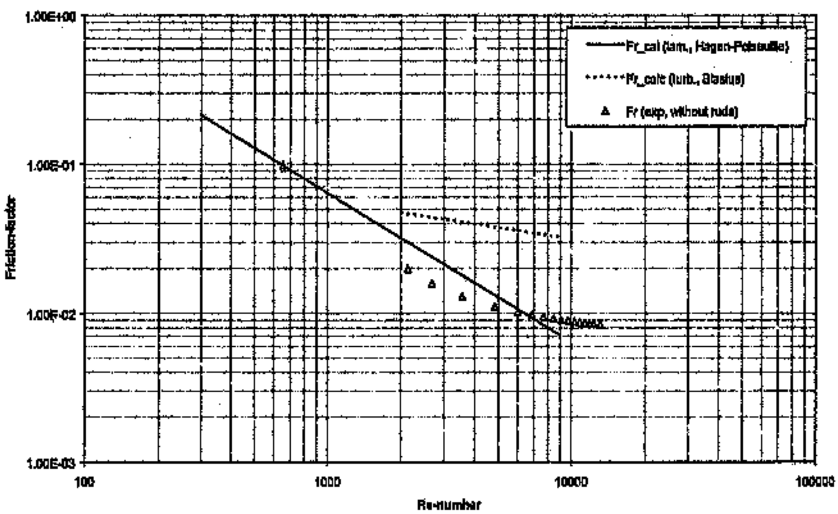

Figure 4.43: Friction-factor for flat plates, experimental and calculated values [29]

The calculated Nusselt-number, derived from Equation (4.3), agrees exactly with the experimental Nusselt-numbers in the Reynolds-region between 3000 and 8000. For higher Reynolds-number the difference between the calculated and the measured Nusselt-number varies about 10 %.

Looking only at the experimental data of the Friction-factor, it is remarkable that the transition from laminar to turbulent only occurs at Re ≈ 7000. This leads to the conclusion that the equation for tubular flow at turbulent conditions is not applicable. In Figure 4.43 it can be seen that the equation for laminar flow (Equation 4.4) best describes the experimental results.

4.5 Regression of test results

To calculate the heat transfer and the pressure drop from the mass flow, equations must be derived which represent the aforementioned results. It was chosen to use regression equations for the Colburn- and the Friction- factor of the following form:

- Colburn-factor:

$$Co = A_1 \cdot Re^{B_1} \tag{4.6}$$

- Friction-factor:

$$F = A_2 \cdot Re^{B_2} \tag{4.7}$$

The graphs and the relevant coefficients for the most commonly used profiles are following.

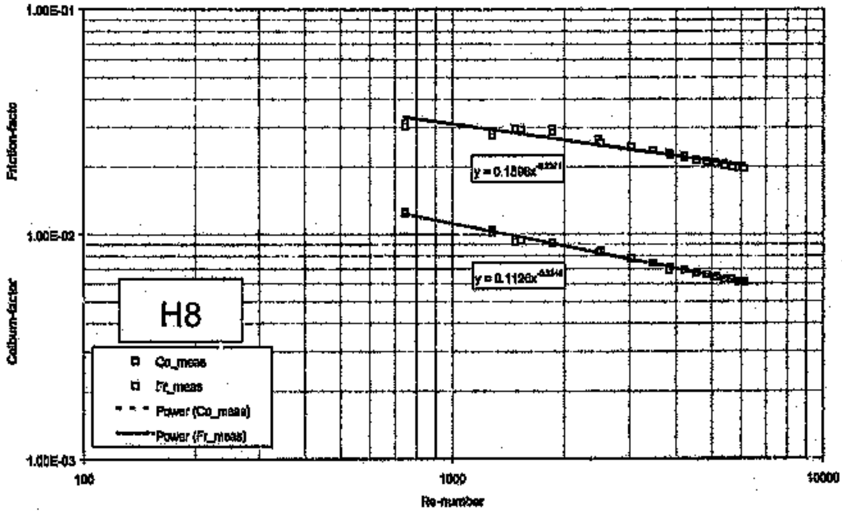

Figure 4.44: Colburn- and Friction-factor vs. Reynolds-number, H8 profile

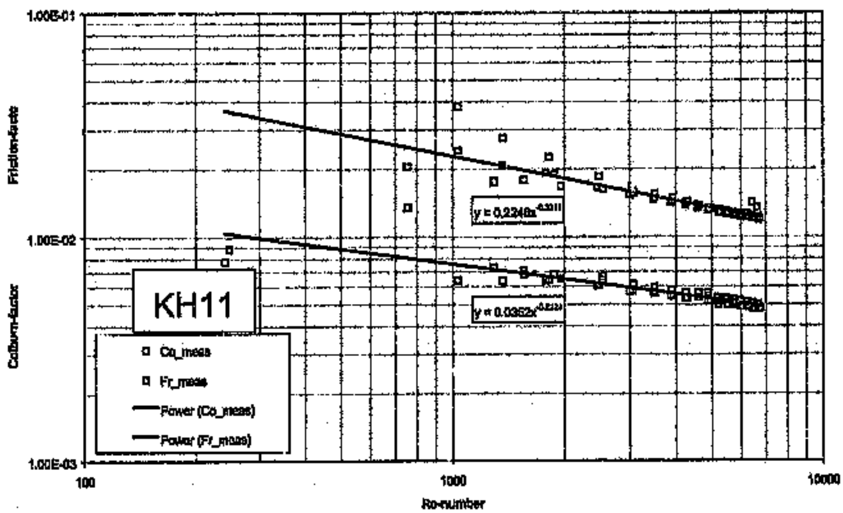

Figure 4.45: Colburn- and Friction-factor vs. Reynolds-number, KH11 profile

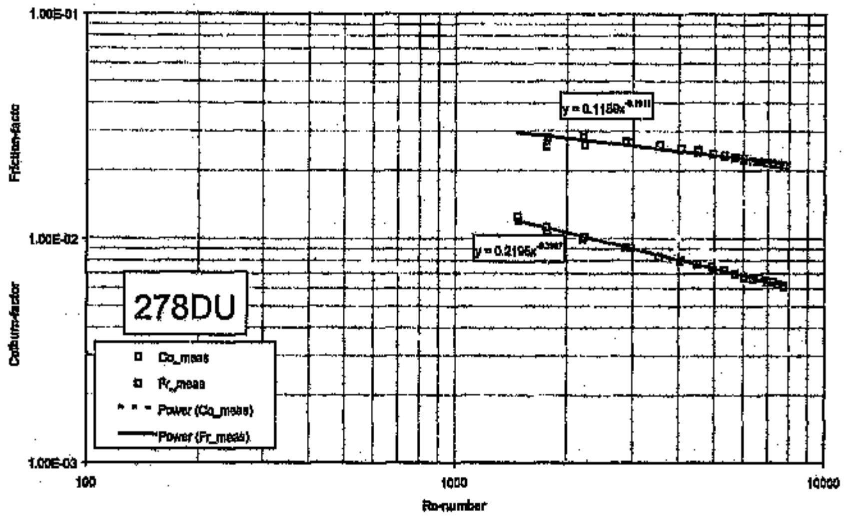

Figure 4.46: Colburn- and Friction-factor vs. Reynolds-number, 278DU profile

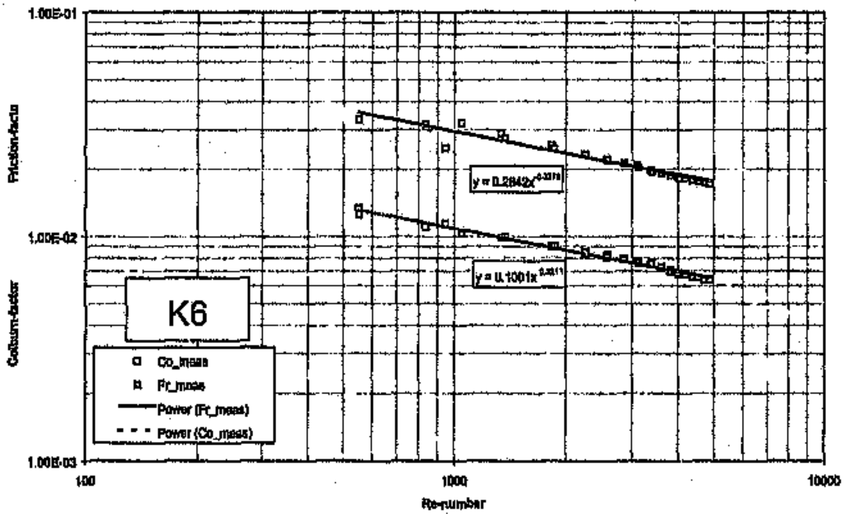

Figure 4.47: Colburn- and Friction-factor vs. Reynolds-number, K6 profile

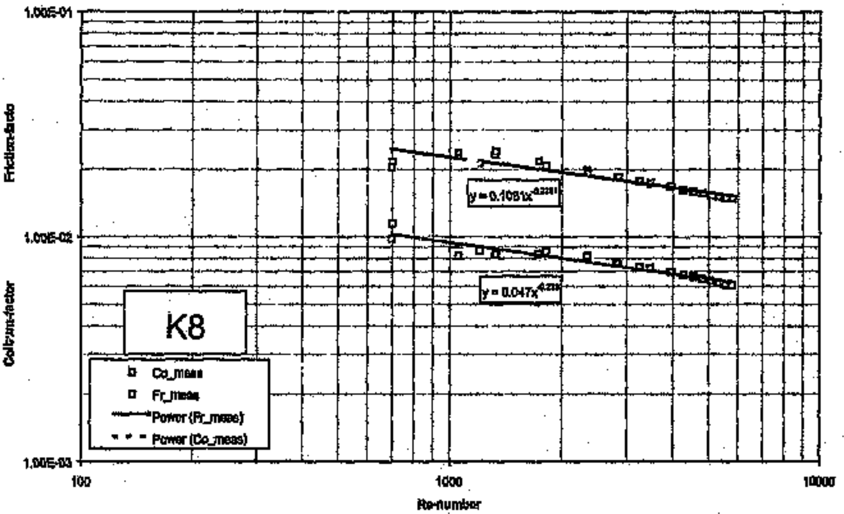

Figure 4.48: Colburn- and Friction-factor vs. Reynolds-number, K8 profile

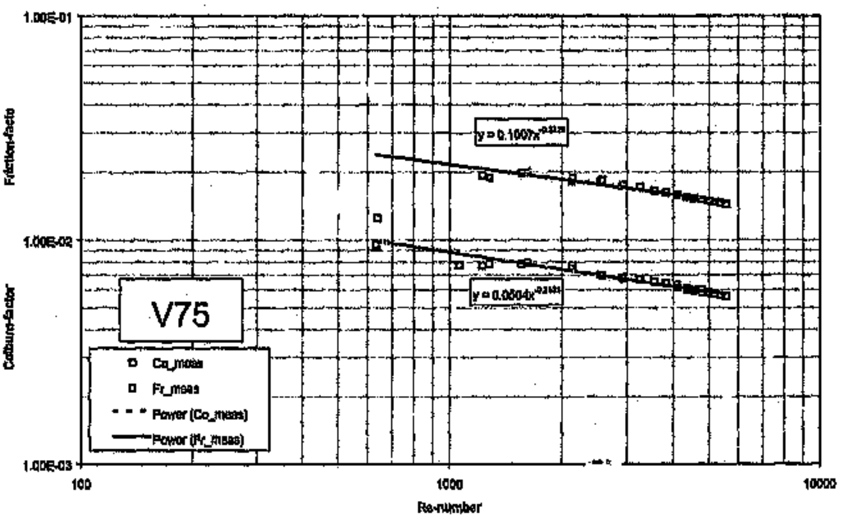

Figure 4.49: Colburn- and Friction-factor vs. Reynolds-number, V75 profile

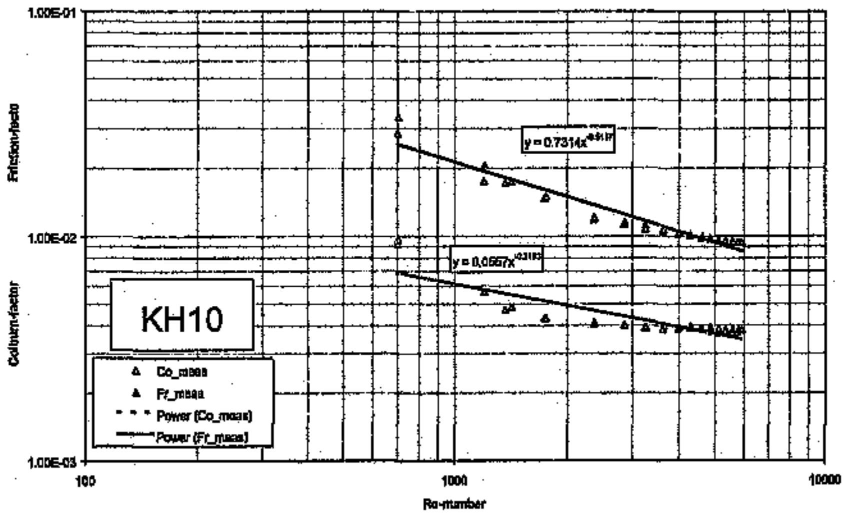

Figure 4.50: Colburn- and Friction-factor vs. Reynolds-number,
KH10 profile

These diagrams show that the experimental results are well represented by one single regression curve, both for the Colburn- as well as for the Friction-factor. It is not necessary to distinguish between different flow regions, like laminar, turbulent or transition because all results fit well to one straight line on a double-logarithm diagram. Only the KH10 profile shows a slightly different behaviour. There is a changing of the linearity in the Colburn- and in the Friction-factor at Re ≈ 1300. To represent these test results two separate curves, one for the laminar and one for the turbulent region, would be better. But to avoid inconsistency this profile type is included such that only one function for the whole Reynolds-number range is derived.

The Reynolds-number range for which the regression equations are valid varies for each profile. It depends firstly on the tested region (minimum and maximum mass flow) and the hydraulic diameters of the different profiles. Secondly, it also depends on the measuring uncertainties, which made it necessary to eliminate some of the test points, especially for the Friction-factor. The curves in the graphs show the valid Reynolds-number region.

These coefficients for the Colburn- and Friction-factor can be used as input data in the air heater performance prediction model developed by Habbitts [1] in parallel with the present project.

4.6 Conclusions of testing uneroded plates

1. The Rothemuehle (RM) H8 test pack confirmed that within the measurement uncertainties, the thermal test facilities in Germany and at TRI give matching results.

2. The RM H8 pack and the Howden Power H8 pack have essentially identical hydraulic and thermal performance

3. The results of testing three different H8 packs show that there is no influence of individual packs on test results. Other pack types have not been tested on this influence.

4. The following table shows the influence of braces on the pressure drop and the heat transfer coefficient for all tested profile types so far.

Table 4.14: Influence of braces on the pressure drop of different profiles

Profile	Pressure loss	Heat transfer coefficient
H8	$\Delta p_{without} < \Delta p_{with}$ (30 Pa)	$h_{without} < h_{with}$
278DU	$\Delta p_{without} < \Delta p_{with}$ (35 Pa)	$h_{without} < h_{with}$
KH11	$\Delta p_{without} < \Delta p_{with}$ (30 Pa)	$h_{without} \leq h_{with}$
KH10	$\Delta p_{without} < \Delta p_{with}$ (30 Pa)	$h_{without} \approx h_{with}$
V75	$\Delta p_{without} < \Delta p_{with}$ (35 Pa)	$h_{without} \approx h_{with}$
K4	$\Delta p_{without} < \Delta p_{with}$ (40 Pa)	$h_{without} < h_{with}$
K5	$\Delta p_{without} < \Delta p_{with}$ (55 Pa)	$h_{without} < h_{with}$
K6	$\Delta p_{without} < \Delta p_{with}$ (30 Pa)	$h_{without} \approx h_{with}$
K8	$\Delta p_{without} < \Delta p_{with}$ (30 Pa)	$h_{without} \approx h_{with}$
K6G	$\Delta p_{without} < \Delta p_{with}$ (30 Pa)	$h_{without} \geq h_{with}$
K8G	$\Delta p_{without} < \Delta p_{with}$ (40 Pa)	$h_{without} \approx h_{with}$

It is seen that for every profile the pressure loss across the pack with braces is higher than without braces. The difference lies between 30 Pa and 40 Pa for a mass flow of 1 kg/s (except the K5 profile). A theoretical sample calculation of additional pressure loss caused by the presence of braces can be found in Appendix I.

As can be seen in this table the influence of the braces on the heat transfer coefficient is not the same for every profile. For some profiles the heat transfer coefficient with braces is higher, as would be expected, and for other profiles .e heat transfer coefficient is the same for packs with and without braces. It appears that for some profiles this increase in pressure drop is not high enough to effect the heat transfer coefficient. The results for the test pack K6G need further investigation.

7. The table below shows the influence of the number of plates on different profiles

Table 4.15: Influence of the number of plates for different profile types

Profile	Pressure loss	Heat transfer coefficient
H8	$\Delta p_{67} \geq \Delta p_{55}$	$h_{57} \geq h_{55}$
KH11	$\Delta p_{63} \geq \Delta p_{61}$	$h_{63} \approx h_{61}$
V75	$\Delta p_{61} \approx \Delta p_{69}$	$h_{61} \leq h_{69}$

These results also do not show any uniformity between the different profile types. It seems that there is a slight increase of the pressure drop caused by an additional pair of plates. This pressure drop increase is not high enough to effect the heat transfer coefficient. A complete summary of all test results can be found in the Appendix D.

8. The profile 278DU shows high heat transfer performance and relatively low pressure drop.

9. Both Friction-factor versus Reynolds-number and Colburn-factor versus Reynolds-number data can be correlated by a power function of the form $y = a \cdot x^b$, where a and b are constants.

5. Erosion

This chapter contains background information on erosion, including erosion in power stations. The chapter also points out the special situation with South African coal and why investigations on erosion are very important for the South African power generating industry.

5.1. Appearance of erosion

Wear on materials can be caused by either abrasion or erosion. The wear caused by sliding particles is known as abrasion and wear resulting from the particle impaction is usually referred to as erosion. The particle properties that influence the rate of abrasion and erosion wear include the size, density, shape, hardness (measured by Vickers or Knoop microindentation techniques), and cohesive strength to resist fracture when stressed by wear-causing forces [19].

The principle function of wear-causing particles in abrasion and erosion is to transmit relatively large quantities of energy to small areas on the surface. The particle energy is dissipated as heat and rebound motion and is partly used for particle fracture. A portion, however, goes to deform and subsequently to remove the surface layer of the target material. The ash particles in the air stream possess potential and kinetic energy. When they contact the surface of the material following energy balance can be made [19]:

$$E_{particle} = E_r + E_d + E_f + E_h + E_s \tag{5.1}$$

where is: E_r = remaining kinetic and potential energy of the rebounding particles
E_d = deformation energy of the particle
E_f = fracture energy of the particle
E_h = energy amount dissipated by heat
E_s = energy transferred to the impacted material

Some of the erosion-influencing parameters will be discussed in the following passages.

5.2. Coal properties

The substance of the coal is soft and of low strength. Only the presence of abrasive mineral species create the wear-causing properties of the coal. The most common abrasives in ash are the silica (SiO_2), alumina (Al_2O_3) and the ferrous oxides (Fe_2O_3). The quartz content can be calculated from the SiO_2 and Al_2O_3 content of ash in percentage weight. The pyrite content depends on the sulphur content of the coal in percentage weight [19]. Raask [20] concluded, that the erosive characteristics of the fly ash are directly related to their quartz and pyrite content.

Raask [19] defines an abrasion-index and a wear-propensity of coal to evaluate the erosion behaviour of different coal types. These values are a function of the sulphur and ash content of the coal, the silica (SiO_2) and the alumina (Al_2O_3) content of the ash (all in percentage weight), and the caloric value (MJ/kg) of the coal.

Table 5.1 shows coal analyses for several South African power stations [19, 24, 25, 30]. It can be seen that all the coals have especially high ash, silica and aluminium oxide contents. The abrasion-index (AI) and the wear-propensity (WP) are calculated, where sufficient data is available, in the last two columns.

Table 5.1: Coal and ash properties of several South African power stations

		coal											ashed coal												calculations			
power		C.V.	H_2O	Ash	V.M.	F.C.	tot. S	Carb.	Hydro.	Nitro.	Co_2	Oxy.	SiO_2	Al_2O_3	Fe_2O_3	TiO_2	P_2O_5	CaO	MgO	Na_2O	SO_2	MnO	K_2O	Quartz	Quartz	Pyrite	AI	WP
station	source	MJ/kg	%	%	%	%	%	%	%	%	%	%	%	%	%	%	%	%	%	%	%	%	%	%	% (coal)	% (coal)		
Arnot	Boshoff	22.[illegible]	4	25	23.4	48	0.79																					
Kriel	Boshoff	21.1	4.7	26	22.3	47	0.86																			0.728		
	Raask												47.5	22.5										13.8	3.5338			
Duvha	Boshoff	22.5	2.2	27	21.8	49	0.95																			0.845		
	Raask												48.9	31										2.4	0.6576			
Kendal	Boshoff	20.2	3.2	32	22.1	43	1.03																					
Matla	Boshoff	22.5	5	22	25.2	48	0.83																			0.689		
	Raask												46.1	27.4										5	1.1			
Hendrina	Boshoff	28.8	3.5	10	31.1	55	0.59																					
	internal	21.8	8.1	24	21.9		0.72	59.5	3.02	1.3			60.6	28.4	3.95	1.6		3.7	0.04	0.35		0	0.9		4.248	0.546	9.24	11
Majuba	Boshoff	22.5	2.2	30	21.8	46	0.98																					
Matimba	Boshoff	20.6	2.8	34	27.3	37	1.13																			1.079		
	Raask												63.2	19.3										34.3	11.508			
	TRI report	19.47	1.6	36	27.6	35	1.05	48.7	3.54	0.99	1.3	7.3	64.3	22	5.7	1	0.3	3	1	0.1	2.3	0.06	1		11.124	0.975	18.7	24
Lethabo	TRI			40																								
	Raask												55.3	29.3										11.4	4.54			

Remarks:

- V.M.: volatile matter of dried coal
- F.C.: fixed carbon of dried coal
- to calculate the abrasion-index and the wear-propensity is only possible for the coal of Hendrina and Matimba Power Station, for the other Power Stations there is not sufficient data available

Besides the chemical properties of coal and ash, properties like the velocity and particle size are also important. According to Raask [19] the following values describing some particle properties for coal used in coal-combustion systems can be taken as typical.

Table 5.2: Coal features, particle size, solids burden, flow velocity, and impaction rates [19]

System	Particle size [µm] mean	max.	solids burden	velocity [m/s]	maximum impaction rates [kg/(m²s)]
fluidised-bed combustion	500	2500	500 - 750 kg/m³	1 - 3	500 - 2000
pulverised-coal pipe lines	40	150	1 - 2 kg/m³	25 - 30	25 - 50
pulverised-coal-fired boiler flue gas	25	100	10 - 20 g/m³	8 - 22	0.1 - 0.4
cyclone-fired boiler flue gas	15	50	2 - 5 g/m³	15 - 20	0.03 - 0.1
coal gas turbine	2	10	50 - 200 mg/m³	150 - 200	0.007 - 0.02

As it can be seen from the table above the size of particles entrained in gas streams in coal-fired power plants range from below 100 µm in pulverised coal-fired boilers to several millimetres in fluidised combustion beds. In the literature [19] there is disagreement concerning the relationship between particle size and wear propensity. It can either be found that the wear increases with the particle size from 5 to 50 µm and remains constant with larger particles or that the wear increases with particle sizes up to several millimetre in diameter.

The velocity of impacting particles is one of the important parameters governing erosion wear because the erosion rate is a function of velocity^n ($n = 2 - 3$). The velocity of ash laden flue gas passing the air heater is relatively low compared to other parts of the power station (usually below 15 m/s, see Table 5.2 and Section 5.3).

5.3. Erosion in air preheaters

Compared with other power station components like the boiler, superheater pipes or the turbines, the fluid velocity in the regenerative air preheater is low. This is necessary firstly to give the flue gas enough residence time to transfer the heat to the storage material and secondly to give the combustion air enough time to heat up while taking energy from the heated steel plates. Depending on the generating load of the unit, the velocity in a regenerative air preheater is between 8 and 12 m/s. This means that ash impaction erosion wear is not as severe as in other components of a power station. But when highly abrasive fuels such as high-ash bituminous coals, quartz-rich brown coals and lignites are used, erosion on heating plates is a problem because of the relatively thin plate thickness (about 0.5 mm).

In the literature [19] some recommended maximum velocities for air preheaters can be found:

Table 5.3: Recommended velocities in air preheaters for different coal types

coal characteristics	velocity
< 15 g/m3 ash burden of flue gas	max. velocity 16 m/s
15 - 40 g/m3 ash burden of flues gas	max. velocity 14 m/s
> 40 g/m3 ash burden of flue gas	max. velocity 12 m/s
German brown coal	velocity 8 - 10 m/s
If quartz content of brown-coal ash exceeds 50 % by weight or when the ash is exceptionally coarse	max. velocity 10 m/s

Vasil'ev and Dombrovskii [31] investigated experimentally the life span of heating plates and tubular heating surfaces for regenerative air preheaters. Their test section was built as a bypass to one of the actual air preheaters in the Russian Troitsk Central Power Station, which uses Ekibastuz coal. The ash of this coal is known as very abrasive. The overall test lasted 4870 hours. The velocity in the heating plates test section was 10 - 12 m/s. The average ash concentration in the flue gas was about 75 g/m³. According to the experimental data, the authors calculated the following erosion-wear life depending on the flue gas velocity:

- 8 m/s 12 to 15 years of life expectancy
- 10 m/s 5 to 8 years of life expectancy
- 12 m/s 3 to 5 years of life expectancy

It should be mentionnd that there is possibly a difference in erosion features between the two different operation techniques of regenerative air heaters, i.e. the Rothemuehle stator principle and the Ljungstroem rotor principle. Raask [19] did not distinguish between these two operating techniques when he described the erosion features in air heaters. According to von Borman [32], however, there is a difference in the erosion behaviour in the two types. He states that in the Ljungstroem air heater design, all packs are exposed to the same conditions, so that there is equal erosion potential for each pack. On the other hand the Rothemuehle type has areas of maximum erosion. These areas of maximum erosion are on the opposite side of the flue gas entrance. That does not, at first sight, make sense because the hoods are rotating so that the flue gas is distributed equally. The reason could be that the ash particles travel without changing direction (i.e. without loosing energy) to the opposite side of the entrance. Therefor they have their maximum kinetic energy when they impact the heating plates while entering the air heater. Figure 5.1 and Figure 5.2 show the different gas- and air-entries of the Ljungstroem and the Rothemuehle air-heater type.

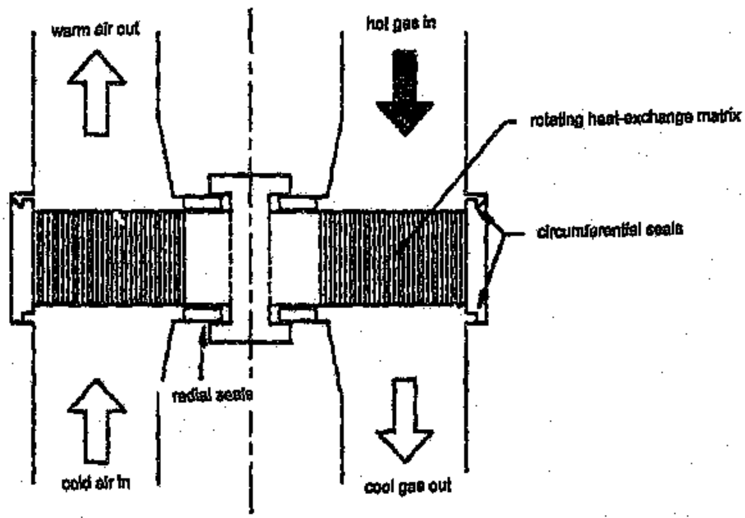

Figure 5.1: Flue-gas and air streams in the Ljungstroem air-heater type
(RM trade literature)

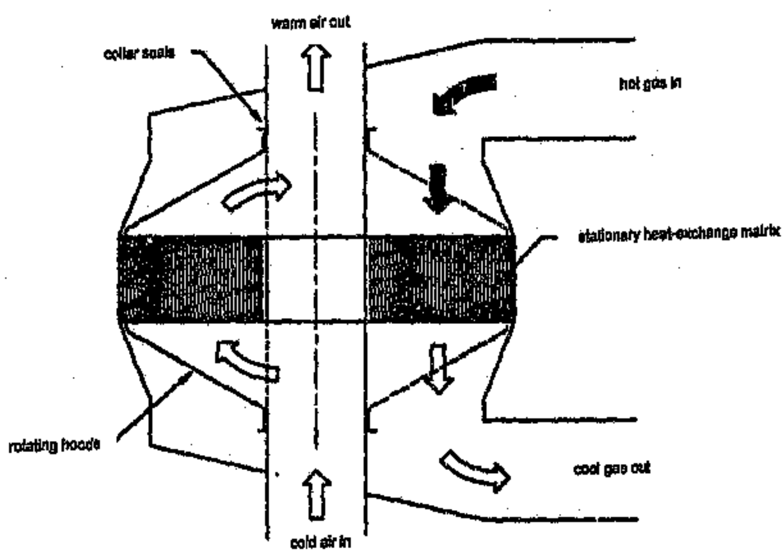

Figure 5.2: Flue-gas and air streams in the Rothemuehle air-heater type
(RM trade literature)

For verification purposes, evaluations at the Matimba Power Station (Rothemuehle type) and at the Kendal Power Station (Ljungstroem type) were carried out. The Matimba air heater had been in operation for 4.5 years and the Kendal air heater for 4 years. The investigation comprised of leading edge erosion measurements, inspection of high erosion areas and determining the difference in erosion behaviour between the Rothemuehle and the Ljungstroem air heater type. *Figure 5.3* to *Figure 5.5) show the leading edge erosion [mm]* in the different rings and cells of the air heaters. In the Rothemuehle type air pre-heater it was impossible to gain access to the packs under the hood. In the Kendal left hand side air heater a direction of erosion could be found. Arrows in Figure 5.4 indicate the direction of the leading edge erosion, which is caused by the flow direction of the ash particles carried in the flue-gas.

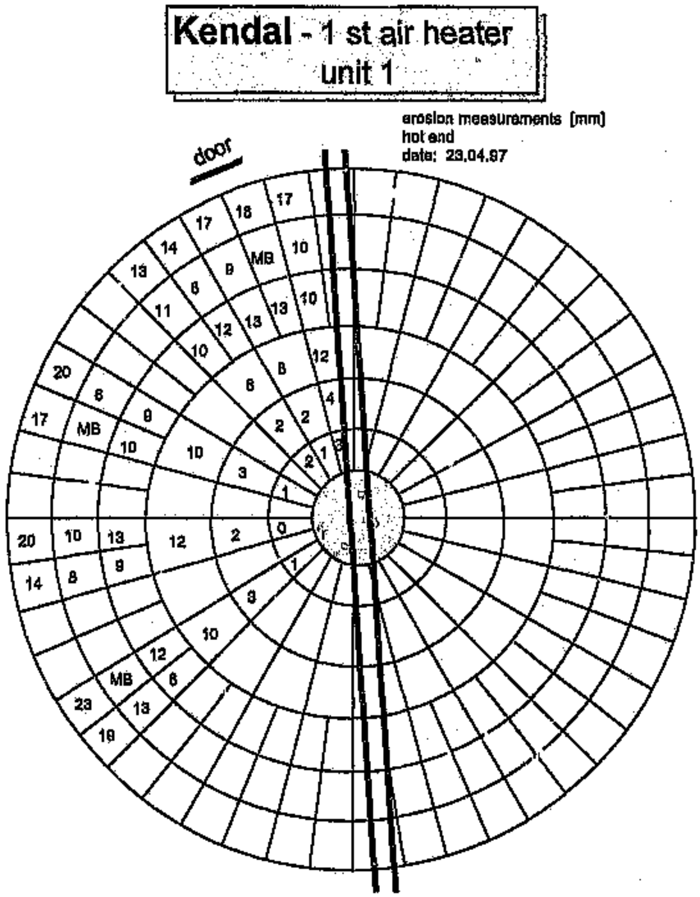

Figure 5.3: Leading edge erosion investigations at the Kendal air heater, unit 1, right hand side

In Figure 5.3 the positions of three Modified Baskets (MB, to be discussed in Chapter 6) are also indicated.

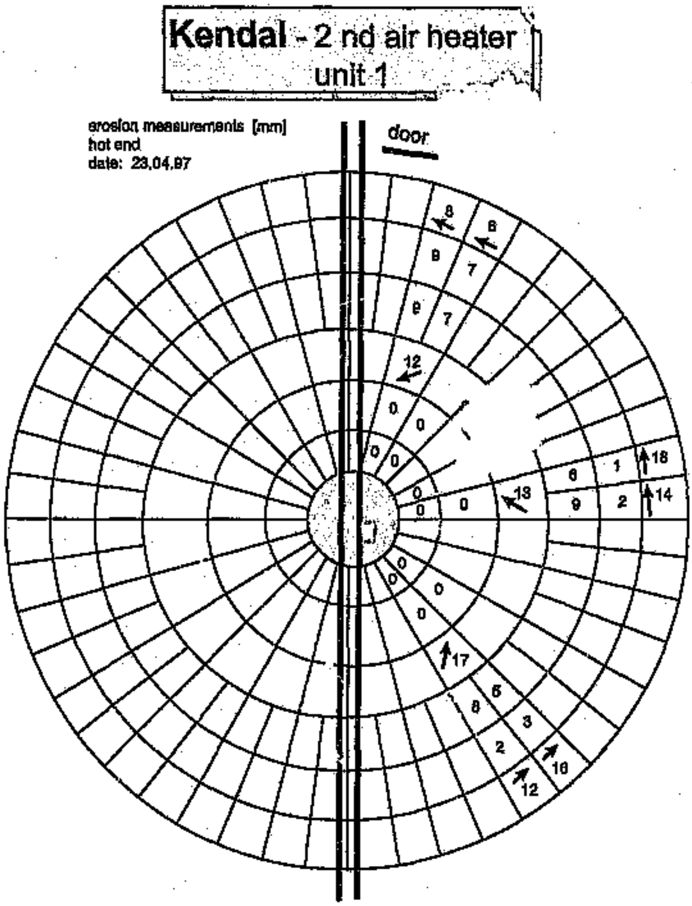

Figure 5.4: Leading edge erosion investigations at the Kendal air heater, unit 1, left hand side

As it can be seen from Figure 5.3 and Figure 5.4 there is essentially no erosion in the two inner rings of the air heater. All the other rows show almost the same erosion behaviour. The leading edge erosion is approximately 10 mm. Only the outermost ring seems to have a slightly higher erosion than the other rings. The distribution of the erosion depth is consistent within concentric circles.

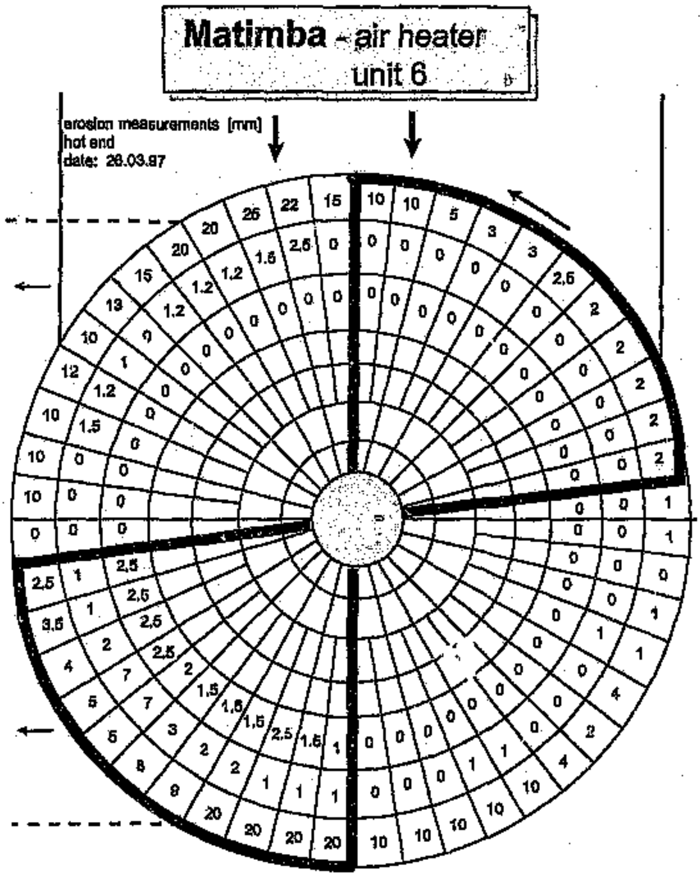

Figure 5.5: Leading edge erosion investigations at the Matimba air heater, unit 6

In the Rothemuehle air heater type at Matimba no erosion features were found in the four inner rings. The third outer ring shows erosion on the opposite side of the flue gas entrance. The two outermost rings show erosion depth between 0 and 20 mm. The spread is not as consistent as was found in the Ljungstroem air heater at Kendal. At Matimba high erosion areas are evident at the entrance of the flue gas and opposite this.

From these two examples it can be concluded that the Ljungstroem air heaters show a more equal distribution of leading edge erosion than Rothemuehle air heaters.

As mentioned earlier the Rothemuehle type shows high erosion areas at the flue gas entrance and opposite to this. The following explanation is possible: if the position of the hood is perpendicular to the gas stream, the flue gas can travel to the opposite side of the air heater. The ash particles hit the heating plates' surface first i.e. without rebounding off the hood. This means that they do not loose any kinetic energy before striking the plates. This possibly explains the high erosive areas in the Rothemuehle air heater.

At the Matimba air heater it was also investigated if there exists any correlation between blockages and erosion patterns. This could not be verified as shown in Figure 5.6. Blockages (in percentage) seem to be distributed equally over the entire flow area.

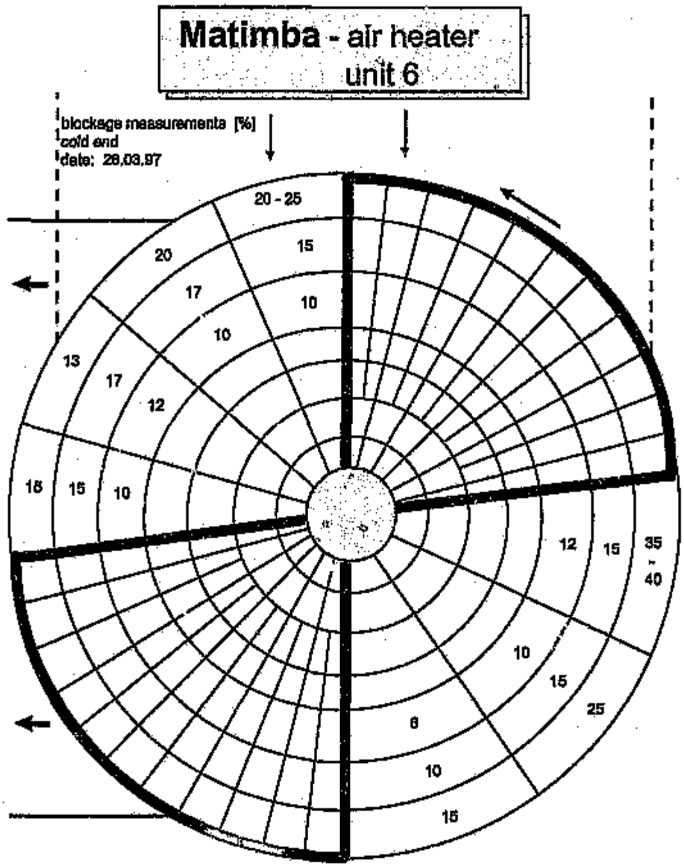

Figure 5.6: Blockage investigations at the Matimba air heater, unit 6

The changing of the hydraulic and thermal performance is not the only important factor, with regards to erosion in air heaters. The decrease of the heat transfer area caused by the appearance of holes in the plates is also of importance. The heat transferred is directly proportional to the heat transfer area. Plates which are eroded to 40% mass loss show an area loss of up to 10%, depending on the profile type (see chapter 7). If the heat transfer coefficient stayed constant, this would mean 10% less transferred heat.

6. Erosion test facilities

To investigate erosion on heating plates TRI ESKOM has established two test methods. One is the Modified Basket Test Facility (MBTF) and the other is the Cold Accelerated Erosion Rig (CAER). Both test facilities are described below.

6.1 Modified Basket Test Facility (MBTF)

The concept of the MBTF is to test the erosion behaviour of air heater packs under real conditions in an air heater. The MBTF is situated in an air pre-heater in a power station. At Kendal Power Station one air heater contains 7 modified baskets (MB) and at Matimba power station one air heater contains 3 modified baskets. It has to be mentioned that the Kendal air heater is a Ljungstroem type and the Matimba air heater is a Rothemuehle type. This implies that for the Kendal air heater the position of the MB is not critical while the MB in the Matimba air heater are all placed in the region of maximum wear on the stator (opposite to the gas inlet, see Chapter 5). Figure 6.1 and Figure 6.2 show the principle of the facility.

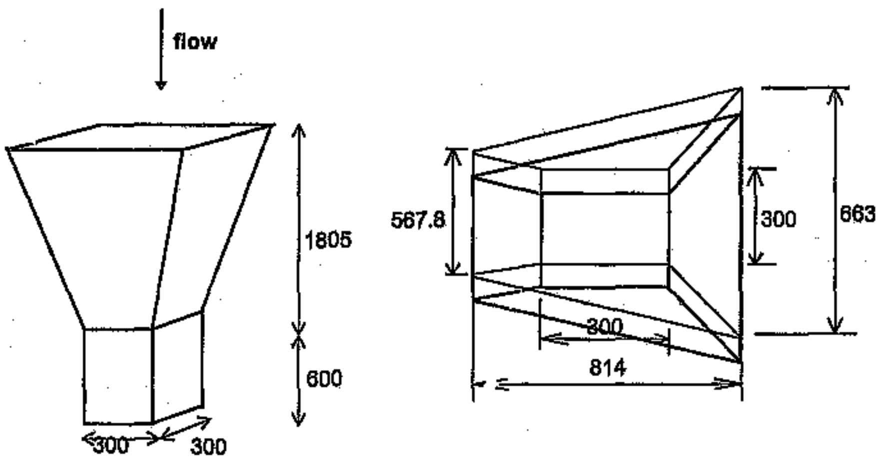

Figure 6.1: Single Modified Basket

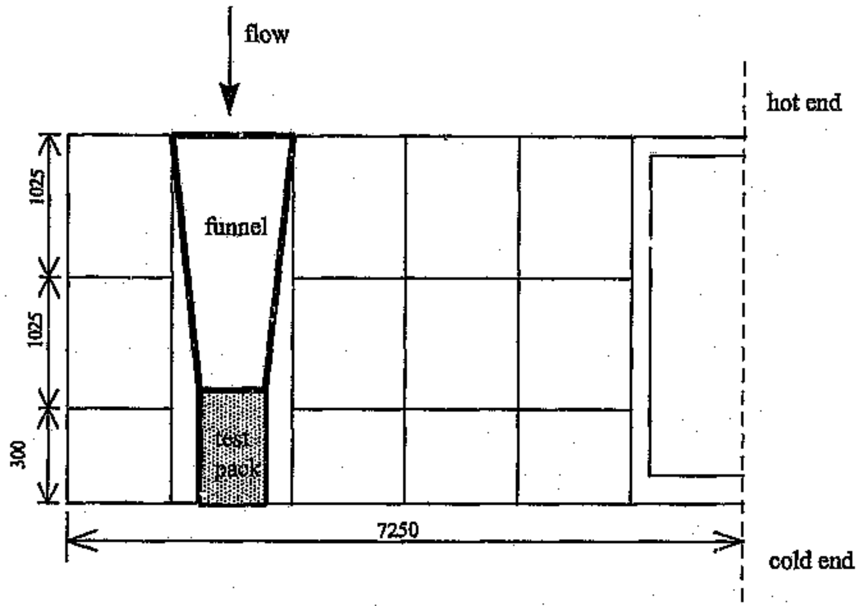

Figure 6.2: Half section of an air heater, with a modified basket in its 2nd outer ring

As can be seen from the diagrams the modified baskets consist of two parts, first the funnel (1.5 to 1.8 m, depending on the depth of the air heater) and the test section. The purpose of the funnel is to accelerate the flue gas. The velocity in the basket is two times higher than in a normal air heater. Modelling with the CFD (Computational Fluid Dynamics) package Star CD indicates that the velocity in the Matimba MB is 14 m/s, as compared to the ordinary velocity which is 6-7 m/s. At the bottom of the MB is an air heater pack with the same dimensions as the packs used in the Thermal Test Facility (TTF) and the Cold Accelerated Erosion Rig (CAER).

The MB-design will accelerate the rate of erosion of the packs by at least a factor of eight as compared to real operating conditions. The disadvantage of this test facility is that the period of time for erosion is entirely dependant on the outage plan for the unit once these packs have been placed. However, this could typically be one year. Therefore it is not practical to use these packs to determine the change in thermal and hydraulic performance of eroded packs. For this purpose the CAER is more practical. This will be explained in the next section.

Experience has shown that the different packs will erode to a different degree and not be as controlled as in the CAER. The thermal and hydraulic evaluation will thus probably only be carried out once, after the first placement of the packs.

At a later stage it would be beneficial to test the eroded packs from the MBTF i. TTF and compare these results with the results of the packs eroded in the CAER.

6.2 Cold Accelerated Erosion Rig (CAER)

The CAER mentioned in the previous section has been designed to reproduce packs which have been eroded to a specific stage. This test facility is not part of the plant, but draws ash from a modified precipitator hopper. As the name of the test facility implies, the erosion rig works at comparatively low temperatures (40 °C). Also the fluid (air and ash) is accelerated to velocities four times of that in a normal air heater when passing the test section. This is the reason the packs erode quickly. It is feasible to erode packs to different stages of erosion, i.e. different stages of mass loss. This is necessary for a systematic investigation into the change in the thermal and hydraulic behaviour of eroded air heater packs.

For this dissertation only a brief description of the CAER is necessary. A complete description of the experimental apparatus can be found in von Bormann [30]. The following diagram shows the schematic layout of the CAER.

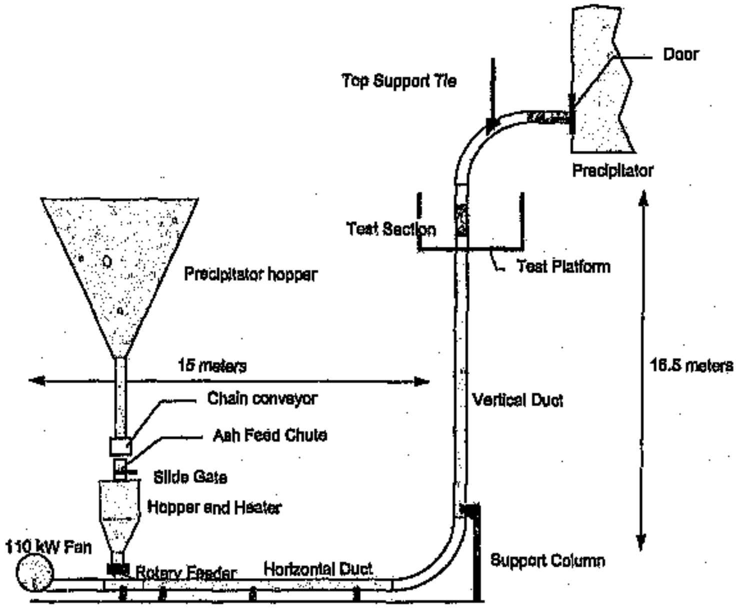

Figure 6.3: Layout of the CAER

The main characteristics of the CAER are as follows:

To use ash directly from the power cycle the hopper of the CAER is connected to one precipitator hopper. The ash travels via a chain conveyor through an ash feeder chute and past a slide gate into the test rig hopper. A rotary feeder insures a constant ash flow throughout the test facility. A 110 kW fan is used to provide an air flow rate of up to 40 m/s, which is approximately four times the velocity in a real air heater. The average mass flow of the ash-air flow rate is 0.6 kg/s. The test section, which contains the test pack, is placed in the vertical shaft of the facility. To ensure that the flow is uniform and straight before entering the test section the vertical duct has a length of 16 m after the bend. The size of the test section is the same as the one in the TTF. This is to ensure that the test packs fit in both test facilities. After passing the test section, the ash-air flow goes back into the precipitator.

The CAER operates as follows:

A test pack is placed into the test section. After setting a constant mass flow rate of ash at a specific velocity the test runs for a specific time, depending on the desired stage of erosion. For example a 40 % mass loss takes about 36 hours, depending on the profile type. The velocity and the mass flow are monitored constantly. To test the weight of the pack, the whole test facility has to be switched off, the test pack has to be removed from the test section and only then it can be weighed.

For the purpose of this study the KH11 profile test pack was tested. The pack was first eroded to 20% mass loss. The pack was then taken out, tested in the TTF to investigate the change in thermal and hydraulic performance after 20% mass loss. After this test, it was put back into the CAER and was eroded a further 10% to a total of 30% mass loss. The pack was then taken out again and tested again in the TTF. After this, the pack was put back into the CAER for a last time where it was eroded to 40 % mass loss. This is the highest safe percentage limit to which these packs can be eroded to without damaging them during transportation. Packs with a higher percentage of mass loss tend to fall apart.

To visualise what heating plates look like at 20%, 30% or 40% mass loss the following photographs were taken. They show four pairs of the profile type KH11 at each stage of erosion. These four pairs represent the whole pack, because the other half of the pack looks identical. The plates are numbered such that, the outermost plate is number 1. The plates which are closer to the middle of the pack tend to have less erosion than the plates which are closer to the outside of the pack.

KH11, 20% erosion

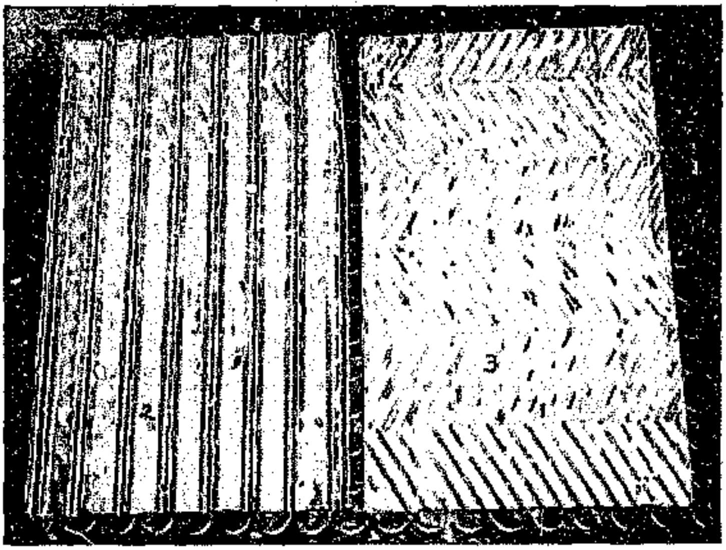

Figure 6.4: Plate 2 and 3, KH11, 20% eroded

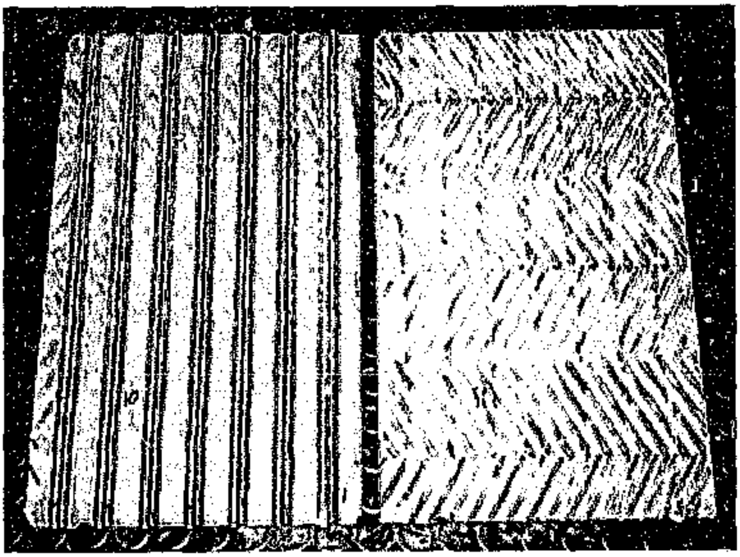

Figure 6.5: Plate 10 and 11, KH11, 20% eroded

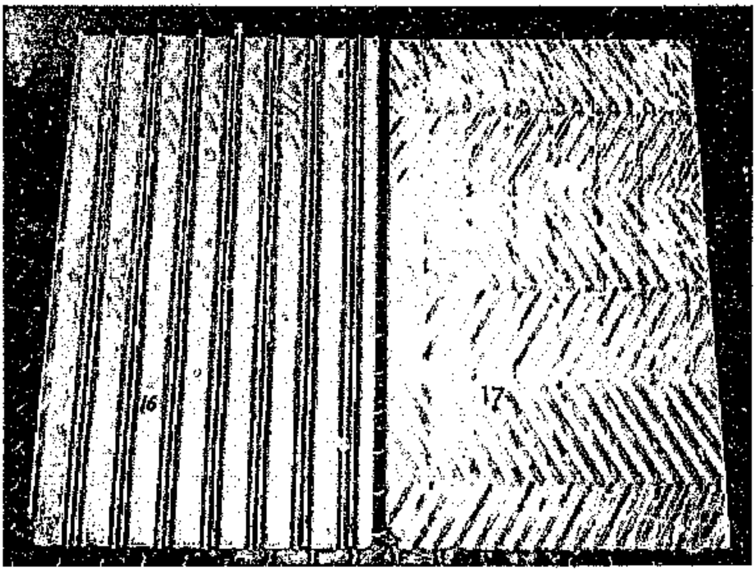

Figure 6.6: Plate 16 and 17, KH11, 20% eroded

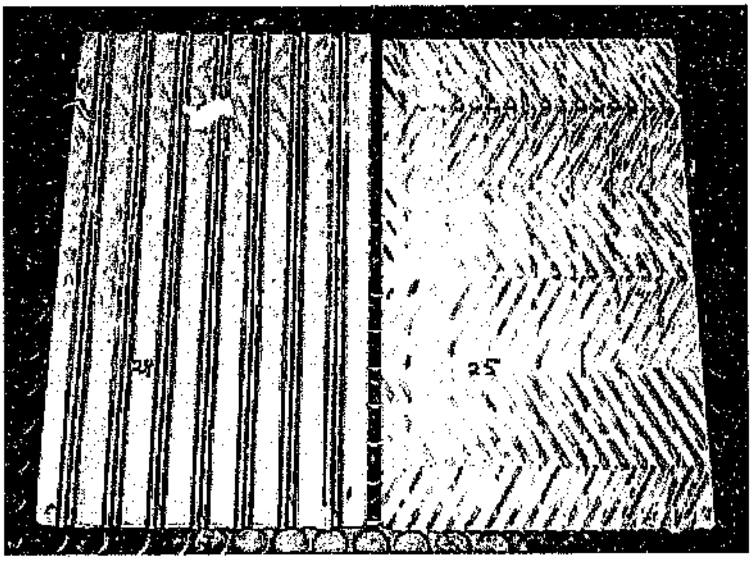

Figure 6.7: Plate 24 and 25, KH11, 20% eroded

KH11, 30% erosion

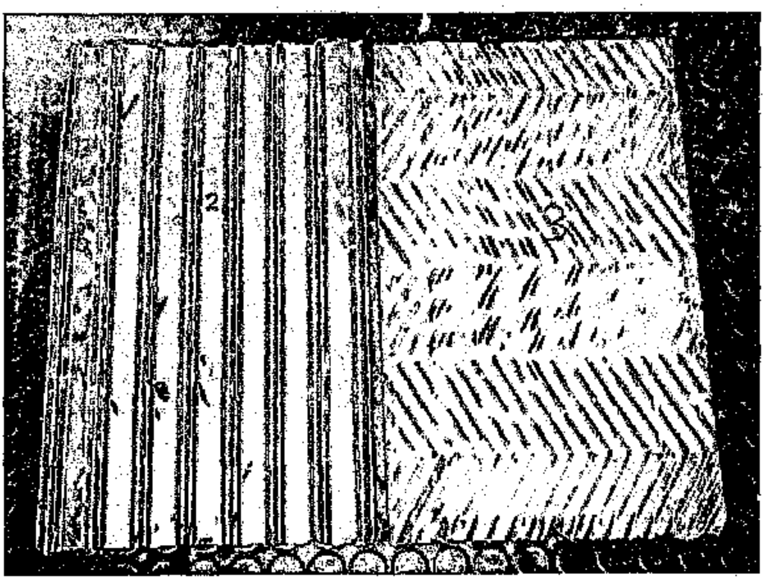

Figure 6.8: Plate 2 and 3, KH11, 30% eroded

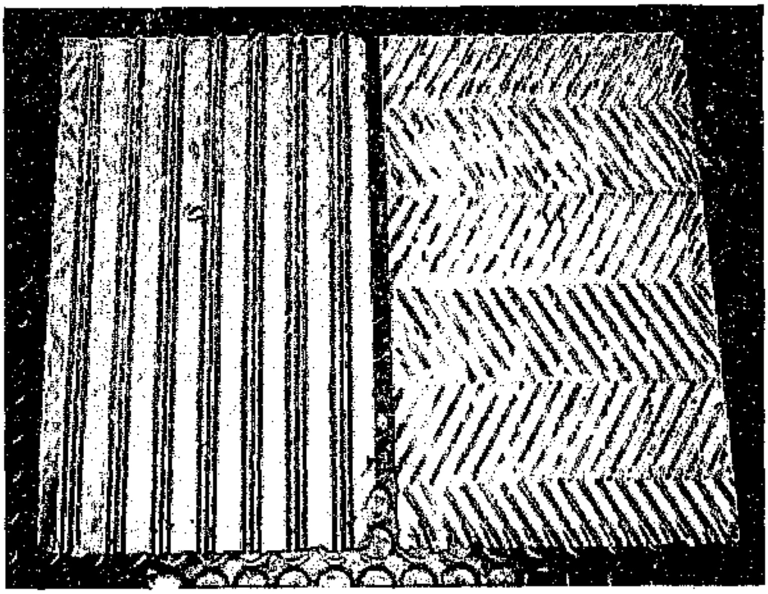

Figure 6.9: Plate 10 and 11, KH11, 30% eroded

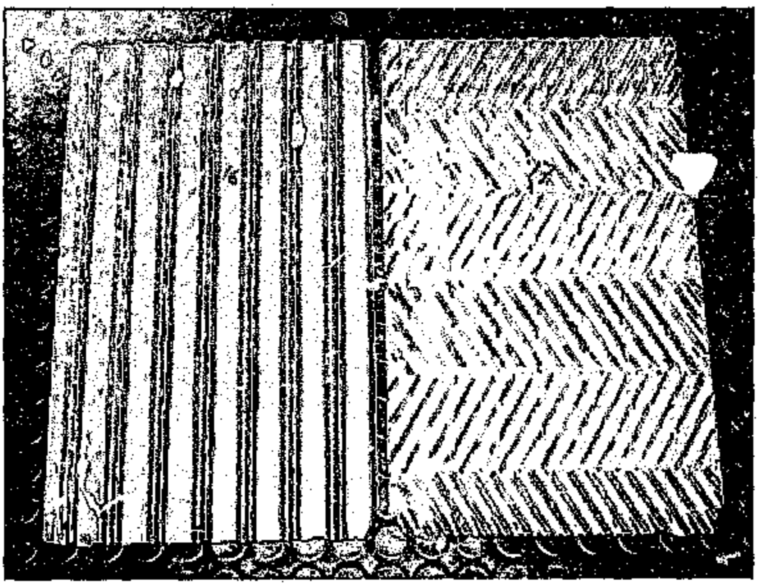

Figure 6.10: Plate 16 and 17, KH11, 30% eroded

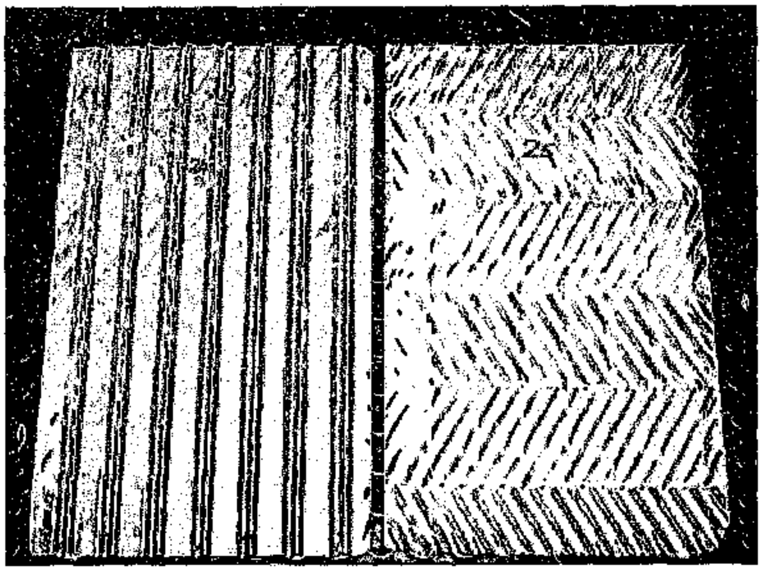

Figure 6.11: Plate 24 and 25, KH11, 30% eroded

KH11, 40% erosion

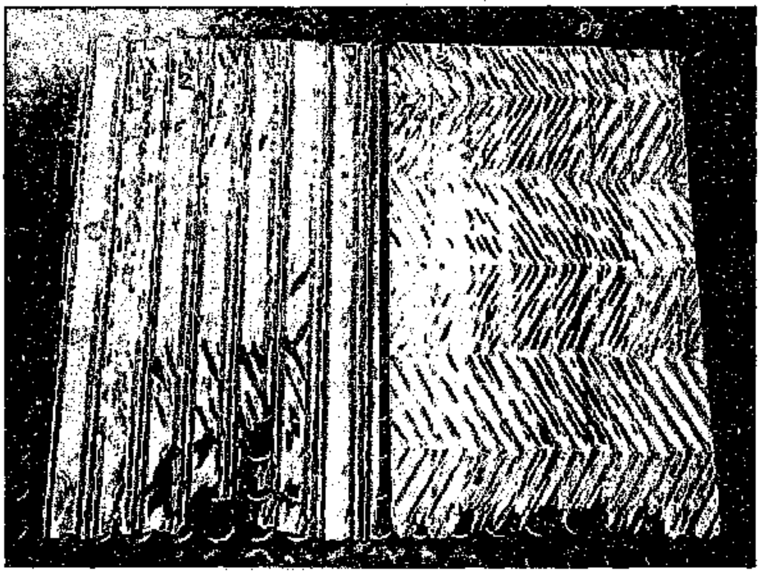

Figure 6.12: Plate 2 and 3, KH11, 40% eroded

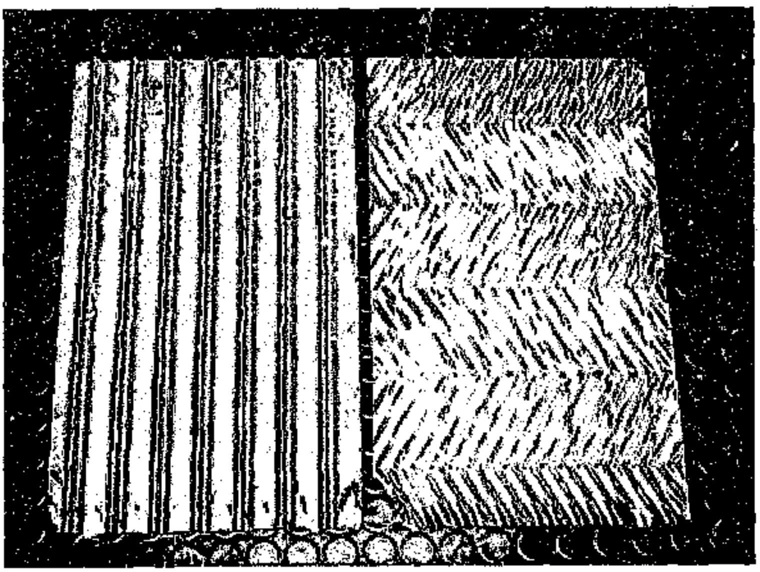

Figure 6.13: Plate 8 and 9, KH11, 40% eroded

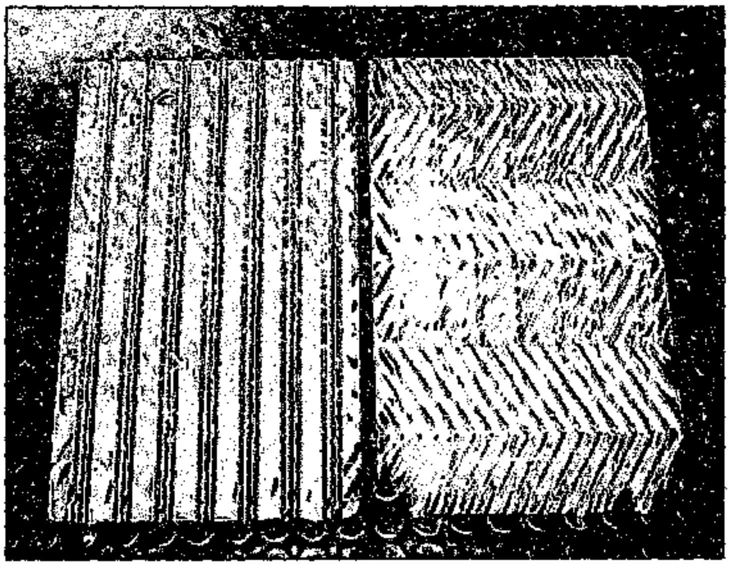

Figure 6.14: Plate 16 and 17, KH11, 40% eroded

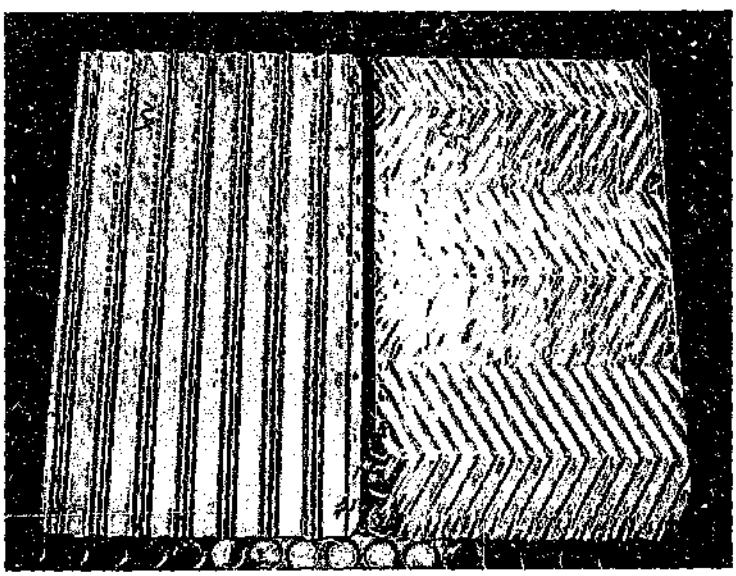

Figure 6.15: Plate 24 and 25, KH11, 40% eroded

It can be seen that the undulated plates have more damage than the notched ones. Also the pattern of the undulated plates are etched into the notched plates. These are the first signs of erosion on the notched plate.

7. Thermal tests of eroded plates

After testing many uneroded heatin^ plates, one commonly used profile types was chosen to be tested at different stages of erosion. Firstly the results of the pressure loss for this pack will be discussed. Secondly the results of the heat transfer coefficient will be presented. The calculation of this coefficient for eroded plates differs from that for uneroded plates.

7.1. Preparation of the eroded plates for the TTF

From the large quantity of profile types tested, one commonly used profiles was chosen to be tested in an eroded stage. This profile type is the KH11. The dimensions of the pack were the same as those used for uneroded thermal testing. Before the pack was sent to Matimba for erosion it was tested in the TTF to ensure that its characteristics were consistent with other new packs. At Matimba this pack was eroded to 20% mass loss. Afterwards it was taken to TRI where the braces were removed to take photographs of a representative number of plates. Before the pack could be tested in the TTF the remaining heat transfer area had to be measured. An automatic image analysis system (LECA) was used for this as follows.

7.1.1. Image analysis system LECA

The main steps of an image analysis system are:

1. input
2. processing
3. measurements
4. output

An image is first visualised through a lens attached to a TV camera. Electronic circuits then digitalise the analogue signal coming from the TV camera so that it can be stored in a computer memory. Once in the memory, various enhancements are performed on the stored image. This resulting image is reconverted to analogue mode and fed to a monitor enabling an operator to observe the effect of the enhancement operations.

The enhanced grey image is then sliced in various sets of grey levels, corresponding to the objects or phases of interest. As these phases or objects are discriminated from the background, they are also coloured according to their grey level spread. These colours are then superimposed to the grey image seen on the monitor. Finally, measurements are made onto each of these coloured objects or phases and results are computed, displayed, or printed.

Procedure to measure the actual heat transfer area of eroded heating plates with the help of the LECO 2001 system

First the plate was put onto the light box. The plate was adjusted such that it fitted exactly on the image screen. It had to be ensured that the leading edge erosion was visible on the screen. The lens and the objectives were adjusted. If necessary the heating plate had to be shaded. Then the picture was frozen. The plate area (dark areas) was coloured with one colour and the holes area (brighter patches) was coloured with another colour. The two areas were connected to one area. Now the fractional area of the holes and the number of holes were measured.

This area measurement was also done for a representative number of plates (4 notched and 4 undulated from one half of the pack) to get a good average. Using the actual heat transfer area, the mass and the density, the average plate thickness and the cross sectional area can be calculated.

After this the packs were put together, the braces were welded on and the pack was tested in the TTF. Then the pack went back to Matimba to be eroded to 30% mass loss, which takes approximately 24 hours. The above mentioned procedure repeats itself for the 30 % and 40% erosion stage.

The following table shows the geometry values for test pack at the different stages of erosion.

Table 7.1: Geometry of the test pack at different stages of erosion

Profile type	Erosion stage	starting date	mass [kg] with braces	mass loss [%]	A_{heat} [m^2]	$A_{cr, s}$ [m^2]	plate thickn. [mm]	% holes notched	% holes undul.
KH11	new	-	36.1	0	17.[illegible]2	8.61E-03	0.5	0	0
	20%	03.08.97	28.5	21.05	16.997	6.75E-03	0.392	0.867	1.769
	30%	12.09.97	25.4	29.64	16.657	5.96E-03	0.346	1.479	5.316
	40%	03.10.97	23.04	36.18	16.054	5.36E-03	0.311	3.29	10.76

Table 7.1 shows that the average plate thickness for 20% eroded plates is 0.4 mm, for 30% erosion 0.35 mm and for 40% 0.3 mm. It is evident that, the percentage of the area of the holes is substantially higher for undulated plates than for notched plates.

7.2. Pressure drop across the pack for eroded packs

The pack that was eroded, was 500 mm in length with braces. In comparison with an uneroded pack the following results were achieved. Figure 7.1 shows the pressure loss for the tested profile type at different stages of erosion.

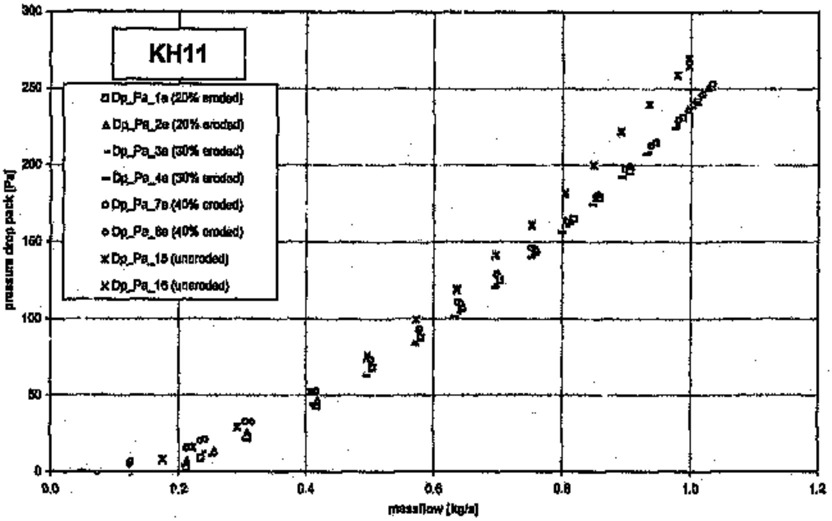

Figure 7.1: Pressure drop across the pack vs. mass flow, KH11, uneroded and eroded plates

Two features of how erosion effects the pressure drop across heating plates are visible from the above graph. Firstly, the stage of erosion does not have any influence on the pressure drop. Once the pack started eroding, the pressure drop was the same for 20%, 30% or 40% mass loss. Secondly, the pressure drop of eroded plates is less than the pressure drop of uneroded plates. At a mass flow rate of 1 kg/s the difference between these pressure drops is at about 40 Pa.

A possible explanation as to why the pressure drop for eroded plates is less than that for uneroded plates could be the presence of the holes in the profiles. Once the plates start eroding and the first holes appear the path for the fluid is easier, it does not have to go around the notches and undulations, but rather go straight through the pack.

7.3. Heat transfer coefficient uncertainties of eroded packs

To measure the heat transfer coefficient of eroded plates was not as easy as for the uneroded plates. The results of all the test runs showed an unacceptably large difference between the experimental and the calculated outlet temperature (see Chapter 3). The iteration program was not able to estimate an heat transfer coefficient, to give the correct temperature outlet history (see Figure 7.2 and Figure 7.4). The convergence criterion is the difference between the dimensionless calculated and the dimensionless experimental outlet temperature. An average absolute difference is calculated to specify the convergence criterion over the test duration:

$$\varepsilon = \sqrt{\sum_{i=0}^{n}\left(T^*_{outlet,i,calc} - T^*_{outlet,i,exp}\right)^2} \tag{7.1}$$

i = 0.....n, time duration approx. 50 sec.

For uneroded plates the error for calculating the heat transfer coefficient is always between 0.05 and 0.2, depending on the Reynolds-number. With increasing Reynolds-numbers the error also increases. The average error value over the Reynolds-number was about 0.1. The difference between the calculated and the experimental temperatures was both positive and negative for one test point (one Reynolds-number). The absolute temperature difference between the calculated and the experimental data was less than 0.15 °C. The difference between the calculated and the experimental data does not increase with the time duration, therefore changing the time duration does not effect the value of the error. Inlet temperature rise duration has no influence on the heat transfer coefficient.

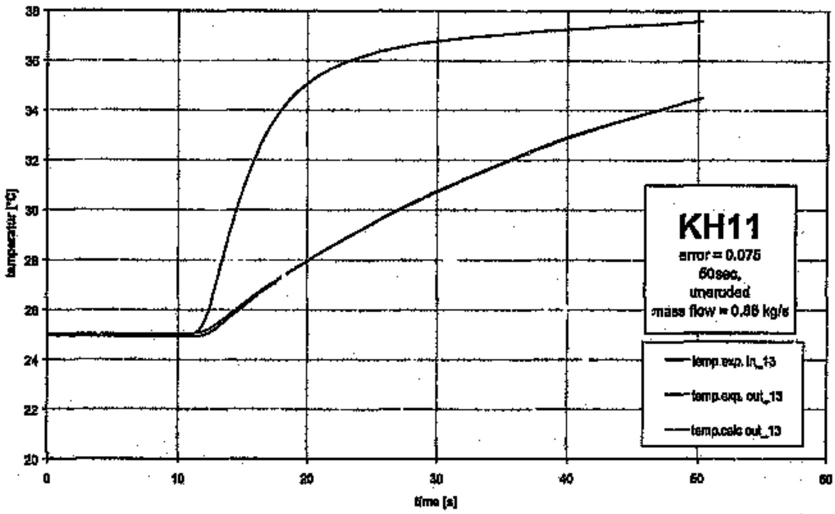

Figure 7.2: Inlet and outlet temperatures histories for an uneroded pack

To establish the reason why the calculation model works for uneroded plates but not for eroded plates, the differences between eroded and uneroded plates should be emphasised.

The mass loss depends on the stage of erosion (20%, 30%, or 40%). The plate thickness decreases from 0.5 mm to a maximum of 0.3 mm. There is one average value taken for the undulated and the notched plates. The presence of holes start at the 20% erosion stage. The areas around the holes are very thin. The undulated plates are more eroded. The loss of heat transfer area is up to 10%. Also because of leading edge erosion, the flow entrance area is not uniform, therefore the flow could be distorted. This could also result in non-uniform temperature distribution at the pack exit.

Some of the features of calculating the heat transfer coefficient for eroded packs should also be mentioned. The dimensionless error (see Equation 7.1) is always between 0.1 and 0.5, depending on the Reynolds-number, with increasing Reynolds-numbers the error is also increasing. That means the error is 5 times higher than for uneroded plates. The curve for the heat transfer coefficient vs. mass flow for an eroded pack does not look similar to one for an uneroded pack. At low Reynolds-numbers the values are similar. In the region of intermediate Reynolds-numbers the spread grows, so that the heat transfer coefficient of the eroded pack is visibly higher than the one of the uneroded pack. At high Reynolds-numbers again there is no difference between the heat transfer coefficient of eroded and uneroded packs. See Figure 7.3.

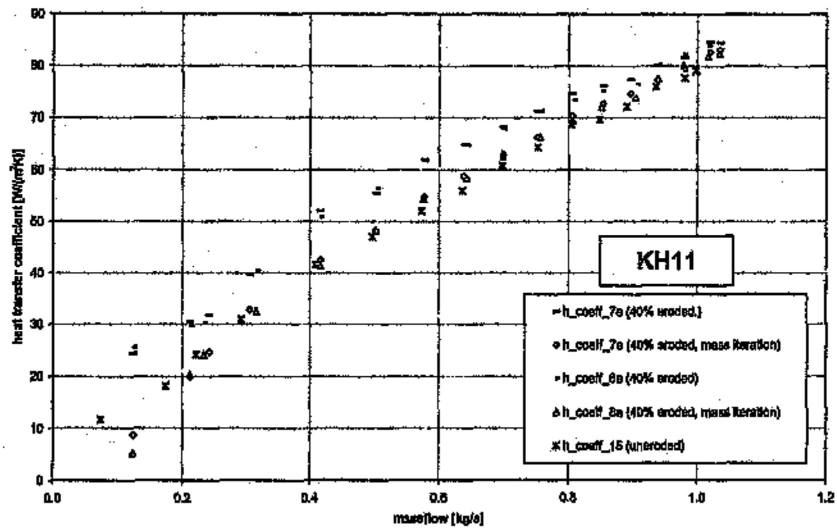

Figure 7.3: Heat transfer coefficient vs. mass flow, KH11 profile, uneroded and eroded (original calculation without any adaptations)

The influence on the heat transfer coefficient and the error is dependant on the stage of erosion. The temperature difference T_{calc} - T_{exp} is always positive, which means that the calculated temperature is always higher than the experimental temperature. The maximum is about 1 °C.

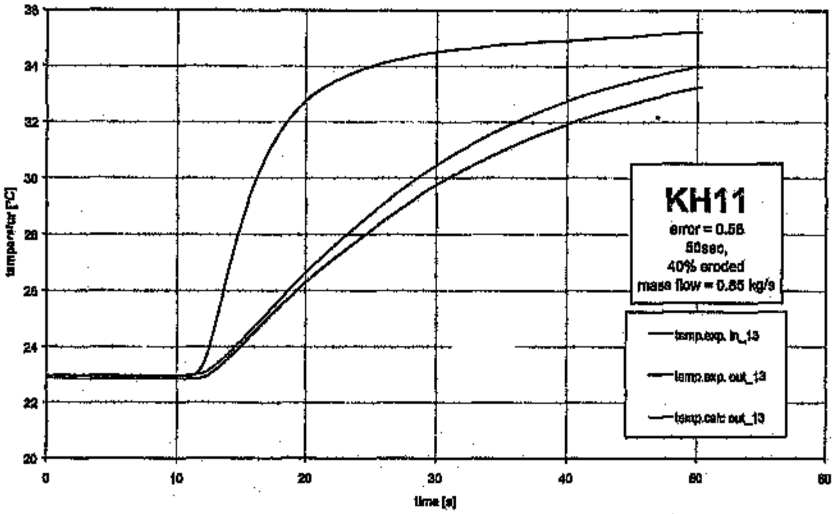

Figure 7.4: Inlet and outlet temperatures histories for an eroded pack

The effect of increasing the difference between the calculated and measured temperature is more significant at 40% mass loss that at 20% mass loss. This difference also increases with time (see Figure 7.4). If the inlet temperature rise duration is shortened the error becomes smaller. This leads to the assumption that shortening the test duration reduces the error. Calculations have been performed for 20 sec., 30 sec., 40 sec. and 50 sec. test duration. Using a time duration of 30 sec. the error (0.1) is acceptable. For this time duration the heat transfer coefficient also does not stay the same; it increases up to 10% at high Reynolds-numbers. The reason why the data for the eroded plates exhibits such a behaviour is unknown and unacceptable.

7.3.1. Flat plates with holes

In order to exclude the possibility that holes in the undulated and notched plates might cause problems when calculating the heat transfer coefficient, experiments on flat plates with holes were conducted. Firstly, a pack consisting only of flat plates, held together by rods, was tested in the TTF. Secondly, a similar pack with holes drilled in it was tested. The area of the holes was chosen to be 8% of the total heat transfer area. This corresponds with the percentage of holes for a 40% eroded pack. The error for both packs was as small as the error for uneroded plates. Figure 7.5 and Figure 7.6 show the results of the heat transfer coefficient and the pressure drop.

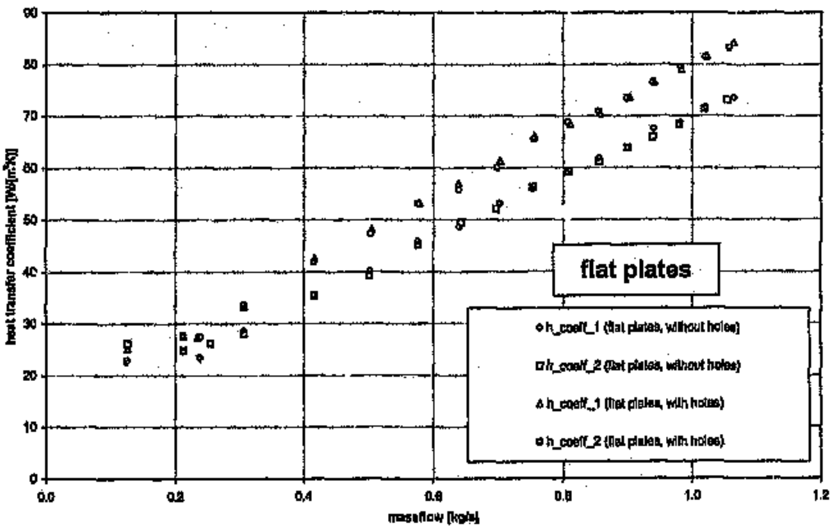

Figure 7.5: Heat transfer coefficient vs. mass flow, flat plates with and without holes

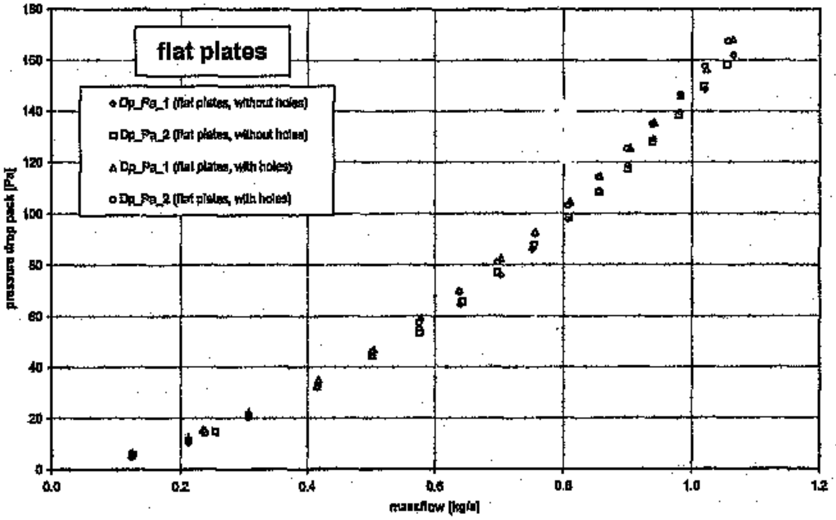

Figure 7.6: Pressure drop vs. mass flow, flat plates with and without holes

It can be seen from the graphs that both the heat transfer coefficient and the pressure drop of the pack with holes are higher than for the pack without holes. This means, in this case the holes do not straighten the flow, as it was seen with the eroded packs, but rather increases the turbulence. This results in a higher pressure drop and higher heat transfer performance.

From this experiment it can be concluded that the presence of the holes do not cause high errors when calculating the heat transfer coefficient.

7.3.2. Steps taken to solve the problem

The following steps were used to approach and solve the problem of the high error when calculating the heat transfer coefficient for eroded plates.

There are two possible reasons why the calculation method can not find the correct solution for eroded plates. Firstly, the Matlab calculation program *htcoef.m* fails because of wrong input data for eroded plates, which are the temperature histories for the inlet and outlet, and geometry values, like the cross sectional area, mass and heat transfer area. Secondly, the model of Mullisen and Loehrke [2] does not work, because one or more assumptions of the model are invalid. As stated before, the presence of the holes can already be excluded as one possibility.

From a visual inspection of the temperature histories of the eroded and the uneroded packs, no difference could be found. In terms of slope and absolute values they seem similar. To determine if input data such as the cross sectional area, heat transfer area or mass are incorrect, these values were varied in the *htcoefa.m*. This procedure yielded to the following results: The increase in the error is not dependant on the value of the heat transfer area. When the heat transfer area is changed the heat balance of the fluid, for the convective part, becomes incorrect. This means that the error stays the same, only the heat transfer coefficient changes. If the input of the heat transfer area is bigger than the original one the heat transfer coefficient becomes smaller and vice versa, as expected.

In order to take longitudinal conduction in the plates into account, it is necessary to consider the cross sectional area. Variations of the cross sectional area do not show any influence on either the error or the heat transfer coefficient. This leads to the conclusion that the conduction is not a major influence on the whole data analysis. Tests where the thermal conductivity was varied between 1 W/(mK) and 100 W/(mK) showed that this definitely did not influence the heat transfer results.

Changing the tolerance in the iteration program or the number of nodes (in longitudinal direction) or the number of iteration steps did not effect the error or the heat transfer coefficient. The iteration stops when the changing of the heat transfer coefficient is less than the value of the tolerance. The function *fmins* (programmed in Matlab) is used to look for a local minimum.

Inputting *h*-values by hand to get a lower error, did not yield any success. Comparisons of temperature graphs with different (hand entered) *h*-values, but the same mass, showed that the heat transfer coefficient influences the slope of the calculated temperature curve. Comparisons of temperature graphs where the mass was varied, but the same heat transfer coefficient was used, showed that the variation of the mass influences the off-set of the calculated temperature curve.

This leads to the following conclusion: Variations in the mass input influences the error. Tests showed that increasing the mass results in a lower error (within limits) and decreasing the mass results in a higher error. The first (by hand) optimisation showed that an additional mass of 5 kg minimises the error for the KH11 pack, 40% eroded and at Re = 5000. The next step was to expand the calculation by putting in the iteration of the mass. The iterated artificial mass increases with the stage of erosion and with the mass flow. Uneroded plates did not show any behaviour of mass dependency.

The theoretical explanation why the calculation method does not work for eroded plates and why artificial mass has to be added to decrease the error can be found be studying the fundamental equations of the model.

7.3.3. Fundamental heat balances

One essential difference between new and eroded plates is the presence of holes in eroded plates. But since the model [23] has been developed for interrupted plates and investigations of plates with holes were done, this should not be a problem. The other main difference is the unevenness of the plate thickness. Figure 7.7 to Figure 7.9 show why there is a problem using differential heat balances. The first picture shows an eroded plate with two specified differential parts, one in the thicker section of the plate and the other one in the thinner section of the plate.

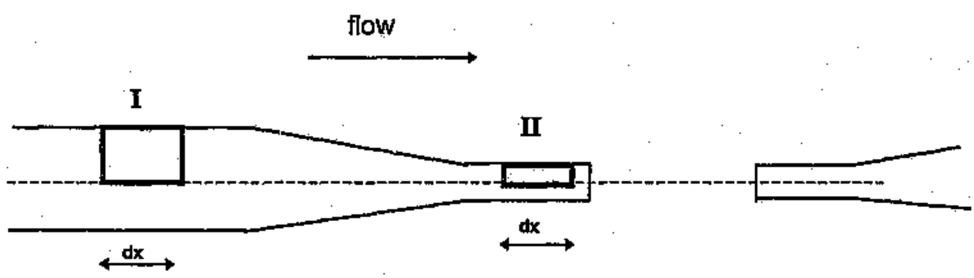

Figure 7.7: Schematic representation of an eroded plate with hole

The following representation shows the different amounts of energy which influence the thicker part of the plate, section I. The appropriate heat balances are written below.

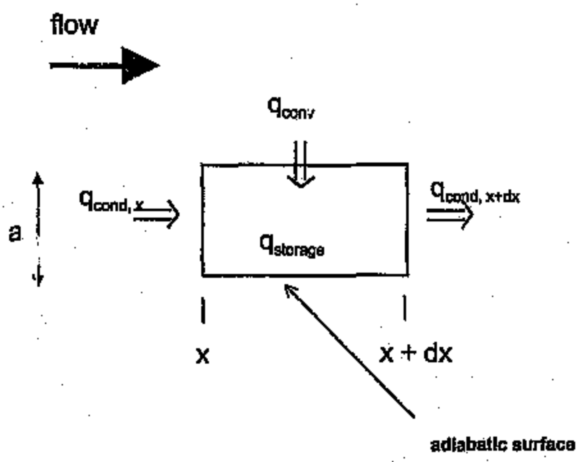

Figure 7.8: Schematic representation of the thicker part of the plate

<u>energy equations of the section I</u> (see also Appendix G)

- heat balance for plate material:

$$\dot{q}_{stor} = \dot{q}_{cond,x} - \dot{q}_{cond,x+dx} + d\dot{q}_{conv} \tag{7.2}$$

- storage term:

$$\dot{q}_{stor} = \int_{x}^{x+dx} a \cdot \rho \cdot c \frac{\partial T_s}{\partial t} dx \tag{7.3}$$

- convective term:

$$\dot{q}_{conv} = \int_{x}^{x+dx} h \cdot (T_f - T_s) dx \tag{7.4}$$

- conduction term:

$$d\dot{q}_{cond,x\rightarrow x+dx} = \frac{k}{\partial x}\cdot a\cdot\frac{\partial T_s}{\partial x} \tag{7.5}$$

- substituting Equation 7.3, 7.4 and 7.5 into Equation 7.2:

$$a\cdot\rho\cdot c\cdot\frac{\partial T_s}{\partial t} = h\left(T_f - T_s\right) + k\cdot a\frac{\partial^2 T_s}{\partial x^2} \tag{7.2a}$$

- rearranging:

$$\frac{\Delta T_s}{\partial t} = \frac{h}{a\cdot\rho\cdot c}\left(T_f - T_s\right) + \frac{k}{\rho\cdot c}\frac{\partial^2 T_s}{\partial x^2} \tag{7.2b}$$

A representation for a thinner part of the plate, section II (half as thick as the other section) together with the appropriate heat balances is written below.

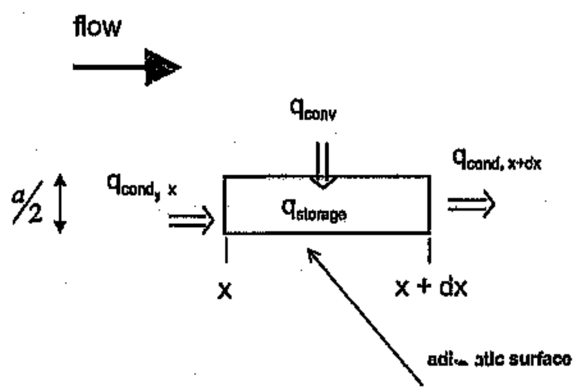

Figure 7.9: Schematic representation of the thinner part of the plate

energy equations of the section II

- heat balance material:

$$\dot{q}_{stor} = \dot{q}_{cond,x} - \dot{q}_{cond,x+dx} + d\dot{q}_{conv} \tag{7.2}$$

- storage term

$$\dot{q}_{stor} = \int_{x}^{x+dx} \frac{a}{2} \cdot \rho \cdot c \frac{\partial T_s}{\partial t} dx \tag{7.3a}$$

- convective term:

$$\dot{q}_{conv} = \int_{x}^{x+dx} h \cdot \left(T_f - T_s\right) dx \tag{7.4}$$

- conduction term:

$$d\dot{q}_{cond,x \to x+dx} = \frac{k}{\partial x} \cdot \frac{a}{2} \cdot \frac{\partial T_s}{\partial x} \tag{7.5a}$$

- substituting Equation 7.3, 7.4 and 7.5 into Equation 7.2:

$$\frac{a}{2} \cdot \rho \cdot c \cdot \frac{\partial T_s}{\partial t} = h\left(T_f - T_s\right) + k \cdot \frac{a}{2} \frac{\partial^2 T_s}{\partial x^2} \tag{7.2c}$$

- rearranging:

$$\frac{\Delta T_s}{\partial t} = \frac{2 \cdot h}{a \cdot \rho \cdot c}\left(T_f - T_s\right) + \frac{k}{\rho \cdot c} \frac{\partial^2 T_s}{\partial x^2} \tag{7.2d}$$

As can be seen from the above energy equations, the energy balance for solid (Equation 7.2) is a function of the mass and not of the heat transfer area. The mass is represented in this equation by the density and the plate thickness. The storage term of the solid is most influenced by the mass (or plate thickness).

The energy balance of the fluid (see Chapter 3, Equation 3.2) is not a function of the mass of the material, but a function of the heat transfer area. This is the reason that this balance is still correct.

As can be seen from Equation 7.2b and 7.2d the input of an average plate thickness is insufficient and incorrect to use in this model. In the Matlab calculation program (*htcoef.m*) the value of the plate thickness is not present, instead the mass is used as the input parameter in the energy balance, see the following equation.

$$-k\frac{\partial^2 T_S^*}{\left(\partial x^*\right)^2}-Ntu\left(T_f^*-T_S^*\right)+\frac{\partial T_S^*}{\partial \Theta^*} \qquad (7.6)$$

whereas: $\Theta^*=\dfrac{\dot{m}\cdot c_f\cdot\Theta}{M_s\cdot c_S}$ (7.7)

It can be seen that by changing the mass, the change in plate thickness can be accommodated.

The following describes the consequence of using in the real situation for uneven plates (plate thickness not constant) an average plate thickness for calculation of the heat transfer coefficient.

- Reality

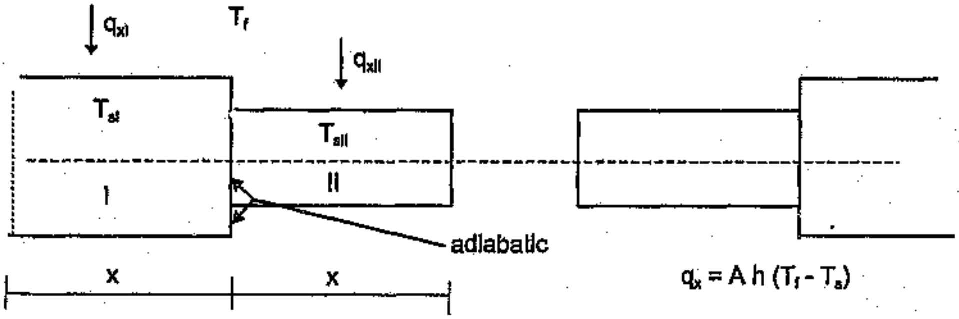

Figure 7.10: Schematic view of an eroded plate with thicker and thinner regions and holes

The eroded plate consists of parts of thicker parts and thinner parts. It can be assumed that both parts are separated by an adiabatic wall, because longitudinal conduction is unimportant in the model (see Section 7.3).

At the time = n the fluid comes into contact with the storage material. Part I and part II receive the same incremental quantity of energy. If the heat transfer coefficient for the two parts can be considered the same, the average temperature of the thicker part is lower than the average temperature of the thinner part (less storage material).

time: n

$$q_{xI} = q_{xII}; \qquad h_I = h_{II} \qquad \Rightarrow \qquad \boxed{T_{sII} > T_{sI}}$$

At the time = n+1 the transferred energy to the two parts of the plate are no longer the same. The thicker parts can absorb more energy than the thinner part, because the difference between the average temperature in the thicker part and the fluid is higher than the difference between the average temperature in the thinner part and the fluid. The temperature in the thinner part will, however, be still higher than in the thicker part.

time: n+1

$$q_{xI} > q_{II}; \qquad h_I = h_{II} \qquad \Rightarrow \qquad \boxed{T_{sII} > T_{sI}}$$

• Model with average plate thickness

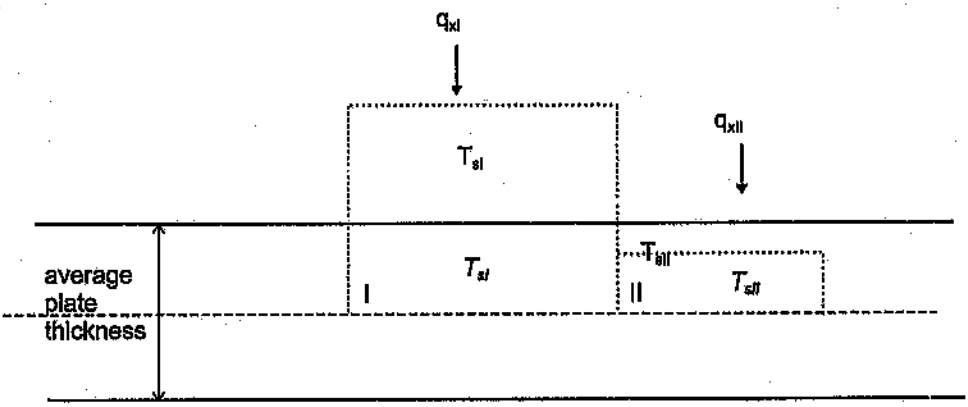

Figure 7.11: Schematic view of an eroded plate with an average plate thickness

whereas: T_{sI}, T_{sII} = calculated temperature
T_{sI}, T_{sII} = real temperature

Figure 7.11 shows that there is a difference between the real temperatures in the uneven plate and the calculated temperatures when considering an average plate thickness.

The following situations need to be considered:

- $T_{sI} > \mathrm{T}_{sI}$:
  The calculated temperature of the thicker section is higher than the real temperature in that part, because in reality there is more mass to absorb the heat than estimated in the calculation model.

- $T_{sII} < \mathrm{T}_{sII}$:
  The calculated temperature of the thinner section is lower than the real temperature in that part, because in reality there is less mass to absorb the heat than it is predicted in the calculation model.

- $T_{sI} = T_{sII}$:
  The calculated temperatures in the thicker and the thinner part of the plates are equal.

- $\mathrm{T}_{sI} < \mathrm{T}_{sII}$:
  In reality the temperature of the thicker part is lower than the temperature of the thinner part.

These considerations lead to the following conclusions:

⇨ The temperatures in the thicker sections are overestimated.
⇨ To decrease these temperatures the average plate thickness should be increased or artificial mass must be added.

⇨ The temperatures in the thinner sections are underestimated.
⇨ To increase these temperatures the average plate thickness should be decreased or artificial mass should be subtracted.

From that point of view the following question should be asked: What does a realistic distribution of plate thickness of an eroded plate as a function of plate length and width look like? Or the other way round, what fraction of the plate of the plate area is thicker than the average plate thickness and what fraction of is thinner?

The answer to these questions would give an indication of how much the original mass must be changed. Either a specific amount must be subtracted, that is the case if a larger fraction of the plate area is thinner than the average plate thickness, or a specific amount of mass must be added, that is the case if a larger fraction of the plate area is thicker than the average plate thickness.

The mass has to be changed as long as the error (difference between the experimental and the estimated temperature outlet history, see Chapter 3) is unacceptably high. This error should be an average value, for the whole mass flow range, of about 0.1, which means a difference between experimental and calculated temperature of 0.15 °C.

By changing the input mass value to either higher or lower values in the Matlab-program it was found that a specific amount of mass had to be added to the original value. This leads to the conclusion that the major portion of the plate area has a higher thickness than the average thickness.

To prove this statement, experimental measurements with a micrometer on several eroded heating plates were carried out. These led to no meaningful conclusions. It became obvious that the measurements comprised too many uncertainties. Additionally the amount of time necessary to measure sufficient plates to get a reliable average was not considered justified in relation to the results which could be obtained.

Finally the Matlab program *htcoef.m* was changed so that the additional mass could be iteratively optimised together with the heat transfer coefficient. The convergence criterion for both iterations is the error (Equation 7.1). Table 7.2 shows the change in mass after the iteration for all profile types and every stage of erosion. In comparison, the mass was also iterated for an uneroded plate. The table shows that the error in this case could not be significantly reduced.

Table 7.2: Results of the mass optimisation for the eroded KH11 pack

Profile	%mass loss	% area loss	orig. mass [kg]	Δmass iter. [kg]	error without correction	error with correction
KH11	20 %	1.318	26.48	1.96	0.182	0.076
				1.95	0.180	0.064
	30 %	3.400	23.38	2.50	0.225	0.051
				2.42	0.232	0.054
	40 %	7.026	21.02	2.95	0.299	0.047
				2.89	0.293	0.059
KH11	0 %	0 %	34.08	0.18	0.077	0.066

Table 7.2 shows that the error for the eroded profile at every stage of erosion becomes smaller after optimising the mass. After the iteration the error is less than 0.1 (average over the whole Reynolds-number range). This value is comparable with errors for uneroded plates. It can be seen that the amount of mass which has to be added to the original mass increases with increasing erosion stage. For 20% erosion the artificial additional mass is about 1.95 kg, for 30% erosion it is 2.45 kg and for 40% erosion it is 2.93 kg. This leads to the assumptions that there might be a function for a mass correction factor between the erosion stage and the mass to be added. Coming back to the reason why mass has to be added (because of plate thickness unevenness), a function containing the percentage of area where the plates are specially thin would be very useful. The value which describes this area of very thin plate parts best is the area percentage of the holes. Around the holes the plates are the thinnest. Figure 7.12 shows the iterated additional mass vs. the percentage of the area of the holes of the total.

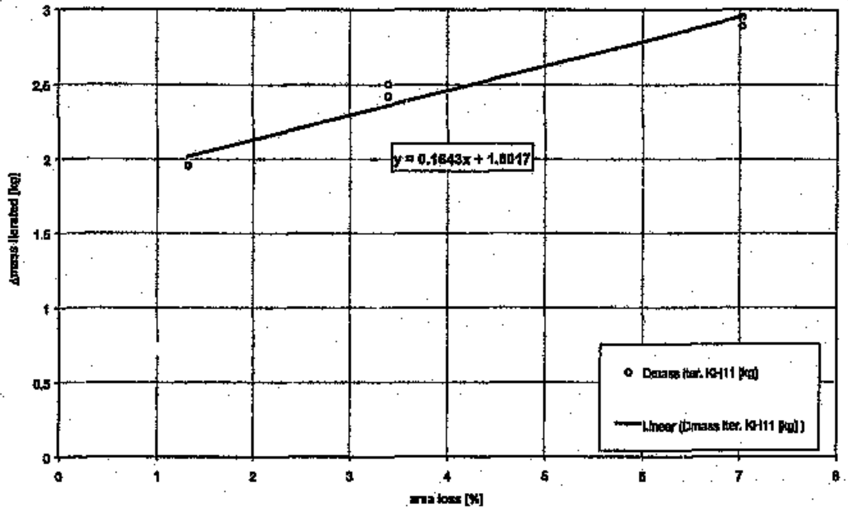

Figure 7.12: Iteratively optimised additional mass at different stages of erosion, profile KH11

Since only one type of heating plates has been tested in the eroded state so far, this graph is not of universal applicability. For the first KH11 profile the correction mass factor is sufficiently represented by the following function.

$$\Delta m_{additional} = 0.1643 \times \%age\ area\ loss + 1.8017 \qquad (7.8)$$

With the help of this mass correction factor the standard calculation program (*htcoef.m*) can be run to obtain the correct heat transfer coefficient with acceptable errors for eroded plates.

7.4. Heat transfer coefficient of eroded plates

The following results of the heat transfer coefficient were achieved with the help of the mass iteration. How much mass was added to the original mass can be seen in Table 7.2. The diagram shows the heat transfer coefficient of the KH11 profile type at different erosion stages. For comparison the results of an uneroded pack are also printed into the same figure.

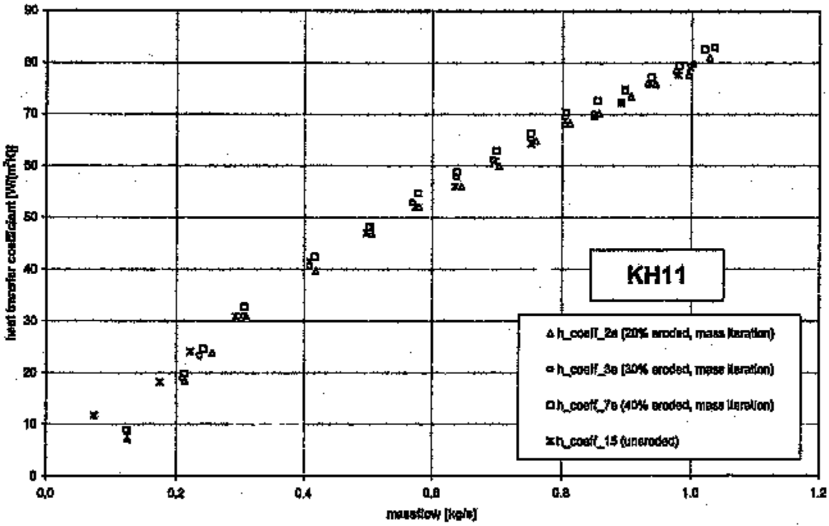

Figure 7.13: Heat transfer coefficient vs. mass flow, uneroded and eroded pack, KH11 profile

It can be seen from this graphs that the heat transfer coefficient is only slightly influenced by erosion. The heat transfer coefficient for eroded plates, independently of the stage of erosion, is a little less than the coefficient for uneroded plates, as expected because of the lower pressure drop for eroded plates than for uneroded plates. The difference in heat transfer coefficient is probably not important. However, it has to be remembered that the heat transfer area decreases with increasing erosion rates. At 40% mass loss the area left is only 90%, which means 10% less heat can be transferred (provided there is still sufficient mass so as not to adversely affect the heat storage).

Regression curves were calculated to facilitate the comparison of eroded and uneroded plates. Figure 7.14 - Figure 7.16 show the Colburn- and the Friction-factor versus Reynolds-number for the KH11 pack at different erosion stages.

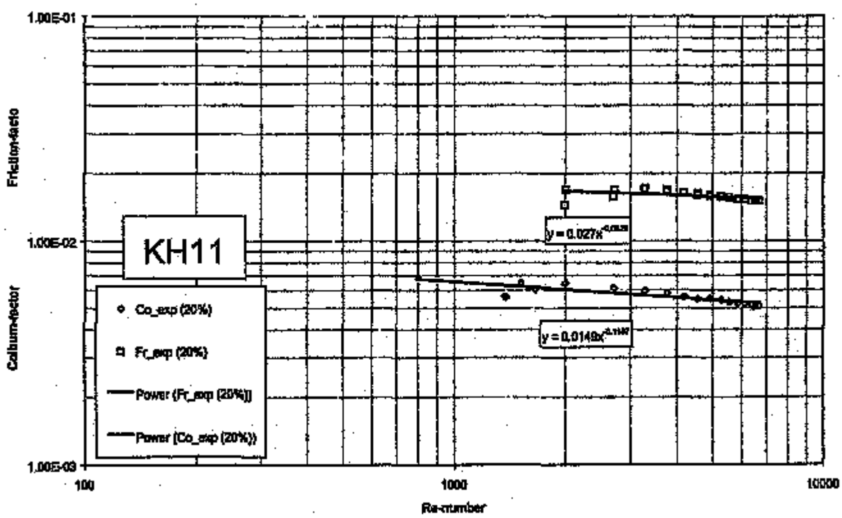

Figure 7.14: Colburn- and Friction-factor vs. Reynolds-number, KH11, 20% erosion, experimental and calculated results

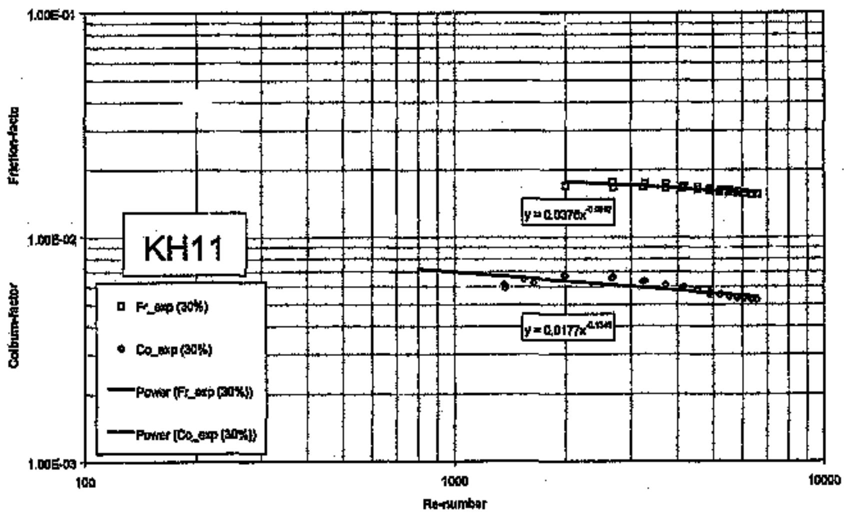

Figure 7.15: Colburn- and Friction-factor vs. Reynolds-number, KH11, 30% erosion, experimental and calculated results

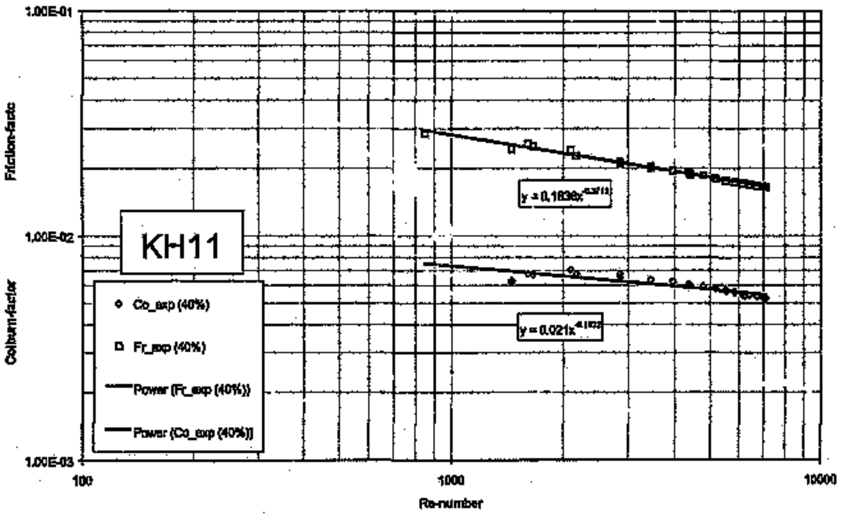

Figure 7.16: Colburn- and Friction-factor vs. Reynolds-number, KH11, 40% erosion, experimental and calculated results

Some Friction-factor data points at low Reynolds-numbers have been omitted from these figures because at low velocities the pressure drop shows some scatter which, though not visible in graphs with linear scales, is magnified by the logarithmic scales.

8. Summary and conclusions

The correctness of the TTF was checked by testing a Rothemuehle (RM) pack of heating elements which had been tested before in the Rothemuehle test facility, and secondly, by testing flat plates and comparing the results with literature data. Testing the RM H8 test pack in the TTF at TRI confirmed that within the measurement uncertainties, the thermal test facilities in Germany and at TRI give matching results. For the flat plates, the calculated Nusselt-number, derived from the Gnielinski equation (see Chapter 4), agrees exactly with the experimental Nusselt-numbers in the Reynolds-region between 3000 and 8000. For higher Reynolds-number the difference between the calculated and the measured Nusselt-number varies about 10 %, which is acceptable.

Twelve different pack designs, which were uneroded, and one pack design, which was eroded, have been tested in the TTF at TRI. The test facility is operating according to the single-blow method. The data reduction method being used involves the numerical solution of finite difference equations describing the heat transfer in the test section. It is shown that for testing eroded plates the procedure had to be changed slightly, because of non-constant plate thicknesses.

All test runs were performed at least twice for each configuration; repeatability was very good. This study of uneroded plates covers the entire range of heating plates available from Howden Power. It is shown that the profile designs with the smallest profile heights have the highest heat transfer coefficient, but also the highest pressure drop, as was expected. Good performance in one parameter always means bad performance in another parameter. Heat transfer coefficients and pressure drops of the various pack designs are in approximately inversely proportion to the hydraulic diameter. Profiles with a flat counterplate have a lower heat transfer coefficient than profiles with an undulated counterplate.

One eroded pack (with 20%, 30% and 40% mass loss) was tested and compared with an uneroded one in terms of heat transfer and pressure drop behaviour. Pressure drop was approximately 15% lower for the eroded plates (irrespective of the extent of erosion) and heat transfer coefficient was essentially unaffected.

9. Recommendations for future work

The heat transfer and pressure drop data gained from these experiments can be used as input for the air-heater model developed by Habbitts [1]. This model allows one to analyse the actual operation of an air-heater. By changing profile designs fictitiously in the program, the effects on the overall heat transfer and the pressure drop can be observed. This allows the operation of the air heater to be optimised. When more erosion data is available the influence of erosion on the heat transfer and pressure drop behaviour should be evaluated with the help of this program.

Even if the whole range of available plate designs have been tested some features need further investigation:

- Individuality of packs for all profile types (i.e. check that different pack types of the same profile have the same thermal performance)
- Influence of braces on the heat transfer coefficient for all profile types
- Influence of number of plates on the heat transfer coefficient and the pressures drop for all profile types
- Influence of the plate thickness on the heat transfer coefficient and the pressure drop
- Influence of the pack length on the heat transfer coefficient and the pressure drop
- More pack designs should be tested in the eroded state to establish firstly the procedure of handling the data of eroded plates and secondly verify the behaviour of eroded plates in terms of change in heat transfer and pressure drop.

Some recommendations can be made to improve the reliability of the test data and decrease the uncertainties:

- Due to the problems experienced with the 16 thermocouples, which measure the inlet and outlet temperature histories, it is recommended that this situation be improved. There are three possibilities, firstly, all the thermocouples could be changed, secondly, more thermocouples could be installed in the cross sectional area, or thirdly, a grid of resistance wire could be installed in the cross sectional area, which measures the average temperature of the fluid stream. In the literature [9, 11] the number of thermocouples installed in the flow area vary between 2 and 20.
- To ensure that the test section is adiabatic, the side walls also need to be insulated with polystyrene and not only the bottom and the top of the test pack.
- To decrease the error of determining the heat transfer coefficient from the temperature histories, the heating period should be shortened (see Appendix E).

After all investigations related to the different types of heating plates have been completed, an overall assessment of the different designs should be undertaken. Therefore several features such as thermal and hydraulic performance as new packs, tendency to erosion, thermal and hydraulic performance at an eroded stage and tendency to blockage have to be taken into account.

Capital cost of packing, the number of re-packings required as well as boiler efficiency and fan power consumption determine the life cycle cost of the system. Prediction of the above parameters will lead to an improvement in cost effectiveness of the air heater.

In addition to the heat transfer and pressure drop measurements on existing plate geometries it is proposed to carry out computational fluid dynamics modelling (CFD) on heating element plates. A successful modelling of air heater elements using CFD would lead to an enhanced understanding of the dynamics of heat transfer and pressure loss for new and existing pack designs as well as for eroded packs. As part of the present project a CFD solution should be developed to predict heat transfer and pressure loss firstly for flat plates. The results of the CFD model should be verified against measurements taken in the TTF. The choice of a suitable turbulence model largely determines the success of the CFD model. These results of the CFD work should be basis for further work in predicting more complex element designs. If successful, this technology could lead to a more economic air heater element design tool. It would also promote the prediction of element erosion behaviour.

Appendix A

Difficulties encountered during the progress of work

As mentioned earlier, the Thermal Test Facility has been in operation for several years. Over the last year several checks were made to compare the accuracy of the test facility. Additional factors were taken into account to give more accurate results. Some mistakes were identified and corrected during this period.

For comparison with results from literature, graphs either at normal conditions (0°C, 1013 mbar) or graphs in dimensionless units must be compared, i.e., Colburn- and Friction-factor vs. Re-number, Nu-number vs. Re-number. Therefore it is important to use the correct fluid properties at laboratory conditions. These fluid properties are: density, kinematic viscosity, Pr-number, specific heat capacity and heat conductivity. The air-density has a significant influence on the calculation of the dimensionless numbers. Therefore the humidity of the laboratory air has to be measured to get the correct value of the air-density.

Tests were done to compare the accuracy of the differential pressure transducer (pressure drop across the test section) with a BETZ-Manometer. Their results showed exact agreement between both devices.

There was concern that the pressure tappings were too close to the test section, especially after the pack. It was suspected that there was not enough flow length to allow the dynamic pressure to stabilise and transform to static pressure, with the result that readings at this point could be too low.
When the pressure tappings were moved further downstream, the thermocouples and their radiation shields were in between the pack and the tapping points. These however, added more resistance to the flow and resulted in a higher pressure drop. This effect was however not quantified.

Towards the end of the present study (March - May 1998) the following errors were discovered:

- During the annual calibration of measuring equipment it was found that wrong corrections were programmed for the 17 thermocouples used to measure the inlet, outlet and the nozzle temperatures. The data acquisition system uses a program written in Labview. In this program the input values to indicate the types of the thermocouples and the values indicating the type of cold junction corrections were interchanged. Since the thermocouples were originally calibrated using a different program, now using the Labview Program 97 gives the incorrect output values in °C. The temperature readings for temperatures above ambient were too low and for below ambient they were too high. At ambient temperature the readings were almost correct, which is why this error was not discovered earlier. At 40°C (true temperature) the faulty program indicated temperatures approximately 6°C lower.

- The Labview Program 97 was then corrected and the thermocouples re-calibrated. Test runs with the new Labview Program 98 (i.e. corrected program) and the new calibrations then showed much lower heat transfer coefficients than the old results (more than 10% lower).

- To be able to use the old results of more than 100 test runs done previously, it was decided to apply a correction function to the old temperature readings.

- The temperature calibration laboratory did an overall calibration for the correct temperatures using Labview Program 97, in order to determine a correction function that can be used to calculate the correct temperatures from the old temperatures.

- The new calculations of the heat transfer coefficient with the corrected temperatures did not give the same heat transfer coefficient as calculations with the new Labview Program 98 (the corrected results were less than 10% higher than the new results).

- To determine the reason why the corrected temperatures did not give similar results of the heat transfer coefficient as measurements with Labview 98, a sensitivity study regarding the temperature readings was undertaken. This study showed the following influences on the heat transfer coefficient when the temperature readings were artificially changed (like uncertainties). The following example was calculated for test run H8_an16.m (after new calibration)

Table A1: Influences of incorrect temperature readings on the heat transfer coefficient

description	heat transfer coef. [W/(m² K)]
original	77.73
$T_{inlet} - T_{outlet} = 0°C$ (before heating)	77.72
T_{outlet} +0.5°C	66.21
T_{outlet} +0.1°C	75.32
T_{outlet} -0.5°C	90.49
T_{outlet} -0.1°C	80.19
T_{inlet} +0.5°C	90.49
T_{inlet} +0.1°C	80.19
T_{inlet} -0.5°C	66.21
T_{inlet} -0.1°C	75.32
T_{inlet} +0.5°C and T_{outlet} +0.5°C	77.73

- This study shows that the influence of incorrect temperature readings has a major influence on the calculation of the heat transfer coefficient. A difference of only 0.5°C in the average temperature measured upstream or downstream results in a change of the heat transfer coefficient of more than 10%.

- Therefore a study of the correction calibration (calibration i.e. values using faulty Labview program 97) of each thermocouple was undertaken. This showed that calibration values for three of the 16 thermocouples were inconsistent with the calibration values of the other thermocouples. The temperatures they indicated are too high (2°C in 45°C). When these three thermocouples were excluded from the heat transfer calculation the heat transfer coefficient would go down, which is the correct direction. Both the average of the inlet and the average of the outlet temperature would go down. However, since two of the faulty thermocouples were at the inlet and the other one at the outlet the inlet temperature was reduced more than outlet temperature (two thermocouples too high), with the results that the heat transfer coefficient was reduced (see table A1).

- There were two possibilities to correct for the faulty three thermocouples, either use only the 6 correct inlet and 7 correct outlet temperatures to calculate the heat transfer coefficient or derive a corrected average correlation to replace the calibration of the three faulty thermocouples. In the latter case the heat transfer coefficient could then be calculated using corrected values for 8 thermocouples upstream and 8 thermocouples downstream of the test pack.

- To determine if the aforementioned considerations with regards to the thermocouples give the same heat transfer coefficient as Labview Program 98 it was decided to use firstly the more easier method to use only 6 inlet and 7 temperatures. The results of each of two test points (high and lower mass flow) for two different profile types are shown in the following table (table A2).

Table A2: Heat transfer coefficients for different temperature calibrations

Flat plates	
low mass flow:	
FF_7_97 (before calibration)	h = 41.57 W/(m² K)
FF_7_97 (wrong correction)	h = 40.51 W/(m² K)
FF_7_97 (without 3 thermocouples)	h = 39.10 W/(m² K)
FF_7_98 (corrected program)	h = 37.68 W/(m² K)
high mass flow:	
FF_16_97 (before calibration)	h = 66.60 W/(m² K)
FF_16_97 (wrong correction)	h = 65.26 W/(m² K)
FF_16_97 (without 3 thermocouples)	h = 63.81 W/(m² K)
FF_16_98 (corrected program)	h = 62.20 W/(m² K)

H8 profile	
low mass flow:	
H8_7_97 (before calibration)	h = 55.70 W/(m² K)
H8_7_97 (wrong correction)	h = 54.11 W/(m² K)
H8_7_97 (without 3 thermocouples)	h = 51.88 W/(m² K)
H8_7_98 (corrected program)	h = 51.35 W/(m² K)
high mass flow:	
H8_16_97 (before calibration)	h = 84.43 W/(m² K)
H8_16_97 (wrong correction)	h = 82.84 W/(m² K)
H8_16_97 (without 3 thermocouples)	h = 80.69 W/(m² K)
H8_16_98 (corrected program)	h = 81.45 W/(m² K)

- The new corrected heat transfer coefficient was now within 1% compared with the Labview Program 98 results, see table A2.

- For the whole range of test runs it was however decided to apply an average correlation function on the three wrong calibrated thermocouples, because of following reason. Firstly the positions of the 8 thermocouples at the inlet and the 8 thermocouples at the outlet is important.

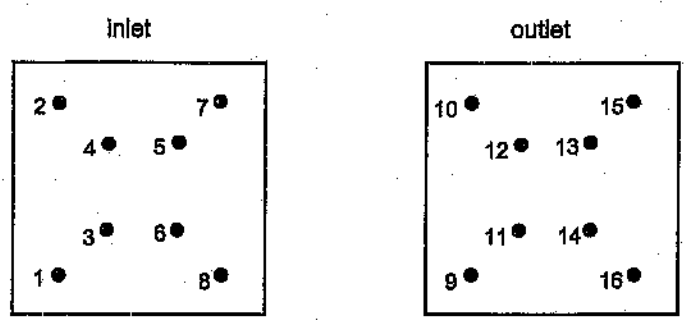

Figure A1: Arrangement of the thermocouples at the inlet and the outlet of the test section, flow into the picture

Due to not absolutely ideal adiabatic conditions in the duct the outermost thermocouples at the inlet show slightly lower temperatures (+/- 1°C) than the inner thermocouples. Consequently the outermost thermocouples at the outlet also show lower temperature readings than the inner ones. It was found that this spread is even more significant for packs with braces (until now no explanation could be found for this behaviour).

Because of this spread of temperatures, it was found that using the average inlet temperature without two thermocouples and the average outlet temperature without one thermocouple did not represent the real average of 8 inlet and 8 outlet thermocouples. Considering the sensitivity of incorrect temperature readings (see table A1) it was decided to derive an average calibration function, so that the values of the 3 wrong calibrated thermocouples could be substituted.

- Comparisons at ambient temperature showed that the thermocouples after the calibration are much more stable. The variations between the 16 thermocouples are now within +/-0.2°C, whereas before the calibration the variation was greater.

Temperature readings without flow at ambient conditions (after calibration):
Since the temperature in the laboratory varies from the ground to the ceiling of 4°C, it is understandable why the temperatures in the duct vary of 0.5°C between the bottom and the top.

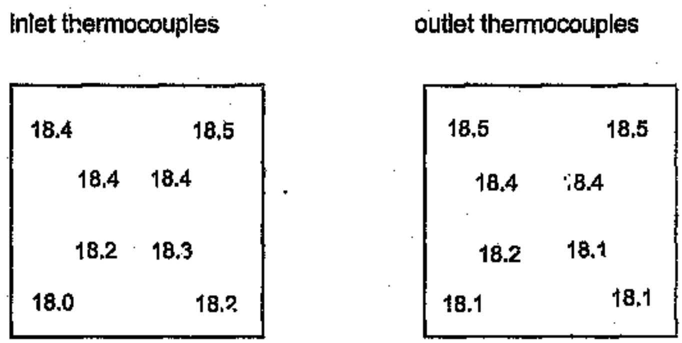

Figure A2: Temperature readings without flow at ambient conditions
(after calibration)

- While stripping the whole ring to look for general uncertainties some small amounts of leakage were found in the rig, which is now sealed.

- In the original Matlab calculation programs the incorrect viscosity for calculating the Re-number (kinematic instead of dynamic) was used. Fortunately this calculation of the Re-number is only used in the mass flow calculation, i.e. to obtain the coefficient of discharge. Here the value of the Re-number has only a small influence. This had very little influence on final results (Co-factor and Re-number) previously calculated, since the Reynolds-numbers were re-calculated undependable again in the correct manner in an Excel-spreadsheet.

- In the calculation for the coefficient of discharge another mistake was found, instead of the pipe Re-number the nozzle Re-number was used (in the Matlab program prepdat.m).

- In the mass flow equation (International Standard ISO 5167)

$$\dot{m} = C \cdot E \cdot \varepsilon \cdot \frac{\pi}{4} \cdot d^2 \cdot \sqrt{2 \cdot \Delta p \cdot \rho} \qquad \text{(A1)}$$

two coefficients were omitted in the original mass flow calculation:

- velocity approach factor E

$$E = (1 - \beta^4)^{-1/2} \qquad \text{(A2)}$$

- expansion factor ε

$$\varepsilon=\left[\left(\frac{\kappa\cdot\tau^{\frac{2}{\kappa}}}{\kappa-1}\right)\cdot\left(\frac{1-\beta^4}{1-\beta^4\tau^{\frac{2}{\tau}}}\right)\left(\frac{1-\tau^{\frac{\kappa-1}{\kappa}}}{1-\tau}\right)\right]^{\frac{1}{2}} \qquad \text{(A5)}$$

The effect of neglecting both coefficients together resulted in a 7% lower mass flow being calculated in previous tests. This has now been changed in the Matlab program prepdat.m.

- In the above mentioned equation for the expansion factor ε, τ represents the ratio of the absolute static pressure before and after the nozzle. At the moment these values are not available from the test rig. An approximation is made, which considers an average pressure ratio (for the minimum and the maximum mass flow). The resulting error for the mass flow is negligible (+/-0.1%);

- After all these corrections a pitot traverse was carried out across the duct upstream from the nozzle according to the standards. The mass flow calculation using the pitot traverse and the nozzle measurements show excellent agreement (+/-0.8%).

- The Re-number range for which the nozzle was calibrated is considerably different from that Re-number range which it is currently operating in the thermal rig. The calibrated range of the nozzle is Re = 400000 - 800000. In the TTF the nozzle is used at Re ≅ 20000 - 230000. According to Liebenberg [33] this extrapolation is acceptable.

- It was found that the turbulator in the test facility was installed upside down in comparison with the way it was fitted by Caby [26].

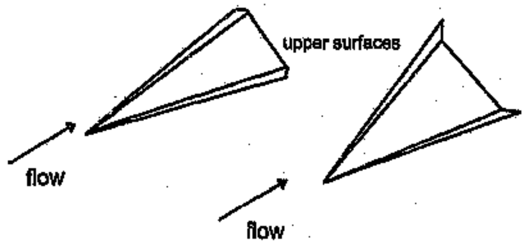

a.) b.)

Figure A3: a.) correct installation of the turbulator (wings down), b.) incorrect installation (wings up) of the turbulator, angle for both installations between turbulator and flow direction is 30° (original according to Caby [26].

When this problem was found, a study was undertaken concerning the effects of different installation configurations of the turbulator, i.e. right way round (wings down), upside down (wings up) for different angles and without turbulator. The velocity and temperature distribution was checked for each installed position at full mass flow; at half mass flow the results are the same. The results are described below.

1.) without turbulator

Pitot traverse [Pa]

63.8	96.8	93.8	72.8	59.4
74.4	111.7	108.2	80.6	64.9
70.3	76.8	74.3	62.2	43.6
37.4	45.1	46.8	43.1	34.9

(In all diagrams flow direction in the paper)

temperatures [°C]

inlet thermocouples

40.7			41.5
	42.8	42.6	
	42.8	43.4	
42.4			42.7

outlet thermocouples

40.5			40.9
	41.8	41.7	
	42.4	42.4	
42.3			42.4

2.) turbulator wings down, at 10° to the flow direction

Pitot traverse [Pa]

102.6	137.7	116.6	106.9	98.3
100.8	91.2	64.5	68.3	94.4
75.0	79.9	64.6	39.3	53.6
43.9	58.8	47.5	32.0	29.4

temperatures [°C]

Inlet thermocouples

40.4			40.4
	41.5	41.4	
	41.3	41.2	
40.6			40.8

outlet thermocouples

40.1			40.4
	41.2	41.2	
	41.2	41.1	
40.6			40.7

3.) turbulator wings down, at 20° to the flow direction

Pitot traverse [Pa]

110.1	98.5	76.9	87.0	103.1
105.2	78.0	69.4	67.6	111.8
67.7	81.0	67.5	46.2	73.8
42.6	50.8	48.2	32.7	39.9

temperatures [°C]

inlet thermocouples

41.4			41.5
	41.8	41.8	
	41.5	41.5	
40.8			41.1

outlet thermocouples

41.1			41.4
	41.8	41.7	
	41.4	41.4	
40.9			41.0

4.) turbulator wings down, at 30° to the flow direction

Pitot traverse [Pa]

103.8	77.5	71.4	74.9	83.0
108.9	93.1	80.6	75.1	109.0
77.9	81.7	63.7	49.0	76.5
40.8	54.7	47.8	32.7	40.0

temperatures [°C]

inlet thermocouples

42.1			42.3
	42.2	42.3	
	42.0	42.1	
41.6			41.8

outlet thermocouples

42.0			42.1
	42.0	42.2	
	41.9	42.0	
41.5			41.7

5.) turbulator wings up, at 10° to the flow direction

Pitot traverse [Pa]

88.1	128.7	117.8	98.3	86.4
91.3	102.3	81.0	68.2	78.1
64.6	84.0	71.2	46.0	42.4
35.9	60.6	59.4	45.2	30.7

temperatures [°C]

inlet thermocouples

41.2			41.3
	42.2	42.2	
	42.3	42.5	
41.7			42.4

outlet thermocouples

40.9			41.3
	41.9	42.0	
	42.0	42.2	
41.6			42.2

6.) turbulator wings up, at 20° to the flow direction

Pitot traverse [Pa]

109.6	105.1	88.8	89.5	94.4
101.9	90.2	73.6	58.7	84.2
71.0	80.8	68.8	49.0	53.9
39.3	58.6	58.6	41.7	35.1

temperatures [°C]

inlet thermocouples

42.1			42.2
	42.6	42.7	
	42.8	42.8	
41.9			42.7

outlet thermocouples

41.8			42.2
	42.5	42.6	
	42.4	42.6	
41.9			42.6

7.) turbulator wings up, at 30° to the flow direction

Pitot traverse [Pa]

100.0	80.3	71.7	77.3	94.7
99.6	89.2	75.8	64.7	92.9
88.3	81.9	68.2	60.9	74.1
44.1	57.1	54.0	40.8	44.9

temperatures [°C]

inlet thermocouples

41.4			41.6
	41.7	41.8	
	41.6	41.8	
41.0			41.6

outlet thermocouples

41.3			41.5
	41.5	41.7	
	41.5	41.6	
41.0			41.5

Conclusions which can be drawn from these temperature and velocity distributions are follows:

- good repeatability of velocity and temperature measurements (not printed),
- no difference in temperature distribution when full or half mass flow (not printed),
- best temperature distribution if the turbulator has an angle at 30° to the flow direction for both configurations, wings up and wings down,
- best velocity distribution at an angle of 30°, for both configurations, wings up and wings down,
- if the turbulator is adjusted to smaller angles (wings down) the flow is concentrated on top of the flow channel,
- for the half mass flow the velocity distribution does not change that much when changing the angle of the turbulator,
- without the turbulator the temperature distribution is much worse ($\Delta t_{min-max}$=1.9°C),
- without the turbulator the velocity distribution is not uniform, similar to the distribution for turbulator angle of 0° (not printed),
- the measurements with the turbulator wings up at 30° show that both the velocity and the temperature distribution are slightly better than the configuration wings down at 30°,
- it should be concluded that these variations in the temperature and velocity distributions of the configuration wings and wings down do not effect the measurements of the pressure drop and the heat transfer coefficient, as can be seen in Figure A4 and Figure A5.

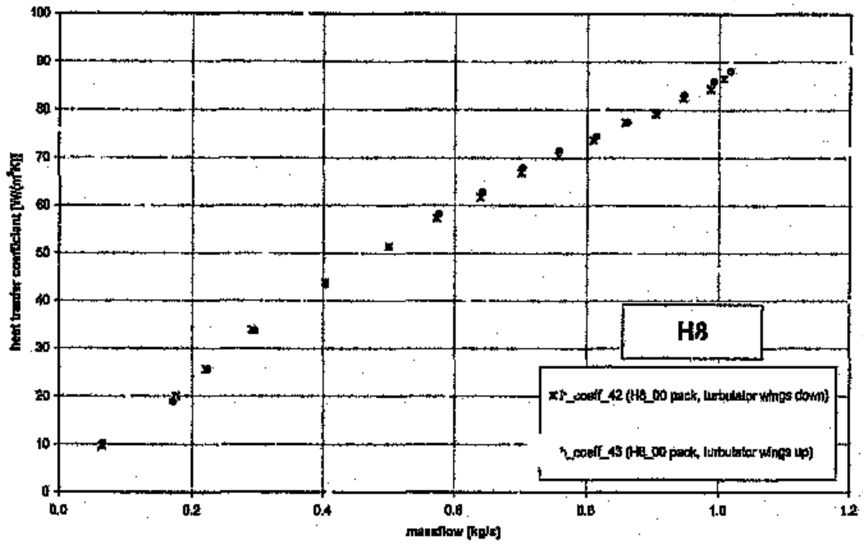

Figure A4: Heat transfer coefficient vs. mass flow, H8 profile, different installations of the turbulator at 30°

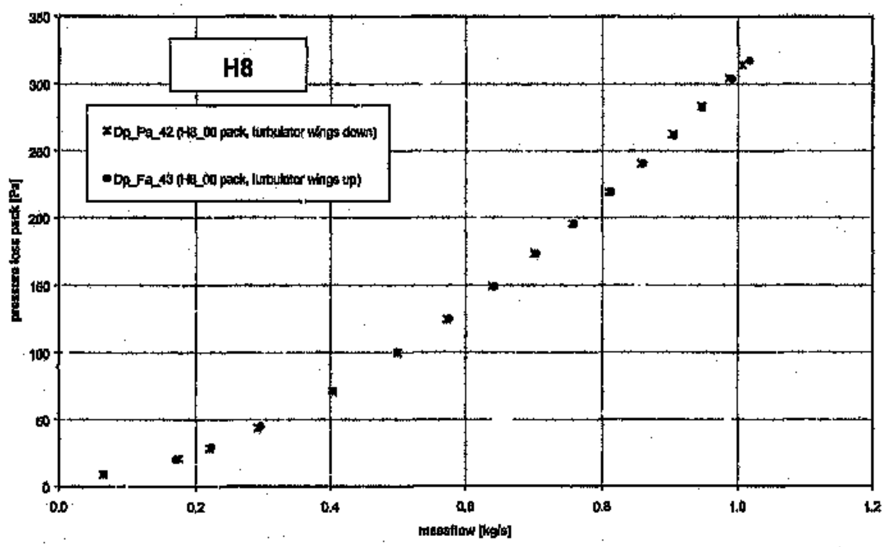

Figure A5: Pressure drop vs. mass flow, H8 profile, different installations of the turbulator at 30°

Even without the turbulator the heat transfer coefficient and the pressure drop do not change much

All these discovered problems and mistakes could lead the reader to the question, why was all this only discovered at the end of this study. The answer is, the present test rig and calculation method was already running for years when the present project started and the obtained results from former studies never gave any reason for suspicion and were therefore never doubted.

Appendix B

Matlab Programs

This appendix includes the Matlab programs for calculating the mass flow and the heat transfer coefficient from the raw experimental data

B1 Prepdat.m calculates mainly the mass flow

```
%**prepdat.m**
clc;
clear;
clear global;
disp('Formatting of Test Data for all test runs (preparation for htcoefa.m)');

%Data for input to this program is recorded by LABVIEW
%tst(1)=time
%tst(2) to tst(9)=air inlet temps to pack (°C)
%tst(10) to tst(17)=air outlet temps from pack (°C)
%tst(18)=air temp before nozzle (°C)
%tst(19)=pack differential pressure (Pa)
%tst(20)=nozzle differential pressure from MEDM (Pa)
%tst(21)=nozzle differential pressure from Furness(Pa)
%tst(22)=average of 'graph 1' temps (normally inlet temps)
%tst(23)=average of 'graph 2' temps (normally outlet temps + nozzle air temp)
%tst(24)=Lab atmospheric pressure (kPa)

%**(raw test data filename.m)**
% Location of the raw test data
% chdir [drive]:\[path]
chdir c:\kg\excel\thermal\results

% This is an edited ASCII file which contains the matrix 'tst'. This
% an m-file i.e. has a file extension = 'm'.
% Note: do not include the file extension when calling an m-file in
% Matlab source code, it is automatically assumed.
%[filename]

for k=1:16,
 clear tst;
 clear mMEDM;
 clear testdata;
 clear NozzleTair;
 clear NozzleDPMEDM;
 clear NozzleDPFC;
 clear PipeReMEDM;
```

```
clear LastCdMEDM;
clear LastCdFC;
clear AirViscosity;
clear packDP;
clear mFC;           %Furness controls
clear NozzleDPFC;    %[Pa]Furness controls
clear PipeReFC;      %Furness controls

%*****opening of test files***
if k==1,
  H8_a01
 elseif k==2
  H8_a02
 elseif k==3
  H8_a03
 elseif k==4
  H8_a04
 elseif k==5
  H8_a05
 elseif k==6
  H8_a06
 elseif k==7
  H8_a07
 elseif k==8
  H8_a08
 elseif k==9
  H8_a09
 elseif k==10
  H8_a10
 elseif k==11
  H8_a11
 elseif k==12
  H8_a12
 elseif k==13
  H8_a13
 elseif k==14
  H8_a14
 elseif k==15
  H8_a15
 elseif k==16
  H8_a16
end

%**Time domain**
% Check that the first two header rows have been deleted in the input file
if tst(1,1)==0  %Then they have been deleted

  testdata(:,1)=tst(:,1);
```

```
%**Determining the average fluid inlet temperature profile
testdata(:,2)=(tst(:,2)+tst(:,3)+tst(:,4)+tst(:,5)+tst(:,6)+tst(:,7)+tst(:,8)+tst(:,9))/8;

%**Determining the average fluid exit temperature profile
testdata(:,3)=(tst(:,10)+tst(:,11)+tst(:,12)+tst(:,13)+tst(:,14)+tst(:,15)+tst(:,16)+tst(:,17))/8;

%**Nozzle mass flow rate
NozzleDiameter=0.235972;              %[m]
PipeDiameter=0.394657;                %[m]
g=9.79;                               %[m/s²]
%LabPr~ss=13.6*LabPress*g;            %[Pa] Baro press. i.e. converting from mmHg to Pa
%LabPress=84.002*1000;                %[Pa] Baro Press.
LabPress=tst(1,24)*1000;              %[Pa] Baro Press. i.e. converting from kPa to Pa
R=287;                                %Specific gas constant [J/(mol K)]
kappa=1.4;                            %Isentropic exponent [-]
tau=(LabPress+1046)/(LabPress+1206);%absolute static pressure ratio between before and
                                      after the nozzle (min - max. flow) [-]
                                      %this is only an approx. value, not correct!!!!!
E=(1-(NozzleDiameter/PipeDiameter)^4)^(-0.5);
                                      %Velocity Approach Factor
 epsilon=((kappa*tau^(2/kappa)/(kappa-1))*((1-(NozzleDiameter/PipeDiameter)^4)/(1-
(NozzleDiameter/PipeDiameter)^4*tau^(2/kappa)))*((1-tau^((kappa-1)/kappa))/(1-tau)))^0.5;
                                      %expansion factor [-]

for i=1:length(tst),
  %tst(20)=nozzle differential pressure (MEDM) (Pa)
  %tst(21)=nozzle differential pressure (Furness) (Pa)
  NozzleDPMEDM(i)=tst(i,20);          %[Pa] MEDM
  NozzleDPFC(i)=tst(i,21);            %[Pa] Furness Controls
  packDP(i)=tst(i,19);                %[Pa] from Schaevitz
  CdMEDM(i,1)=0.976;                  %initial guess for nozzle Cd
  CdFC(i,1)=0.976;                    %initial guess for nozzle Cd
  NozzleTair(i)=tst(i,18);            %Air temp just before nozzle
  AirKelvin=NozzleTair(i)+273.15;

  %The following formula calculated for the range 275 - 400 Kelvin using data from
  %the table in "findcoef.m" , kinematic viscosity, equation is accurate enough
 AirViscosity(i)=9.5142855726E-11*AirKelvin^2+3.561857242e-8*AirKelvin-3.5620716252e-6;
 AirDensity=(LabPress/(R*(NozzleTair(i)+273.15)));

  for j=1:5,   %looping 5 times should enable us to get a good enough estimate of true Cd
mMEDM(i)=CdMEDM(i,j)*E*epsilon*(pi/4)*NozzleDiameter^2*sqrt(2*NozzleDPMEDM(i)*AirDe
nsity);                               %MEDM
   PipeReMEDM(i)=4*mMEDM(i)/pi/PipeDiameter/AirViscosity(i)/AirDensity;
                                      %MEDM
   %The following formula got from nozzle calibration certificate
   CdMEDM(i,j+1)=0.98419-0.06426*sqrt(10000/PipeReMEDM(i));
                                      %MEDM
```

```
mFC(i)=CdFC(i,j)*E*epsilon*(pi/4)*NozzleDiameter^2*sqrt(2*NozzleDPFC(i)*AirDensity);
                                          %Furness controls
   PipeReFC(i)=4*mFC(i)/pi/PipeDiameter/AirViscosity(i)/AirDensity;
                                          %Furness controls
   %The following formula got from nozzle calibration certificate
   CdFC(i,j+1)=0.98419-0.06426*sqrt(10000/PipeReFC(i));
                                          %Furness controls
  end

LastCdMEDM(i)=CdMEDM(i,5);                %MEDM
LastCdFC(i)=CdFC(i,5);                    %Furness controls
end

testdata(:,4)=mMEDM';                     %MEDM
testdata(:,5)=NozzleTair';
testdata(:,6)=NozzleDPMEDM';              %[Pa] MEDM
testdata(:,7)=PipeReMEDM';                %MEDM
testdata(:,8)=LastCdMEDM';
testdata(:,9)=AirViscosity';              %kinematic [m^2/s]
testdata(:,10)=packDP';
testdata(:,11)=mFC';                      %Furness controls
testdata(:,12)=NozzleDPFC';               %[Pa] Furness controls
testdata(:,13)=PipeReFC';                 %Furness controls

 % Save the formatted test data in a mat-file containing the matrix
 % testdata. This file will be used in e.g. heatcoef.m to iteratively
 % solve for the heat transfer coefficient.
 %save [drive]:\[path]\[filename].mat testdata

 if k==1,
  save c:\kg\excel\thermal\results\H8_a01.mat testdata LabPress
 elseif k==2
  save c:\kg\excel\thermal\results\ H8_a02.mat testdata LabPress
 elseif k==3
  save c:\kg\excel\thermal\results\ H8_a03.mat testdata LabPress
 elseif k==4
  save c:\kg\excel\thermal\results\ H8_a04.mat testdata LabPress
 elseif k==5
  save c:\kg\excel\thermal\results\ H8_a05.mat testdata LabPress
 elseif k==6
  save c:\kg\excel\thermal\results\ H8_a06.mat testdata LabPress
 elseif k==7
  save c:\kg\excel\thermal\results\ H8_a07.mat testdata LabPress
 elseif k==8
  save c:\kg\excel\thermal\results\ H8_a08.mat testdata LabPress
 elseif k==9
  save c:\kg\excel\thermal\results\ H8_a09.mat testdata LabPress
 elseif k==10
  save c:\kg\excel\thermal\results\ H8_a10.mat testdata LabPress
 elseif k==11
```

```
  save c:\kg\excel\thermal\results\ H8_a11.mat testdata LabPress
 elseif k==12
  save c:\kg\excel\thermal\results\ H8_a12.mat testdata LabPress
 elseif k==13
  save c:\kg\excel\thermal\results\ H8_a13.mat testdata LabPress
 elseif k==14
  save c:\kg\excel\thermal\results\ H8_a14.mat testdata LabPress
 elseif k==15
  save c:\kg\excel\thermal\results\ H8_a15.mat testdata LabPress
 elseif k==16
  save c:\kg\excel\thermal\results\ H8_a16.mat testdata LabPress
end

else %first 2 header rows were not deleted
 disp('First two header rows of input file were not deleted - operation cancelled');
end
end
chdir \kg\excel\thermal\results
```

B2 findcoef.m contains the iteration for the heat transfer coefficient

```
% Function call for findcoef.m
function error=findcoef(h);

% Global variables being passed from the main p    am e.g. Heatcoef.m.
global N freq. passdata              %findcoe.  puts
global k Cs Ar As Ms                 %matrix physical props
global error L a                     %findcoef outputs


%   Air properties at 1 atm in matrix form 'AIR'.
%       T       Cp          k           Pr      rho     nu
%       K       kJ/(kg K)   W/(m K)     -       kg/m³   m²/s

AIR=[250 1.0031 2.227e-2 0.720 1.412  1.132e-5;
    275 1.0038 2.428e-2 0.713 1.284  1.343e-5;
    300 1.0049 2.624e-2 0.707 1.177  1.568e-5;
    325 1.0063 2.816e-2 0.701 1.086  1.807e-5;
    350 1.0082 3.003e-2 0.697 1.009  2.056e-5;
    375 1.0106 3.186e-2 0.692 0.9413 2.317e-5;
    400 1.0135 3.365e-2 0.688 0.8824 2.591e-5;
    450 1.0206 3.710e-2 0.684 0.7844 3.168e-5;
    500 1.0295 4.041e-2 0.680 0.7060 3.782e-5;
    550 1.0398 4.357e-2 0.680 0.6418 4.439e-5;
    600 1.0511 4.661e-2 0.680 0.5883 5.128e-5;
    650 1.0629 4.954e-2 0.682 0.5430 5.853e-5;
    700 1.0750 5.236e-2 0.684 0.5043 6.607e-5;
    750 1.0870 5.509e-2 0.687 0.4706 7.399e-5;
    800 1.0987 5.774e-2 0.690 0.4412 8.214e-5];

%****FUNCTION PROGRAM****

%**(time domain)**
t=passdata(:,1);
%tst=passdata(1,1);
tlength=length(t);
dt=1/freq;                           %[sec]

Ti=passdata(1,2);                    %[°C] initial fluid & solid temperature
Tfm=passdata(tlength,2);             %[°C] maximum stable fluid temperature
Tb=0.5*(passdata(1,2)+passdata(1,3));

%**(fluid properties at Tb)**
Cf=(inter(Tb+273.15,AIR,2))*1e3;     %[J/kg/K]
m=passdata(:,4);                     %[kg/s]

%**(dimensionless time domain)**
td(1)=((m(1)*Cf)/(Ms*Cs))*t(1);
```

```
%**(experimental fluid inlet function)**
Tfi=passdata(:,2);
Tfid=(Tfi-Ti)/(Tfm-Ti);

%**(experimental fluid exit function)**
Tfee=passdata(:,3);
Tfeed=(Tfee-Ti)/(Tfm-Ti);

%**(construction of node network)**
dx=L/N;                                  %[m]
dxd=1/N;                                 %[dim]

%**(setting initial boundary conditions)**
Tsold=ones(1,N).*Tfid(1);
Tfold=ones(1,N).*Tfid(1);

Tsed(1)=Tfid(1);
Tfed(1)=Tfid(1);

%**(time step)**
for tstep = 2:tlength,

  %**(dimensionless time domain)**
  Tb=0.5*(Tfi(tstep)+Tfee(tstep));
  Cf=(Inter(Tb+273.15,AIR,2))*1e3;       %[J/(kg K)]
  dtd=((m(tstep)*Cf)/(Ms*Cs))*dt;
  td(tstep)=((m(tstep)*Cf)/(Ms*Cs))*t(tstep);

  %**(non-dimensionalised groups)**
  lamda=(k*As)/(m(tstep)*Cf*L);
  Ntu=(h*Ar)/(m(tstep)*Cf);
  Rs1=(lamda*dtd)/(2*(dxd)^2);
  Rs2=Ntu*dtd;
  Rf=Ntu*dxd;

  %**(tridiagonal matrix {H})**
  main=ones(1,N).*(1+2*Rs1);

  submain=ones(1,N-1).*(-Rs1);

  H=diag(submain,1) + diag(main,0) + diag(submain,-1);
  H(1,1)=H(1,1)-Rs1;
  H(N,N)=H(N,N)-Rs1;
```

```
 for M = 1:N,
  if M == 1 | M == N
   A(M)=(1-Rs1-Rs2)*Tsold(M);
  else
   A(M)=(1-2*Rs1-Rs2)*Tsold(M);
  end

  if M == 1
   B(1)=(Rs1)*Tsold(2);
  elseif M == N
   B(M)=(Rs1)*Tsold(M-1);
  else
   B(M)=(Rs1)*(Tsold(M-1)+Tsold(M+1));
  end

  if M == 1
   C(M)=(Rs2)*Tfld(tstep-1);
  else
   C(M)=(Rs2)*Tfold(M);
  end
 end

 D=A+B+C;
 D=D';

 Tsnew=H\D;

 for P = 1:N,
  if P == 1
   Tfnew(1)=Tfld(tstep);
  else
   Tfnew(P)=((Rf*Tsnew(P))+Tfnew(P-1))/(1+Rf);
  end
 end

 Tsed(tstep)=Tsnew(N);
 Tfed(tstep)=Tfnew(N);
 Tsold=Tsnew;
 Tfold=Tfnew;

end

% Difference array between the experimental and predicted air
% temperature vs. time profiles.
difference=Tfed-Tfeed';

% Normalising the difference array.
error=norm((difference),'fro');
```

B3 htcoef.m calculates the heat transfer coefficient, uses findcoef.m

```
%***htcoef.m****
%for running please switch off power save (screen) and perhaps screen saver
clc;
clear;
clear global;
disp('HEAT TRANSFER PERFORMANCE COEFFICIENT  -original-');

%****DEFINED INPUTS****

N=50;                   % Number of nodes
freq=3;                 % Data acquisition rate [Hz]
initguessFC=50;         % Initial guess for convective H/T coeff [W/(m² K)]
initguessMEDM=50;       % Initial guess for convective H/T coeff [W/(m² K)]
k=64;                   % Matrix thermal conductive coeff [W/(m K)]
Cs=458.8;               % Matrix specific heat [J/(kg K)]
R=287;                  % specific gas constant  [J/(kg K)]
disp('The following calculations assume the following values:');
disp('     N=50;          % Number of nodes');
disp('     freq=3;        % Data acquisition rate [Hz]');
disp('     Initguess=50;  % Initial guess for convective H/T coeff [W/(m² K)]');
disp('     k=64;          % Matrix thermal conductive coeff [W/(m K)]');
disp('     Cs=458.8;      % Matrix specific heat [J/(kg K)]');
disp('     PackLength=0.5; %[m]');
disp('     NozzleDiameter=0.235972; %[m]');
disp('     ************************* ');

Ms=input('Enter matrix mass [kg]:35.89: ');
Ar=input('Enter matrix H/T area [m²]:18.222: ');
As=input('Enter matrix X-sectional area available for heat conduction [m²]:9.111e-3: ');

% Length of the test pack or plates in [m].
L=0.5;

% Half-plate thickness of the plates constituting the pack in [m].
% a=0.25e-3;

for i=1:16,
% where XX is the number of test runs.

  % Location of the test data mat-files.
  % chdir [drive]:\[path]
  chdir \kg\excel\thermal\results
```

```
% Test data should be called in order of ascending or descending
% mass flow rates. This allows the program to more efficiently
% solve the heat transfer coefficient from one test run to the
% next.
if i==1,
  load H8_a01.mat
elseif i==2
  load H8_a02.mat
elseif i==3
  load H8_a03.mat
elseif i==4
  load H8_a04.mat
elseif i==5
  load H8_a05.mat
elseif i==6
  load H8_a06.mat
elseif i==7
  load H8_a07.mat
elseif i==8
  load H8_a08.mat
elseif i==9
  load H8_a09.mat
elseif i==10
  load H8_a10.mat
elseif i==11
  load H8_a11.mat
elseif i==12
  load H8_a12.mat
elseif i==13
  load H8_a13.mat
elseif i==14
  load H8_a14.mat
elseif i==15
  load H8_a15.mat
elseif i==16
  load H8_a16.mat
end

%Set up array of pertinent data to be passed to 'findcoef'
passdata(:,1)=testdata(:,1);
passdata(:,2)=testdata(:,2);
passdata(:,3)=testdata(:,3);
passdata(:,4)=testdata(:,4);          %MEDM

% Global variables to be passed to the function findcoef.
global N freq passdata                %findcoef inputs
global k Cs Ar As Ms                  %matrix physical props
global error L a                      %findcoef outputs
```

```
% Location of the file findcoef.m
% chdir [drive]:\[path]
chdir \kg\calcu

% Minimising the error between the exit experimental and predicted
% air temperature vs. time profiles by manipulating the initial guess
% of the heat transfer coefficient entered by the user.
H_coeffMEDM=fmins('findcoef',initguessMEDM,[0,1e-2]);
errorMEDM=error;
%Optima=fmins('fndcffs',[initguess ; initguess2 ; initguess3],[0,1e-1]);

% To facilitate a quicker solution of subsequent test runs the
% solution of the preceding test run is submitted as an initial
% guess for the solution of the following test run.
initguessMEDM=H_coeffMEDM;

% For Furness controls
passdata(:,4)=testdata(:,11);
H_coeffFC=fmins('findcoef',initguessFC,[0,1e-2]);
errorFC=error;
initguessFC=H_coeffFC;

% Determining the average mass flow rate & air temp. & air viscosity over
% the entire test run. This is used in calculating the Colburn
% j-factor when presenting heat transfer results.
AvgMassflowFC=0;
AvgMassflowMEDM=0;
AvgNozzleAir=0;   %average air temperature upstream from nozzle (for nozzle calcs)
avgtemp=0;
for e=1:length(testdata),
  AvgMassflowFC=AvgMassflowFC+testdata(e,11);          %Furness Controls
  AvgMassflowMEDM=AvgMassflowMEDM+testdata(e,4);       %MEDM
  avgtemp=avgtemp+((testdata(e,2)+testdata(e,3))/2);
  AvgNozzleAir=AvgNozzleAir+testdata(e,5);
end
AvgMassflowFC=AvgMassflowFC/length(testdata);           %[kg/s]
AvgMassflowMEDM=AvgMassflowMEDM/length(testdata);       %[kg/s]
avgtemp=avgtemp/length(testdata);
AvgNozzleAirKelvin=AvgNozzleAir/length(testdata)+273.15;

%The following formula calculated for the range 275 - 400 Kelvin using data of
%the table in "findcoef.m", equation is accurate enough
AvgAirViscosity=9.5142855726E-11*AvgNozzleAirKelvin^2+3.561857242e-
8*AvgNozzleAirKelvin-3.5620716252e-6;
AirDensity=(LabPress/(R*AvgNozzleAirKelvin));
% Determining the initial mass flow rate, air temp, packDP and nozzleDP before
% switching on the heaters. This is used in calculating the
% fanning friction factor when presenting pressure drop results.
InitMassflowFC=0;                                       %[kg/s]
InitMassflowMEDM=0;                                     %[kg/s]
```

```
 Initemp=0;
 InitNozzleDPFC=0;
 InitNozzleDPMEDM=0;
 InitPackDP=0;
 for s=1:10,
   InitMassflowFC=InitMassflowFC+testdata(s,11);              %Furness Controls
   InitMassflowMEDM=InitMassflowMEDM+testdata(s,4);           %MEDM
   Initemp=Initemp+((testdata(s,2)+testdata(s,3))/2);
   InitNozzleDPFC=InitNozzleDPFC+testdata(s,12);              %Furness Controls
   InitNozzleDPMEDM=InitNozzleDPMEDM+testdata(s,6);           %MEDM
   InitPackDP=InitPackDP+testdata(s,10);
 end
 InitMassflowFC=InitMassflowFC/10;
 InitMassflowMEDM=InitMassflowMEDM/10;
 Initemp=Initemp/10;
 InitNozzleDPFC=InitNozzleDPFC/10;                  %[Pa]
 InitNozzleDPMEDM=InitNozzleDPMEDM/10;              %[Pa]
 InitPackDP=InitPackDP/10;                          %[Pa]

% Determine Reynolds numbers in test pack and nozzle, and pack face vel.
 PackLength=0.5;                                    %[m]
 NozzleDiameter=0.235972;                           %[m]
 DuctArea=0.093025;                                 %[m^2] ie 0.305*0.305
 PackReFC=4*AvgMassflowFC*PackLength/Ar/AvgAirViscosity/AirDensity;
 NozzleReFC=4*AvgMassflowFC/pi/NozzleDiameter/AvgAirViscosity/AirDensity;
 PackFaceVelFC=AvgMassflowFC/DuctArea;
 PackReMEDM=4*AvgMassflowMEDM*PackLength/Ar/AvgAirViscosity/AirDensity;
 NozzleReMEDM=4*AvgMassflowMEDM/pi/NozzleDiameter/AvgAirViscosity/AirDensity;
 PackFaceVelMEDM=AvgMassflowMEDM/DuctArea;

 clear testdata;
% Storing results in a matrix form by the name of 'sol'.
 sol(i,1)=AvgMassflowFC;                            % average mass flow rate.
 sol(i,2)=H_coeffFC;                                % heat transfer coefficient.
 sol(i,3)=InitMassflowFC;                           % initial mass flow rate.
 sol(i,4)=InitPackDP;                               % initial pack ΔP [Pa].
 sol(i,5)=avgtemp;                                  % average air temperature.
 sol(i,6)=Initemp;                                  % initial air temperature.
 sol(i,7)=errorFC;                                  % normalised error between the
                                                    experimental and predicted air temp.
                                                    vs. time profiles.

 sol(i,8)=InitNozzleDPFC;                           % initial pressure drop across
                                                    nozzle [Pa].

 sol(i,9)=LabPress/1000;                            % Lab barometric pressure [kPa].
 sol(i,10)=PackReFC;                                % Pack Reynolds number.
 sol(i,11)=NozzleReFC;                              % Nozzle Reynolds number.
 sol(i,12)=PackFaceVelFC;                           % Pack face velocity [m/s].
 sol(i,13)=N;                                       % number of nodes
 sol(i,14)=freq;                                    % data acquisition rate [Hz]
```

```
  sol(i,15)=k;                          % matrix thermal conductivity
                                        [W/(m K)]
  sol(i,16)=Cs;                         % matrix specific heat capacity
                                        [J/(kg K)]
  sol(i,17)=Ms;                         % pack mass [kg]
  sol(i,18)=Ar;                         % matrix heat transfer area [m^2]
  sol(i,19)=As;                         % matrix cross sectional area
                                        available for heat conduction
  sol(i,20)=AvgMassflowMEDM;            % average mass flow rate.
  sol(i,21)=H_coeffMEDM;                % heat transfer coefficient.
  sol(i,22)=InitMassflowMEDM;           % initial mass flow rate.
  sol(i,23)=errorMEDM;                  % normalised error between the
                                        experimental and predicted air temp.
                                        vs. time profiles.
  sol(i,24)=InitNozzleDPMEDM;           % initial pressure drop across
                                        nozzle [Pa].
  sol(i,25)=PackReMEDM;                 % pack Reynolds number.
  sol(i,26)=NozzleReMEDM;               % nozzle Reynolds number.
  sol(i,27)=PackFaceVelMEDM;            % pack face velocity [m/s].

  %Set up a matrix to display certain channels only during runtime
  mydisp(i,1)=sol(i,1);
  mydisp(i,2)=sol(i,2);
  mydisp(i,3)=sol(i,7);
  mydisp(i,4)=sol(i,8);
  mydisp(i,5)=sol(i,10)/100;
  mydisp(i,6)=sol(i,11)/10000;
  mydisp(i,7)=sol(i,12)

  % Save the results to an output file [filename].mat containing
  % the matrix 'sol'. Do not alter the file extension or the subsequent
  % matrix description 'sol'. This is a backup file which gets written
  % every time a result from a test run have beer. determined.
  % save [drive]:\[path]\[filename].mat sol
  save \kg\excel\thermal\results\tempsol.txt sol -ascii

  % Purge memory of all data to ensure that calculations for the
  % subsequent test run are not influenced by data left in memory
  % from the preceding test run.
  clear global passdata testdata error
end

% Save the results of the program
save \kg\excel\thermal\results\H8_a.txt sol -ascii
```

Appendix C

No.	Date	Pack type	Test name	Test number	Braces (with or without)	new or eroded	Pack no.	Super-visor	Comments
Table of test runs at the thermal test facility TTF									
01	04.03.97	H8	H8_x (b)	1	without	new	H8_00	Njabulo	first calculation was with wrong mass initial name: h8bsol, data sheet missing
02	12.03.97	H8	H8_n	2	without	new	H8_00	Njabulo	first calculation was with wrong mass flow control was not working well
03	14.03.97	H8	H8_j	3	without	new	H8_00	Njabulo	first calculation. with wrong mass, FC not connected, 1st Betz and press. trans. both inner tappings
04	08.04.97	KH11	KH11_a	1	with	new	KH11_02	Njabulo	all 3 curves match perfect, round bra., door clo.
05	10.04.97	KH11	KH11_b	2	with	new	KH11_02	Njabulo	all 3 runs agree with Caby, round bra., door clo.
06	11.04.97	KH11	KH11_c	3	with	new	KH11_02	Njabulo	door closed, round braces
07	24.03.97	K6	K6_n	1	with	new	K6_01	Njabulo	mass = mass_tot - mass_braces_calc. FC prob. out of order,
08	26.03.97	K6	K6_j	2	with	new	K6_01	Njabulo	mass = mass_tot - mass_braces_calc. Betz a. press. trans. both inner tappings, door op.
09	01.04.97	K6	K6_b	3	with	new	K6_01	Njabulo	mass = mass_tot - mass_braces_calc. slid. door op., new motherboard, humid. measured, Betz a. press. trans. inner tappings
10	02.04.97	K6	K6_c	4	with	new	K6_01	Njabulo	mass = mass_tot - mass_braces_calc. slid. door op., Betz a. press. trans. inner tappings
11	04.04.97	K6	K6_f	5	with	new	K6_01	Njabulo	mass = mass_tot - mass_braces_calc. door closed, Betz a. press. trans. inner tappings
12	14.04.97	K6	K6_z	6	with	new	K6_01	Njabulo	mass = mass_tot - mass_braces_calc. 1st Betz man. inner a. press. trans. outer tappings
13	16.04.97	K6	K6_g(1)	7	without	new	K6_01a	Njabulo	K6_g with measured mass, K6_g1 with mass=m_tot- m_brac_calc., Betz. inner, pr. tr. outer tappings, packing similar way
14	17.04.97	K6	K6_h	8	without	new	K6_01a	Njabulo	mass = mass_tot - mass_braces_calc. Betz man. inner and press. trans. outer tappings

Table of test runs at the thermal test facility TTF									
No.	Date	Pack type	Test name	Test number	Braces (with or without)	new or eroded	Pack no.	Supervisor	Comments
15	18.04.97	H8	H8_a	4	without	new	H8_00	Njabulo	verification but 1 additional pair (57 pairs of plates)
16	27.02.97	H8	H8	0	without	new	H8_00	Njabulo	no computer-results, 1st test after installation of new prc ram, FC are abnormal
17	24.04.97	H8	H8_b	5	without	new	H8_00	Njabulo	repetition of H8_a
18	30.04.97	H8	H8_c	6	with	new	H8_01	Njabulo	1st test with braces, 57 plates, but 1.9 kg less weight than H8_00 pack (braces already subtracted)
19	02.05.97	H8	H8_d	7	with	new	H8_01	Njabulo	repetition of H8_c
20	07.05.97	KH11	KH11_d	4	with	new	KH11_03	Njabulo	flat braces
21	12.05.97	KH11	KH11_e	5	with	new	KH11_03	Njabulo	repetition of KH11_d
22	13.05.97	KH11	KH11_f	6	without	new	KH11_03a	Njabulo	braces taken off from KH11_03
23	14.05.97	KH11	KH11_g	7	without	new	KH11_03a	Njabulo	repetition of KH11_f
24	15.05.97	KH11	KH11_h	8	without	new	KH11_03a	Njabulo	one additional pair of plates than KH11_f
25	16.05.97	KH11	KH11_I	9	without	new	KH11_03a	Njabulo	repetition of KH_h
26	20.05.97	Cheese grater	Chg_a	1	without	new	Chgr_01	Njabulo	1 st test
27	21.05.97	Cheese grater	Chg_b	2	without	new	Chgr_01	Njabulo	repetition of Chg_a, last measurement with Betz parallel
28	28.05.97	Cheese grater	Chg_c	3	without	new	Chgr_01	Themba	no MEDM and Betz-manometer, only measurem. at inner tappings (press. transd.)
29	29.05.97	Cheese grater	Chg_d	4	without	new	Chgr_01	Themba Richard	no MEDM and Betz-manometer, only measurem. at inner tappings (press. transd.), 5 test points

Table of test runs at the thermal test facility TTF									
No.	Date	Pack type	Test name	Test number	Braces (with or without)	new or eroded	Pack no.	Super-visor	Comments
30	09.06.97	H8	H8_e	8	without	new	H8_00	Nja.	without MEDM
31	12.06.97	KH11	KH11_j	10	without	new	KH11_03a	Nja.	checking test, without MEDM gap between plates and side wall test section
32	13.06.97	KH11	KH11_k	11	without	new	KH11_03a	Nja.	without MEDM, repetition of KH11_j gap between plates and side wall test section
33	19.06.97	KH11	KH11_l	12	without	new	KH11_03a	Nja.	without MEDM, wooden plate between plates and side wall test section
34	23.06.97	278DU	278DU_a	1	without	new	278DU_01a	Rich.	wrong MEDM, braces are cut off
35	23.06.97	278DU	278DU_b	2	without	new	278DU_01a	Rich.	wrong MEDM, braces are cut off
36	25.06.97	V75	V75_a	1	without	new	V75_01a	Rich.	wrong MEDM, braces are cut off
37	25.06.97	V75	V75_b	2	without	new	V75_01a	Rich.	wrong MEDM, braces are cut off
38	27.06.97	278DU	278DU_c	3	with	new	278DU_02	Rich.	different test pack comp. to tests 278DU_a,b correct MEDM, pack for CAER
39	30.06.97	278DU	278DU_d	4	with	new	278DU_02	Rich.	as above, geometry taken from the pack 278DU_01
40	01.07.97	V75	V75_c	3	with	new	V75_02	Rich.	different test pack comp. to tests V75_a,b pack for CAER
41	01.07.97	V75	V75_d	4	with	new	V75_02	Rich.	as above, geometry taken from the pack V75_01
42	03.07.97	H8	H8_f	9	with	new	H8_02	Rich.	pack little bit rusty
43	03.07.97	H8	H8_g	10	with	new	H8_02	Rich.	repetition
44	04.07.97	KH11	KH11_m	13	with	new	KH11_04	Rich.	difficult to put the pack into the test section
45	04.07.97	KH11	KH11_n	14	with	new	KH11_04	Rich.	repetition

Table of test runs .. .e thermal test facility TTF									
No.	Date	Pack type	Test name	Test number	Braces (with or without)	new or eroded	Pack no.	Super -visor	Comments
46	08.07.97	H8	H8_h	11	with	new	H8_02	Richard	pack for CAER, Error max.: 0.15
47	08.07.97	H8	H8_l	12	with	new	H8_02	Richard	Error max.: 0.18
48	16.07.97	H8	H8_k	13	without	new	H8_00	Richard	RM pack repetition
49	18.07.97	H8	H8_l	14	with	new	H8_03	Kristina	new pack of store room, same geometry like H8_02, same results
50	18.07.97	H8	H8_m	15	with	new	H8_03	Kristina	repetition
51	22.07.97	278DU	D278_e	5	with	new	278DU_03	Kristina	new pack, no FC 1st time new and thicker insulation
52	23.07.97	278DU	D278_f	6	with	new	278DU_03	Kristina	repetition, no FC
53	25.07.97	V75	V75_e	5	with	new	V75_02a	Kristina	2 plates cut off, Betz installed
54	25.07.97	V75	V75_f	6	with	new	V75_02a	Kristina	repetition with Betz
55	26.07.97	H8	H8_p	16	with	new	H8_02a	Kristina	1 plate cut off
56	26.07.97	H8	H8_q	17	with	new	H8_02a	Kristina	repetition
57	30.07.97	KH11	KH11_p	15	with	new	KH11_04a	Kristina	2 plates cut off, braces grinded
58	31.07.97	KH11	KH11_q	16	with	new	KH11_04a	Kristina	repetition
59	01.08.97	278DU	D278_g	1e	with	20% er.	278DU_03	Kristina	1st test eroded pack, MEDM wrong
60	04.08.97	278DU	D278_h	2e	with	20% er.	278DU_03	Kristina	2nd test eroded pack, MEDM new batteries
61	06.08.97	H8	H8_r	1e	with	20% er.	H8_02a	Kristina	1st test eroded pack

Table of test runs at the thermal test facility TTF									
No.	Date	Pack type	Test name	Test number	Braces (with or without)	new or eroded	Pack no.	Super -visor	Comments
62	07.08.97	H8	H8_s	2e	with	20% er.	H8_02a	Kristina	2nd test eroded pack
63	08.08.97	V75	V75_g	1e	with	20% er.	V75_02a	Kristina	
64	11.08.97	V75	V75_h	2e	with	20% er.	V75_02a	Njabulo	
65	13.08.97	KH11	KH11_r	1e	with	20% er.	KH11_04a	Njabulo	
66	14.08.97	KH11	KH11_s	2e	with	20% er.	KH11_04a	Njabulo	fan bearing made noise
67	15.08.97	278DU	D278_i	3e	with	40% er.	278DU_03	Njabulo	Δp_{Pa} 10 Pa too low
68	18.08.97	278DU	D278_j	4e	with	40% er.	278DU_03	Njabulo	no higher mass flow possible (only until point 14) Δp_{Pa} 10 Pa too low
69	19.08.97	278DU	D278_k	7	with	new	278DU_04	Njabulo	only 13 meas. points possible Δp_{Pa} 10 Pa too low
70	20.08.97	278DU	D278_l	8	with	new	278DU_04	Njabulo	only 14 meas. points possible Δp_{Pa} 10 Pa too low
71	26.08.97	H8	H8_t	18	without	new	H8_04a	Njabulo	after cleaning the fan Δp_{Pa} 10 Pa too low
72	27.08.97	H8	H8_u	19	without	new	H8_04a	Njabulo	Δp_{Pa} 10 Pa too low
73	02.09.97	H8	H8_v	20	with	new	H8_04	Njabulo	pressure transducer pack new calibrated
74	03.09.97	H8	H8_w	21	with	new	H8_04	Njabulo	
75	05.09.97	278DU	D278_m	5e	with	40% er.	278DU_03	Njabulo	repetition, because of high error at former test runs
76	08.09.97	278DU	D278_n	6e	with	40% er.	278DU_03	Njabulo	
77	10.09.97	H8	H8_x	22	without	new	H8_00	Bheki	RM pack, repetition test

Table of test runs at the thermal test facility TTF									
No.	Date	Pack type	Test name	Test number	Braces (with or without)	new or eroded	Pack no.	Super -visor	Comments
78	11.09.97	KH10	KH10_a	1	with	new	KH10_01	Bheki	
79	12.09.97	KH10	Kh10_b	2	with	new	KH10_01	Bheki	
80	15.09.97	KH10	KH10_c	3	without	new	KH10_01a	Bheki	
81	16.09.97	KH10	KH10_d	4	without	new	KH10_01a	Bheki	
82	18.09.97	K4	K4_a	1	without	new	K4_01a	Bheki	only 14 test points
83	19.09.97	K4	K4_b	2	without	new	K4_01a	Bheki	
84	25.09.97	H8	H8_y	3e	with	30% er.	H8_02a	Bheki	
85	26.09.97	H8	H8_z	4e	with	30% er.	H8_02a	Bheki	
86	29.09.97	KH11	KH11_t	3e	with	30% er.	KH11_04a	Bheki	
87	29.09.97	KH11	KH11_u	4e	with	30% er.	KH11_04a	Bheki	
88	02.10.97	K4	K4_c	3	with	new	K4_01	Bheki	funny results for heat transfer coefficient calculated with MEDM
89	02.10.97	K4	K4_d	4	with	new	K4_01	Bheki	
90	06.10.97	V75	V75_I	3e	with	30% er.	V75_02a	Bheki	
91	06.10.97	V75	V75_J	4e	with	30% er.	V75_02a	Bheki	
92	09.10.97	K5	K5_a	1	without	new	K5_01a	Bheki	pressure transducer for measuring Dp across pack completely out of order (Dp_pack wrong)
93	10.10.97	K5	K5_b	2	without	new	K5_01a	Bheki	Dp_pack wrong

Table of test runs at the thermal test facility TTF									
No.	Date	Pack type	Test name	Test number	Braces (with or without)	new or eroded	Pack no.	Super -visor	Comments
94	13.10.97	K5	K5_c	3	with	new	K5_01	Bheki	Dp_pack wrong
95	14.10.97	K5	K5_d	4	with	new	K5_01	Bheki	Dp_pack wrong different MEDM in use => MEDM results wrong
96	15.10.97	K6G	K6G_a	1	without	new	K6G_01	Bheki	Dp_pack wrong MEDM results wrong
97	16.10.97	K6G	K6G_b	2	without	new	K6G_01	Bheki	Dp_pack wrong MEDM results wrong
98	20.10.97	H8	H8_aa	5e	with	40% er.	H8_02	Bheki	Dp_pack wrong MEDM results wrong
99	20.10.97	H8	H8_ab	6e	with	40% er.	H8_02	Bheki	Dp_pack wrong MEDM results wrong
100	21.10.97	DU278	D278_o	7e	with	30% er.	278DU_04	Bheki	Dp_pack wrong MEDM results wrong
101	21.10.97	DU278	D278_p	8e	with	30% er.	278DU_04	Bheki	Dp_pack wrong MEDM results wrong
102	22.10.97	KH11	KH11_v	5e	with	40% er.	KH11_04	Bheki	Dp_pack wrong MEDM results wrong
103	22.10.97	KH11	KH11_w	6e	with	40% er.	KH11_04	Bheki	Dp_pack wrong MEDM results wrong
104	23.10.97	K6G	K6G_c	3	with	new	K6G_01	Bheki	Dp_pack wrong MEDM results wrong
105	23.10.97	K6G	K6G_d	4	with	new	K6G_01	Bheki	Dp_pack wrong MEDM results wrong
106	30.10.97	H8	H8_ac	23	without	new	H8_05	Dakalo	Dp_pack wrong MEDM results wrong
107	30.10.97	H8	H8_ad	24	without	new	H8_05	Dakalo	Dp_pack wrong MEDM results wrong
108	03.11.97	H8	H8_ac1	25	without	new	H8_05	Dakalo	another pressure transducer (Dp_pack) in use our MEDM back, repetition of H8_ac

Table of test runs at the thermal test facility TTF									
No.	Date	Pack type	Test name	Test number	Braces (with or without)	new or eroded	Pack no.	Super -visor	Comments
109	04.11.97	H8	H8_ad1	26	without	new	H8_05	Bheki	repetition of H8_ad
110	05.11.97	K8	K8_a	1	without	new	K8_01a	Dakalo	
111	05.11.97	K8	K8_b	2	without	new	K8_01a	Dakalo	
112	06.11.97	H8	H8_ae	27	with	new	H8_05	Bheki	another H8 pack
113	06.11.97	H8	H8_af	28	with	new	H8_05	Bheki	
114	07.11.97	K8	K8_c	3	with	new	K8_01	Bheki	
115	07.11.97	K8	K8_d	4	with	new	K8_01	Bheki	
116	11.11.97	278DU	D278_o1	9e	with	30%	278DU_04	Dakalo	repetition of D278_o
117	11.11.97	278DU	D278_p1	10e	with	30 %	278DU_04	Bheki	repetition of D278_p
118	17.11.97	KH11	KH11_v1	7e	with	40 %	KH11_04	Dakalo	repetition of KH11_v
119	17.11.97	KH11	KH11_w1	8e	with	40 %	KH11_04	Dakalo	repetition of KH11_w
120	18.11.97	H8	H8_aa1	7e	with	40 %	H8_02	Dakalo	repetition of H8_aa, higher error than H8_aa h-values don't seem correct
121	18.11.97	H8	H8_ab1	8e	with	40 %	H8_02	Dakalo	repetition of H8_ab, higher error than H8_ab h-values don't seem correct
122	19.11.97	H8	H8_ag	9e	with	40 %	H8_02	Bheki	to check the h-values of H8_aa1 same as H8_aa1
123	19.11.97	H8	H8_ah	10e	with	40 %	H8_02	Bheki	to check the h-values of H8_ab1 same as h8_ab1
124	20.11.97	K5	K5_a1	5	without	new	K5_01	Dakalo	

Table of test runs at the thermal test facility TTF									
No.	**Date**	**Pack type**	**Test name**	**Test number**	**Braces (with or without)**	**new or eroded**	**Pack no.**	**Super -visor**	**Comments**
125	20.11.97	K5	K5_b1	6	without	new	K5_01	Dakalo	
126	24.11.97	K5	K5_c1	7	with	new	K5_01	Dakalo	
127	24.11.97	K5	K5_d1	8	with	new	K5_01	Dakalo	
128	25.11.97	K6G	K6G_a1	5	without	new	K6G_01	Dakalo	
129	25.11.97	K6G	K6G_b1	6	without	new	K6G_01	Dakalo	
130	27.11.97	K6G	K6G_c1	7	with	new	K6G_01	Dakalo	
131	27.11.97	K6G	K6G_d1	8	with	new	K6G_01	Dakalo	
132	28.11.97	Chgr	Chgr_e	5	without	new	Chgr_01	Dakalo	Dp_Pack higher as before
133	01.12.97	Chgr	Chgr_f	6	without	new	Chgr_01	Dakalo	Dp_Pack higher as before
134	02.12.97	K6G	K6G_e	9	without	new	K6G_02	Dakalo	
135	03.12.97	K6G	K6G_f	10	without	new	K6G_02	Dakalo	
136	05.12.97	K6G	K6G_g	11	with	new	K6G_02	Dakalo	
137	05.12.97	K6G	K6G_h	12	with	new	K6G_02	Dakalo	
138	08.12.97	H8	H8_ai	29	without	new	H8_00	Dakalo	Dp_betz = Dp_pressure transducer
139	08.12.97	H8	H8_aj	30	without	new	H8_00	Dakalo	Dp_betz = Dp_pressure transducer
140	10.12.97	Chgr	Chgr_g	7	without	new	Chgr_01	Dakalo	DpPack higher than before

Table of test runs at the thermal test facility TTF									
No.	Date	Pack type	Test name	Test number	Braces (with or without)	new or eroded	Pack no.	Super -visor	Comments
141	15.12.97	KH11	KH11_x	17	without	new	KH11_05	Dakalo	
142	15.12.97	KH11	KH11_y	18	without	new	KH11_05	Dakalo	
143	17.12.97	KH11	KH11_z	19	with	new	KH11_05	Dakalo	
144	17.12.97	KH11	KH11_aa	20	with	new	KH11_05	Dakalo	
145	05.01.98	K8G	K8G_a	1	without	new	K8G_01a	Dakalo	
146	05.01.98	K8G	K8G_b	2	without	new	K8G_01a	Dakalo	
147	06.01.98	K8G	K8G_c	3	with	new	K8G_01	Dakalo	
148	09.01.98	K8G	K8G_d	4	with	new	K8G_01	Dakalo	
149	19.01.98	278DU	D278_q	11e	with	40%	278DU_04	Bheki	2nd pack
150	20.01.98	278DU	D278_r	12e	with	40%	278DU_04	Bheki	2nd pack
151	21.01.98	V75	V75_k	5e	with	40%	V75_02	Bheki	
152	22.01.98	V75	V75_l	6e	with	40%	V75_02	Bheki	
153	04.02.98	FF	FF_a	1	rods	new	FF_01	Bheki	completely without holes
154	09.02.98	FF	FF_b	2	rods	new	FF_01	Bheki	completely without holes
155	11.02.98	FFh	FFh_a	1	rods	new	FFh-01	Bheki	completely with holes
156	11.02.98	FFh	FFh_b	2	rods	new	FFh_01	Bheki	completely with holes

Table of test runs at the thermal test facility TTF									
No.	Date	Pack type	Test name	Test number	Braces (with or without)	new or eroded	Pack no.	Super -visor	Comments
157	13.02.98	FFh	FFh_c	1	rods	new	FFh_02	Bheki	half with holes and half without holes
158	17.02.98	FFh	FFh_d	2	rods	new	FFh_02	Bheki	half with holes and half without holes
159	18.02.98	FFh	FFh_e	3	rods	new	FFh_01	Bheki	only holes

Appendix D

Profile	Influence of braces		Influence of form of braces		Influence of no. of plates		Influence of individuality	
	Δh	Δp_{Pa} (at 1 kg/s)	Δh	Δp_{Pa}	Δh	Δp_{Pa}	Δh	Δp_{Pa}
H8	$h_{with} > h_{without}$ (same pack)	$\Delta p_w > \Delta p_{wo}$ (30 Pa)	-	-	$h_{55} < h_{57}$ (RM-pack)	$p_{55} < p_{57}$	3 packs no (4th pack diff.)	3 packs no (4th pack diff.)
278DU	$h_{with} > h_{without}$ (diff. pack)	$\Delta p_w > \Delta p_{wo}$ (35 Pa)	-	-	-	-	3 packs yes	3 packs yes
KH11	$h_{withround} > h_{without}$ (diff. pack) $h_{withflat} = h_{without}$ (same pack)	$\Delta p_{w\_flat} = \Delta p_{w\_round} > \Delta p_{wo}$ (30 Pa)	$h_{round} > h_{flat}$ (slightly)	$\Delta p_{round} > \Delta p_{flat}$	$h_{61} = h_{63}$ (same pack, without braces)	$\Delta p_{61} < \Delta p_{63}$	2 packs yes	2 packs yes
KH10	$h_{with} > h_{without}$ (same pack)	$\Delta p_w > \Delta p_{wo}$ (30 Pa)	-	-	-	-	-	-
V75	$h_{with} = h_{without}$ (diff. pack)	$\Delta p_w > \Delta p_{wo}$ (35 Pa)	-	-	$h_{59} > h_{61}$ (diff. pack, with braces)	$\Delta p_{59} = \Delta p_{61}$ (10 Pa)	-	-
K4	$h_{with} > h_{without}$ (same pack)	$\Delta p_w > \Delta p_{wo}$ (40 Pa)	-	-	-	-	-	-
K5	$h_{with} > h_{without}$ (same pack)	$\Delta p_w > \Delta p_{wo}$ (55 Pa)	-	-	-	-	-	-
K6	$h_{with} = h_{without}$ (same pack, flat braces)	$\Delta p_w > \Delta p_{wo}$ (30 Pa)	-	-	-	-	-	-
K8	$h_{with} = h_{without}$ (same pack)	$\Delta p_w > \Delta p_{wo}$ (30 Pa)	-	-	-	-	-	-
K6G	$h_{with} < h_{without}$ (same pack)	$\Delta p_w > \Delta p_{wo}$ (30 Pa)						
K8G	$h_{with} = h_{without}$ (same pack)	$\Delta p_w > \Delta p_{wo}$ (40 Pa)	-	-	-	-	-	-

Appendix E

Uncertainty analysis

All data gained from experiments requires evaluation according to their uncertainties. In the present study an uncertainty analysis for presenting the results was undertaken for the pressure drop across the pack versus mass flow and heat transfer coefficient versus mass flow rate. The second analysis being for the Colburn-factor versus Reynolds-number and Friction-factor versus Reynolds-number. There are different forms of uncertainties. In the present study it has to be distinguished between measured uncertainties during the experiment, uncertainties in determining the geometry of the test pack and an error due to deviation from the mathematical model to calculate the heat transfer coefficient.

The uncertainty analysis in this section will be presented according to Kline and McClintock [34]. The mass flow rate in this sample calculation will be 1 kg/s and the test pack will be the H8-pack.

E1 Mass flow

The mass flow rate will be determined by following equation:

$$\dot{m} = C \cdot E \cdot e \cdot \frac{\pi}{4} \cdot d^2 \cdot \sqrt{2 \cdot \Delta p \cdot \rho} \qquad \text{(E1)}$$

with density defined as follows:

$$\rho = \frac{p_{stat}}{R \cdot T} \qquad \text{(E2)}$$

The considered uncertainties for the single elements are:

- Coefficient of discharge: $\frac{\partial C}{C} = 0.1\%$
- velocity approach factor: $\frac{\partial E}{E} = 0.1\%$
- expansion factor: $\frac{\partial e}{e} = 0.1\%$
- diameter: $\frac{\partial d}{d} = 0.4\%$
- pressure drop: $\frac{\partial \Delta p}{\Delta p} = 5.0\%$ (± 10Pa, calibration)
- static pressure: $\frac{\partial \Delta p_{stat}}{\Delta p_{stat}} = 0.011\%$
- air temperature: $\frac{\partial T}{T} = 0.17\%$

From these single uncertainties the uncertainties for the density and the mass flow can be determined:

- density:

$$\frac{\partial \rho}{\rho} = \sqrt{\left(\frac{\partial T}{T}\right)^2 + \left(\frac{\partial \Delta p_{stat}}{\Delta p_{stat}}\right)^2} \quad \text{(E3)}$$

$$= 0.17\%$$

- mass flow:

$$\frac{\partial \dot{m}}{\dot{m}} = \sqrt{\left(\frac{\partial C}{C}\right)^2 + \left(\frac{\partial E}{E}\right)^2 + \left(\frac{\partial e}{e}\right)^2 + \left(2\frac{\partial d}{d}\right)^2 + \left(\frac{1}{2}\frac{\partial \Delta p}{\Delta p}\right)^2 + \left(\frac{1}{2}\frac{\partial \rho}{\rho}\right)^2}$$

$$= 2.6\% \quad \text{(E4)}$$

E2 Pressure drop

The pressure drop across the pack is measured with a pressure transducer Rosemount, maximum scale 1 kPa.
The uncertainty of this device is 0.1% of full scale, which is 1 Pa.

- pressure drop across the pack: $\frac{\partial \Delta p}{\Delta p} = 0.35\%$

E3 Heat transfer coefficient

The heat transfer coefficient is evaluated according to the numerical scheme of Mulilsen and Loehrke [2]. It is difficult to determine the uncertainties involved in this calculation. There are four different types of uncertainties to distinguish:

- measuring and fluid properties uncertainties
- uncertainties where the test procedure does not correspond to ideal assumptions
- uncertainties describing the pack properties
- uncertainties in the data reduction

These different forms of uncertainties should be described in detail.

E3.1 Measuring and fluid properties uncertainties

In the model following values are required. These values are measured with certain uncertainties:

- temperatures

average inlet-temperature $\frac{\partial T_{in}}{T_{in}} = 0.5\%$

average outlet-temperature $\frac{\partial T_{out}}{T_{out}} = 0.5\%$

- fluid properties

density $\frac{\partial \rho}{\rho} = 0.17\%$

viscosity $\frac{\partial \upsilon}{\upsilon} = 1.0\%$

humidity $\frac{\partial \varphi}{\varphi} = 1.0\%$

conductivity $\frac{\partial k}{k} = 0.5\%$

specific heat $\frac{\partial c_p}{c_p} = 0.5\%$

The uncertainty of the Pr-number, which is defined as follows

$$Pr = \frac{c_p \cdot \rho \cdot \upsilon}{k} \tag{E5}$$

yield to:

- Pr-number

$$\frac{\partial Pr}{Pr}=\sqrt{\left(\frac{\partial \upsilon}{\upsilon}\right)^2+\left(\frac{\partial c_p}{c_p}\right)^2+\left(\frac{\partial k}{k}\right)^2+\left(\frac{\partial \rho}{\rho}\right)^2} \tag{E6}$$

$$= 1.24\%$$

E3.2 Uncertainties describing the pack properties

- geometry of the pack

length	$\frac{\partial L}{L}=0.2\%$
width	$\frac{\partial W}{W}=0.3\%$
height	$\frac{\partial H}{H}=0.3\%$
plate thickness	$\frac{\partial 2a}{2a}=2.0\%$
expanded length ratio	$\frac{\partial S_n}{S_n}=1.25\%$ (notched)
	$\frac{\partial S_u}{S_u}=1.0\%$ (undulated)

- storage material properties

density	$\frac{\partial \rho_{st}}{\rho_{st}}=1.0\%$
specific heat	$\frac{\partial c_{st}}{c_{st}}=2.0\%$
mass	$\frac{\partial m_{st}}{m_{st}}=0.25\%$

From these single uncertainties following uncertainties for composed values can be determined:

- cross sectional area

$$\frac{\partial A_{cross}}{A_{cross}} = \sqrt{\left(\frac{\partial S_u}{S_u}\right)^2 + \left(\frac{\partial S_n}{S_n}\right)^2 + \left(\frac{\partial W}{W}\right)^2 + \left(\frac{\partial 2a}{2a}\right)^2} \qquad \text{(E7)}$$

$$= 2.58\%$$

- free flow area

$$\frac{\partial A_{free}}{A_{free}} = \sqrt{\left(\frac{\partial S_u}{S_u}\right)^2 + \left(\frac{\partial S_n}{S_n}\right)^2 + \left(\frac{\partial W}{W}\right)^2 + \left(\frac{\partial 2a}{2a}\right)^2 + \left(\frac{\partial H}{H}\right)^2} \qquad \text{(E8)}$$

$$= 2.59\%$$

- heat transfer area

$$\frac{\partial A_{heat}}{A_{heat}} = \sqrt{\left(\frac{\partial S_u}{S_u}\right)^2 + \left(\frac{\partial S_n}{S_n}\right)^2 + \left(\frac{\partial W}{W}\right)^2 + \left(\frac{\partial 2a}{2a}\right)^2 + \left(\frac{\partial H}{H}\right)^2 + \left(\frac{\partial L}{L}\right)}$$

$$= 2.6\% \qquad \text{(E9)}$$

It is not possible to calculate the influence of these aforementioned uncertainties (E3.1 and E3.2) on the heat transfer coefficient. There is not one single relationship but a set of differential equations to calculate the heat transfer coefficient. So the method of Kline and McClintock is not appropriate.

E3.3 Uncertainties due to the fact that the actual test procedure does not correspond to the ideal assumptions assumed in the mathematical model

Firstly the assumptions on which the model is based should be repeated here:

- the fluid velocity profile is uniform across the cross sectional flow area over the testing time;
- the fluid temperature profile is uniform across the cross sectional flow area;
- the properties of the test pack surface remain constant throughout the whole test pack (see [26]);
- the thermal conductivity of the air is zero;
- the thermal conductivity of the steel plates perpendicular to the flow direction is infinite;
- only the thermal conductivity of the steel plate in longitudinal direction is considered;
- the side walls of the test section are adiabatic;
- the thermal capacity of the fluid is zero.

The evaluation of the uncertainties caused by deviation from these assumptions are not possible to quantify. But during the test runs every possibility was undertaken to ensure that these assumptions were fulfilled.

It was ensured that the test section was as adiabatic as possible. There was no gap between the test pack and the side walls of the test section. There was polystyrene insulation on top and at the bottom of the test section.

To ensure that the velocity distribution is uniform across the cross sectional area, velocity traverses have been undertaken at the inlet and at the outlet of the test section. The results are shown in Appendix A. Especially the uniform outlet distribution of the velocity indicates an uniform flow inside the test pack. Also a temperature traverse has been undertaken to proof an uniform temperature distribution across the test section.

The steel plates fulfil perfect the assumption that the properties of the test pack surface should remain constant throughout the whole test pack.

The assumptions concerning the conductivity of the air and the storage material should not influence the test results very much. One test was undertaken, where the longitudinal conductivity of the storage material was changed from 1 W/(kg K) to 115 W/(kg K) and the change in heat transfer coefficient was only 0.01%. From this evaluation it can be concluded that conductivity is of minor influence on these test runs.

E3.4 Uncertainties in the data reduction

The uncertainties which are caused by data reduction method are quantified by the error, which was discussed in Appendix A. The error determines the difference between the calculated and the experimental outlet temperature. Therefore the uncertainty of the heat transfer coefficient can be expressed by following equation [26]:

$$\frac{\delta h}{h}=\sqrt{\sum_{i=1}^{n}\left(\frac{T_{f,out,theo}^{i}-T_{f,out,exp}^{i}}{T_{f,out,exp}^{i}}\cdot 100\right)^{2}} \tag{E10}$$

for: i = 1,2,3....n, n is the number of discreet points in the recorded time response curve after starting the heating.

Equation (D4) has been solved for several test runs of different pack types. The average uncertainty of these packs is below 10 %, which is less than what can be found in the literature (see Chapter 2). The average uncertainties are:

H8:	8.9 %
KH11:	6.5 %
V75:	8.1 %
278DU:	7.8 %

It was found that the time duration of the heating period has a great influence on the error; the longer the heating period the higher the error. The calculated outlet temperature matches with the experimental one only up to a certain time. If the heating period is shortened to 25 sec. (instead of 50 sec.) the error decreases drastically without much influencing the heat transfer coefficient. For the above mentioned packs the error is reduced by 50 % and the average change in heat transfer coefficient is 1.7 % when shortening the heating period to 25 sec. This shows that the above mentioned error can be reduced without changing the heat transfer coefficient. For further test runs it is proposed to reduce the heating period to keep the error smaller.

E4 Reynolds-number

The Reynolds-number is determined by following equation:

$$Re = \frac{v \cdot d_h}{\upsilon} = \frac{\dot{m} \cdot d_h}{A_{free} \cdot \rho \cdot \upsilon} \tag{E11}$$

Whereas the hydraulic diameter d_h is defined as follows:

$$d_h = \frac{4 \cdot A_{free} \cdot L}{A_{heat}} \tag{E12}$$

The uncertainties for the single elements have been determined earlier. The uncertainties for the hydraulic diameter and the Reynolds-number are:

- hydraulic diameter

$$\frac{\partial d_h}{d_h} = \sqrt{\left(\frac{\partial A_{free}}{A_{free}}\right)^2 + \left(\frac{\partial L}{L}\right)^2 + \left(\frac{\partial A_{heat}}{A_{heat}}\right)^2} \tag{E13}$$
$$= 3.68\%$$

- Reynolds-number:

$$\frac{\partial Re}{Re} = \sqrt{\left(\frac{\partial A_{free}}{A_{free}}\right)^2 + \left(\frac{\partial \dot{m}}{\dot{m}}\right)^2 + \left(\frac{\partial d_h}{d_h}\right)^2 + \left(\frac{\partial \upsilon}{\upsilon}\right)^2 + \left(\frac{\partial \rho}{\rho}\right)^2} \tag{E14}$$
$$= 5.29\%$$

E5 Friction-factor

The Friction-factor is calculated by following equation:

$$F = \frac{1}{2}\,\Delta p\,\frac{A_{free}^{\,2}\rho}{\dot{m}^2}\,\frac{d_h}{L} \tag{E15}$$

The uncertainty analysis yields to:

- Friction-factor

$$\frac{\partial F}{F} = \sqrt{\left(2\frac{\partial A_{free}}{A_{free}}\right)^2 + \left(2\frac{\partial \dot{m}}{\dot{m}}\right)^2 + \left(\frac{\partial d_h}{d_h}\right)^2 + \left(\frac{\partial \rho}{\rho}\right)^2 + \left(\frac{\partial \Delta p}{\Delta p}\right)^2 + \left(\frac{\partial L}{L}\right)^2}$$
$$= 6.38\% \tag{E16}$$

E6 Colburn-factor

The Colburn-factor is defined by following equation:

$$Co = \frac{Nu}{Re \cdot Pr^{\frac{1}{3}}} = \frac{h \cdot d_h}{k \cdot Re \cdot Pr^{\frac{1}{3}}} \tag{E17}$$

The uncertainty of the Colburn-factor can be calculated as follows:

$$\frac{\partial Co}{Co} = \sqrt{\left(\frac{\partial h_{average}}{h_{average}}\right)^2 + \left(\frac{1}{3}\frac{\partial Pr}{Pr}\right)^2 + \left(\frac{\partial d_h}{d_h}\right)^2 + \left(\frac{\partial k}{k}\right)^2 + \left(\frac{\partial Re}{Re}\right)^2} \tag{E18}$$
$$= 10.14\ \%$$

Appendix F

Error between the experimental and calculated temperatures

For the calculation of the heat transfer coefficient an approximate value for the heat transfer coefficient is assumed and is used in the heat balances to calculate a theoretical exit fluid temperature history (see Chapter 3). This history is then compared with the measured fluid exit temperature history. If both histories match within specified limits, the assumed value of the heat transfer coefficient is the correct average heat transfer coefficient of the pack. If the history does not match, the heat transfer coefficient is changed iteratively until the specified agreement is achieved. For the convergence criterion an average absolute difference value ε is used, which is calculated as follows:

$$\varepsilon = \sqrt{\sum_{i=0}^{n}\left(T^{*}_{out,i,calc} - T^{*}_{out,i,exp}\right)^{2}} \qquad \text{(F1)}$$

where: i = 0...n, time steps of 0.33 sec. (test duration is normally approx. 50 sec.)

$T^{*}_{out,i,calc}$ = dimensionless, calculated outlet temperature for each time step i

$T^{*}_{out,i,exp}$ = dimensionless, experimental outlet temperature for each time step i

The dimensionless temperatures are defined as follows:

- e.g. dimensionless outlet temperature:

$$T^{*}_{out,i} = \frac{T_{out,i} - T_{out,1}}{T_{out,max} - T_{out,1}} \qquad \text{(F3)}$$

where: $T_{out,i}$ = outlet temperature for each time step
$T_{out,max}$ = maximum outlet temperature
$T_{out,1}$ = outlet temperature for time i = 1

Following features could be found regarding the error:

- The error is increasing with increasing mass flow.
- The error for packs with braces is higher than the error for packs without braces. It is also found that the spread of the temperatures behind the pack is wider for packs with braces than without braces. This is a possible explanation for this increased error.
- The maximum error (at maximum mass flow) for the majority of the test runs is close to 0.15.
- Some test runs had a maximum error below 0.02. The highest maximum error was 0.35.
- The error increases if the readings of the thermocouples are not uniform, i.e. one or more thermocouples show higher or lower readings (± 0.5°C) than the average.
- Some questions which needed answered were,
  - when there is an increased error, how does the calculated outlet temperature history look compared to the experimental history and,
  - how does this increased error influence the heat transfer coefficient?
- The following table shows some sample calculations which answer the above mentioned questions:

Table F1: Dependency of the error on the temperature difference and the heat transfer coefficient

error ε	$\Delta T_{average}$ (calc - exp) [°C]	Δh [%]
0.02	0.004	0.0
0.14	0.130	3.8
0.21	0.200	5.7
0.27	0.230	6.6
0.40	0.350	9.9

- It can be seen from the table that an error of 0.2 already gives an inaccurate heat transfer coefficient of 5%.
- This indicates that the accuracy of the temperature readings is quite important (see Appendix A).
- For this reason the maximum accepted error is 0.2. Preferably the error should not exceed 0.15.
- Test runs which have higher errors should be repeated. These are caused possibly by faulty temperature readings.
- To avoid these difficulties either more thermocouples could be installed in the flow area (so that the average is not that sensitive to one or two faulty thermocouples) or a grid of wire could be installed which measures the average temperature.

Appendix G

Numerical scheme according to Mullisen and Loehrke [2]

Mullisen and Loehrke [2] developed their data reduction procedure for interrupted-plate surfaces (see Figure G1).

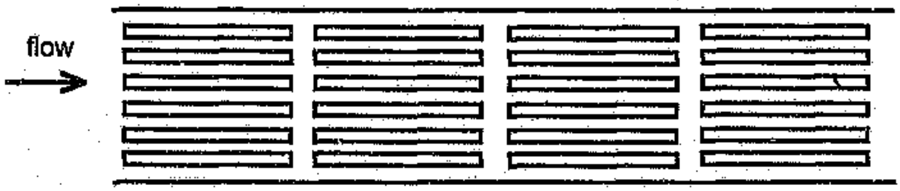

Figure G1: Multiple in-line plates

One flow channel consists of two plates (see Figure G2).

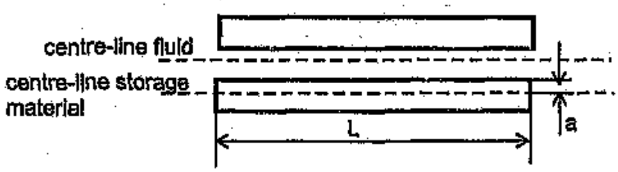

Figure G2: Single pair of plates

Considering the symmetry of the flow channel, the heat balances are applied to half of the material and half of the flow channel (between centre-line storage material and centre-line flow channel, see Figure G3)

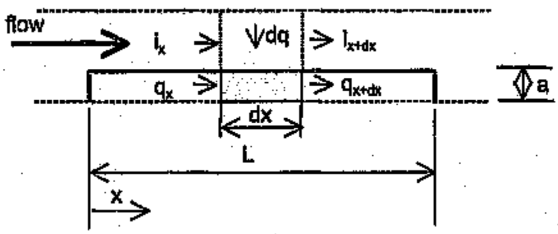

Figure G3: Half flow passage and half plate

Figure G4 shows the division of the half flow passage and the half plate into finite-difference nodes.

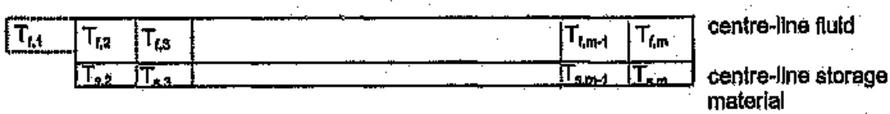

Figure G4: Division into finite-difference nodes

The heat balance for the difference nodes are made under the following assumptions:

- steady flow
- finite wall conduction in flow direction
- infinite wall conduction perpendicular to flow direction
- zero fluid conduction in flow direction
- zero fluid capacity
- constant properties
- adiabatic side walls

The heat balance of the storage material is described by following equation,

$$\dot{q}_{stor} = \dot{q}_{cond,x} - \dot{q}_{cond,x+dx} + d\dot{q}_{conv} \tag{G1}$$

where the single terms are as follows:

- storage term:

$$\dot{q}_{stor} = \int_{x}^{x+dx} a \cdot \rho \cdot c \frac{\partial T_s}{\partial t} dx \tag{G2}$$

- convective term:

$$\dot{q}_{conv} = \int_{x}^{x+dx} h \cdot (T_f - T_s) dx \tag{G3}$$

- conduction term:

$$d\dot{q}_{cond,x\rightarrow x+dx} = \frac{k}{\partial x} \cdot a \cdot \frac{\partial T_s}{\partial x} \tag{G4}$$

Substituting equations G2, G3 and G4 in equation G1 results:

$$a \cdot \rho \cdot c \cdot \frac{\partial T_s}{\partial t} = h(T_f - T_s) + k \cdot a \frac{\partial^2 T_s}{\partial x^2} \tag{G5}$$

$$\frac{\Delta T_s}{\partial t} = \frac{h}{a \cdot \rho \cdot c}(T_f - T_s) + \frac{k}{\rho \cdot c}\frac{\partial^2 T_s}{\partial x^2} \tag{G5a}$$

The heat balance of the fluid is described by following equation:

$$\frac{\partial T_f}{\partial x}+\frac{W\cdot h}{\dot{m}\cdot c_p}\left(T_f-T_s\right)=0 \qquad \text{(G6)}$$

The initial conditions are:

$$T_s(x, t=0)=T_f(x, t=0)=T_0 \quad \text{or} \qquad T^1_{s,i}=T^1_{f,i}=T_0$$

where T_0 is known from the experiment. The inlet and outlet temperatures of the fluid, as a function of time, are also known from the experiment:

$$T_f(x=0, t)=T_1(t) \qquad \text{or} \qquad T^n_{f,1}=T_1(t)$$

$$T_f(x=L, t)=T_2(t) \qquad \text{or} \qquad T^n_{f,m}=T_2(t)$$

The equations G5a and G6 are converted to finite-difference equations. Equation G5a becomes:

$$\frac{T^{n+1}_{s,i}-T^n_{s,i}}{\Delta t}=\frac{k}{2\rho c}\left[\frac{T^{n+1}_{s,i-1}-2T^{n+1}_{s,i}+T^{n+1}_{s,i+1}}{(\Delta x)^2}\right]+\frac{k}{2\rho c}\left[\frac{T^n_{s,i-1}-2T^n_{s,i}+T^n_{s,i+1}}{(\Delta x)^2}\right]+\frac{h}{\rho a c}\left[T^n_{f,i}-T^n_{s,i}\right] \qquad \text{(G5b)}$$

for i = 2 to m (steps in length direction).

When the following conditions prevail, i.e.:

- no heat is conducted over the ends (i = 2 and i = m),
- $T^n_{s,1} = T^n_{s,2}$ and $T^n_{s,m+1} = T^n_{s,m}$, where the nodes 1 and m+1 are fictitious,

equation G5b becomes a single matrix:

$$\begin{bmatrix} & & C_i \\ & B_i & \\ A_i & & \end{bmatrix}\left[T^{n+1}_{w,i}\right] = \left[D^n_i\right] \qquad \text{(G5c)}$$

where:

$A_i = Z$; for i = 3,m

$B_i = -2Z - 1$; for i = 3, m-1

$C_i = Z$; for i = 2, m-1

$D_i = T^n_{s,i}\left[2Z + \left(\frac{h\Delta t}{\rho ac}\right) - 1\right] - Z\left[T^n_{s,i-1} + T^n_{s,i+1}\right] - \left[\frac{h\Delta t}{\rho ac}\right]T^n_{f,i}$; for i = 2,m

$A_2 = 0$

$B_2 = -Z - 1$

$B_m = B_2$

$C_m = 0$

$Z = \frac{k\Delta t}{2\rho c(\Delta x)^2}$

Equation G6 becomes a finite difference equation as follows:

$$T^{n+1}_{f,i} = \frac{Y \cdot T^{n+1}_{s,i} + T^{n+1}_{f,i-1}}{1 + Y} \qquad \text{(G6a)}$$

where:

$$Y = \frac{h \cdot \Delta x \cdot W}{\dot{m} \cdot c_p}$$

The procedure to determine the correct heat transfer coefficient is as follows: Firstly equations G5c and G6a must be solved using an estimated value for the heat transfer coefficient, the boundary conditions and the measured inlet temperature history. From this a theoretical exit temperature history is calculated, which must be compared with the measured experimental history. The heat transfer coefficient has to be changed iteratively until the measured and the calculated exit temperature histories match within certain limits. This procedure is described in detail in Chapter 3 and need not be repeated.

Appendix H

Fluid Properties

H1 Correction of barometric pressure [35]

H1.1 Temperature correction

$$K_t = -b_t \cdot \frac{182 \cdot 10^{-6} \cdot t - 11 \cdot 10^{-6} \cdot (t-20)}{1 + \left[182 \cdot 10^{-6} \cdot t - 11 \cdot 10^{-6} \cdot (t-20)\right]} \qquad \text{(H1)}$$

with: K_t = temperature correction factor
b_t = barometric pressure at lab temperature t [°C]

$b_0 = b_t + K_t$ (barometric pressure reduced to 0°C) (H2)

H1.2 Gravity correction

- <u>influence of geographic latitude</u> (because of rotation, centrifugal force)

$$K_{g\varphi} = \left[\frac{9{,}80616}{9{,}80665} \cdot (1 - 0{,}002637 \cdot \cos 2\varphi) - 1\right] \cdot b_0 \qquad \text{(H3)}$$

with: $K_{g\varphi}$ = gravity correction caused by geographic latitude φ [°]
b_0 = barometric pressure reduced to 0°C
9.080665 = gravity at equator
9.080616 = gravity at angle 45° (see figure)

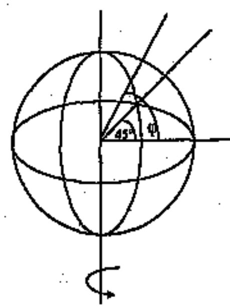

- <u>Influence of altitude</u>

$$K_{gH} = -0{,}195 \cdot 10^{-6} \cdot H \cdot b_0 \qquad \text{(H4)}$$

with: K_{gH} = gravity correction caused by geographic altitude H [m]
b_0 = barometric pressure reduced to 0°C

For the place Johannesburg (φ = 26.2°, H = 1600 m) following correction is necessary:

$$K_g = (K_{g\varphi} + K_{gH}) \cdot b_0 = (-0.001659 - 0.000312) \cdot b_0 = -0.001971 \cdot b_0 \qquad \text{(H5)}$$

H1.3 Capilliary fo: :e (height of the tip, meniscus)

$$K_c = h_c^{0,42} - 0,448 \qquad \text{(H6)}$$

with K_c = correction of height of the tip caused by capilliary force
h_c = height of the tip, meniscus

$\Rightarrow$ corrected barometric pressure : $p_{corr} = b_0 + K_g + K_c$
$p_{corr} = 0,998029(b_t + K_t)$

(H7)

H2 Humidity (according to [36])

The following calculations are based on a humidity measurement by means of a psychrometer. Values which are to be measured are the dry bulb t_d and the wet bulb temperature t_w. The corresponding saturation pressure can be taken either from DIN 24163, sheet 2, or can be calculated according to the following procedure [28].

For the two temperatures t_d and t_w the appropriate saturation pressures $p_{s,d}$ and $p_{s,w}$ are to be calculated by means of the following equations:

for $t > 0$ °C

$$p_{s,w} = 611,20 \cdot e^{\left\{15,634\left[1-\left(\frac{273,15K}{t_w+273,15K}\right)^{1,27}\right]\right\}} \quad \text{[Pa]} \qquad \text{(H8)}$$

$$p_{s,d} = 611,20 \cdot e^{\left\{15,634\left[1-\left(\frac{273,15K}{t_d+273,15K}\right)^{1,27}\right]\right\}} \quad \text{[Pa]} \qquad \text{(H9)}$$

for $t < 0$ °C

$$p_{s,w} = 611{,}20 \cdot e^{\left\{21 \cdot \left[1-\left(\frac{273{,}15K}{t_w+273{,}15K}\right)^{1{,}07}\right]\right\}} \qquad \text{[Pa]} \qquad \text{(H10)}$$

$$p_{s,d} = 611{,}20 \cdot e^{\left\{21 \cdot \left[1-\left(\frac{273{,}15K}{t_d+273{,}15K}\right)^{1{,}07}\right]\right\}} \qquad \text{[Pa]} \qquad \text{(H11)}$$

the "Sprunç" formula yields to:

$$= \frac{p_{s,w}}{p_{s,d}} - \frac{p_{lab}}{p_{s,d}} \cdot \left(\frac{t_d - t_w}{1542K}\right) \qquad \text{[\%]} \qquad \text{(H12)}$$

so the vapor pressure can be calculated in the following way

$$p_v = \varphi_w \cdot p_{s,d} \qquad \text{[Pa]} \qquad \text{(H13)}$$

the mass of water is then according to [36]

$$x_{H_2O} = 0{,}622 \cdot \frac{p_v}{p_{lab} - p_v} \qquad \text{[kg/kg]} \qquad \text{(H14)}$$

H3 Gas constant (according to [37])

The gas constant can be calculated by means of

$$R_w = \frac{287 \frac{J}{kg\,K}}{1 - 0{,}377 \frac{p_v}{p_{lab}}} \qquad \text{[J/(kg K)]} \qquad \text{(H15)}$$

H4 Density calculation (according to [37])

$$\rho = \frac{p}{R_w \cdot (t + 273{,}15\,K)} \qquad [\mathrm{kg/m^3}] \qquad \text{(H16)}$$

H5 Kinematic viscosity (according to [36])

The kinematic viscosity can be calculated as follows

$$\nu = \frac{10^{-6}}{\rho}\left(\sum_{i=0}^{5} c_i\, t^i\right) \qquad [\mathrm{m^2/s}] \qquad \text{(H17)}$$

with

$$c_i = a_i + \frac{x_{H_2O}}{1 + x_{H_2O}}\, b_i \qquad \text{(H18)}$$

and the coefficients

$a_0 = 0{,}1714237 \cdot 10^{2}$ $b_0 = -0{,}9108949 \cdot 10^{1}$

$a_1 = 0{,}4636040 \cdot 10^{-1}$ $b_1 = 0{,}2654355 \cdot 10^{-1}$

$a_2 = -0{,}2745836 \cdot 10^{-4}$ $b_2 = -0{,}6432423 \cdot 10^{-4}$

$a_3 = 0{,}1811235 \cdot 10^{-7}$ $b_3 = 0{,}1307$[illegible]$5 \cdot 10^{-6}$

$a_4 = -0{,}6744970 \cdot 10^{-11}$ $b_4 = -0{,}8190284 \cdot 10^{-10}$

$a_5 = 0{,}1027747 \cdot 10^{-14}$ $b_5 = 0$

Appendix I

Sample calculation of additional pressure loss caused by the presence of braces

An example calculation for additional pressure loss caused by the presence of braces is following. For this calculation the case of flat braces is assumed.

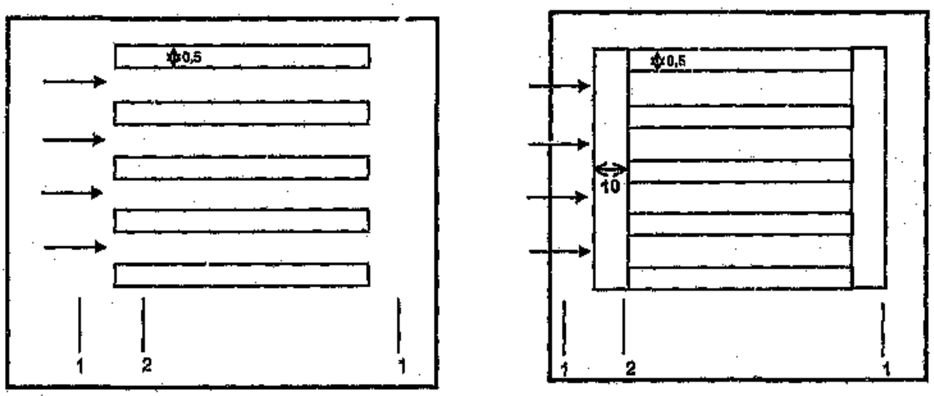

Figure I.1: Flow through a pack without and with braces, definition of the different cross sections

The pressure drop due to entrance and exit losses can be calculated according to different references in the literature. Only the VDI-Waermeatlas [38] and Kays and London [3] should be mentioned below. These calculations should be done for the Reynolds-numbers 2000 and 4500.

The following equations are for calculating the entrance and exit losses of an air heater pack according to the VDI-Waermeatlas [38]

contraction

$$\Delta p_{contraction} = \xi_E \cdot \frac{\rho}{2} \cdot v_2^{\,2} \qquad \text{with: } \xi_E = f\left(\frac{A_2}{A_1}\right) \tag{I.1}$$

expansion (Carnot)

$$\Delta p_{expansion} = \left(1 - \frac{A_2}{A_3}\right)^2 \cdot \frac{\rho}{2} \cdot v_2^{\,2} \tag{I.2}$$

with: ρ = density of air [0.99 kg/m³]
v_2 = velocity in the pack [6 m/s and 10 m/s respectively]

Using the above mentioned equations (I.1) and (I.2) the additional pressure loss due to contraction and expansion with and without braces is:

- without braces

Re = 2000		Re = 4500	
$\Delta p_{contraction}$ =	3.74 Pa	$\Delta p_{contraction}$ =	8.91 Pa
$\Delta p_{expansion}$ =	0.35 Pa	$\Delta p_{expansion}$ =	0.97 Pa
Δp_{tot} =	4.09 Pa	Δp_{tot} =	9.88 Pa

- with braces

Re = 2000		Re = 4500	
$\Delta p_{contraction}$ =	4.46 Pa	$\Delta p_{contraction}$ =	9.9 Pa
$\Delta p_{expansion}$ =	0.77 Pa	$\Delta p_{expansion}$ =	2.14 Pa
Δp_{tot} =	5.23 Pa	Δp_{tot} =	12.04 Pa

The additional pressure loss according to Kays and London is calculated with the help of diagrams showing coefficients for the entrance (K_c) and exit loss (K_e). With these coefficients and the following equations the pressure loss can be calculated.

- contraction

$$\Delta p_{contraction} = \frac{v_2^2 \rho}{2}\left(1 - \sigma^2 + K_c\right) \quad [N/m^2] \tag{I.3}$$

- expansion

$$\Delta p_{exansion} = \frac{v_2^2 \rho}{2}\left(1 - \sigma^2 - K_e\right) \quad [N/m^2] \tag{I.4}$$

with σ = core free-flow area to frontal-area ratio, with or without braces [m²/m²]
ρ = density of air [0.99 kg/m³]

The following calculation is related to the K6 profile ($\sigma_{without\ braces}$ = 0.86, $\sigma_{with\ braces}$ = 0.8), turbulent flow with a reference Reynolds-number of 2000 and 4500, which represents a velocity of 6 m/s or 10 m/s in the heat exchanger pack. For values of higher Reynolds-numbers the influence on the pressure loss is more important, but for lower Reynolds-numbers the influence is negligible.

Following coefficients for the exit and entrance losses can be found in [3]:

- without braces

Re = 2000	Re = 4500
K_e = -0.11	K_e = -0.08
K_c = 0.34	K_c = 0.3

- with braces

Re = 2000	Re = 4500
K_e = -0.14	K_e = -0.1
K_c = 0.3	K_c = 0.25

According to equation (I.3) and (I.4) the additional pressure loss due to exit and entrance losses with and without braces is:

- without braces

Re = 2000		Re = 4500	
$\Delta p_{contraction}$ =	10.7 Pa	$\Delta p_{contraction}$ =	27.7 Pa
$\Delta p_{expansion}$ =	6.6 Pa	$\Delta p_{expansion}$ =	16.9 Pa
Δp_{tot} =	17.3 Pa	Δp_{tot} =	44.6 Pa

- with braces

Re = 2000		Re = 4500	
$\Delta p_{contraction}$ =	11.8 Pa	$\Delta p_{contraction}$ =	30.2 Pa
$\Delta p_{expansion}$ =	8.9 Pa	$\Delta p_{expansion}$ =	22.8 Pa
Δp_{tot} =	20.7 Pa	Δp_{tot} =	53.0 Pa

These calculations point out some interesting features. First, there is little coincidence between both calculation methods. The pressure drop calculated by Kays and London is considerably higher than the one calculated by the VDI - Waermeatlas. Second, the calculated difference between a pack with and without braces is not as high as the experimental results show. Theoretically the difference should be between 1 Pa and 10 Pa (depending on the calculation method and the Reynolds-number). It has to be considered that the calculation does not take into account the expansion at the entrance after the flow passes the braces and another contraction at the exit when the flow passes the braces.

REFERENCES

[1] Habbitts, S.A. — Simulation and measurement of thermal performance of rotary regenerative boiler air pre-heaters, MSc Dissertation, Faculty of Engineering, University of the Witwatersrand, Johannesburg (1992)

[2] Mullisen, R.S., Loehrke, R.I. — A transient heat exchanger evaluation for arbitrary fluid inlet temperatures variation and longitudinal core conduction, *Journal of Heat Transfer*, vol. 108, pp. 370 - 376 (1986)

[3] Kays, W.M, London, A.L. — *Compact Heat Exchanger*, 2nd edition, McGraw Hill Book Co., New York (1964)

[4] Anzelius, A. — Ueber Erwaermung vermittels durchstroemender Medien, *Z. Angew. Math. Mech.* 6, pp. 291 - 294 (1926)

[5] Schumann, T.E. — Heat transfer: A liquid flowing through a porous prism, J. Franklin Trust Ins., 208, pp. 405 - 416 (1929)

[6] Locke, G.L. — Heat transfer and flow characteristics of porous solids, Technical report no. 10, Department of Mechanical Engineering, Stanford University, Stanford (1950)

[7] Howard, C.P. — The single blow problem including the effects of longitudinal conduction, ASME paper No. 64-GT2-11 (1964)

[8] Pucci, P.F., Howard, C.H., Piersall, C.H. — The single-blow transient testing technique for compact heat exchanger surfaces, *ASME J. Engng. Power* 89, pp. 29 - 40 (1967)

[9] Liang, C.Y., Yang, W.-J. — Modified single-blow technique for performance evaluation on heat transfer surfaces, *Transactions of the ASME*, pp. 16 - 21 (1975)

[10] Cheng, C.-H., Huang, C.-S. — Extended model for single-blow transient testing method in evaluation thermal performance of heat transfer surfaces, *Int. Comm. Heat Mass Transfer* Vol. 21, pp. 53 - 63 (1994)

[11] Chen, P.-H., Chang, Z.-C. Measurements of thermal performance of cryocooler regenerators using an improved single-blow method, *Int. J. Heat Mass Transfer*, Vol. 40, No. 10, pp. 2341 - 2349 (1997)

[12] Heggs, P.J., Burns, D. Single-blow experimental prediction of heat transfer coefficients; a comparison of four commonly used techniques, *Experimental Thermal and Fluid Science*, pp. 243 - 251 (1988)

[13] Darabi, F. Heat and momentum transfer in packed beds, Ph.D. thesis, University of Leeds (1982)

[14] Baclic, B.S., Heggs, P.J., *Ziyan, H.A.* The differential fluid enthalpy method, *Proc. 8th International Heat Transfer Conference San Francisco*, Vol. 5, pp. 2616 - 2622 (1986)

[15] Migay, V.K. Refinement of plate-type heated surfaces for rotary air preheater, *Heat Transfer*, Soviet Research, Vol. 2, No. 4, pp. 151 - 156 (1970)

[16] Karlsson, H., Holm, S. Heat transfer and fluid resistance in Ljungstrom regenerative-type air preheaters, *Transactions of the ASME*, Jan. 1943 pp. 61 - 72 (1943)

[17] Stasiek, J., Collins, M.W. Ciofalo, M., Chew, P.E. Investigations of flow and heat transfer in corrugated passages - I. Experimental results, *Int. J. Heat Mass Transfer*, Vol.39, No.1 pp. 149 - 164 (1996)

[18] Ciofalo, M, Stasiek, J. Collins, M.W. Investigation of flow and heat transfer in corrugated passages - II. Numerical simulations, *Int. J. Heat Mass Transfer*, Vol. 39, No.1 pp. 165 - 192 (1996)

[19] Raask, E. *Erosion Wear in Coal Utilisation*, (1988)

[20] Raask, E. Tube erosion by ash impaction, *Wear*, 13, pp. 301 - 315 (1969)

[21] Finnie, I., Levy, A., McFadden, D.H. — Fundamental mechanisms of the erosive wear of ductile metals by solid particles, in: *Erosion: Prevention and useful Applications*, W.F. Adler, editor, ASTM, pp. 36 - 58 (1979)

[22] Hutchings, I.M. — Mechanisms of the erosion of metals by solid particles, in: *Erosion: Prevention and useful Applications*, W.F. Adler, editor, ASTM, pp. 59 - 76 (1979)

[23] Suckling, M.B., Allen, C. — Ash erosivity differences between coal fired power generating units, confidential information (1992)

[24] Blenkinsop, M. — TRI ESKOM Report: TRR/P94/045 (1994)

[25] Blenkinsop, M. — TRI ESKOM private communication (1998)

[26] Caby, M. — Experimental investigation of heat transfer in regenerative heat exchangers MSc Dissertation, Faculty of Engineering University of the Witwatersrand, Johannesburg (1996)

[27] Uys, R.F. — Internal report, ESKOM (1997)

[28] Baerwald, T. — Howden Power private communication (1997)

[29] Incropera, F.P. De Witt, D.P. — *Introduction to Heat Transfer*, 3rd edition, John Wiley & Son, New York, pp 434 - 457 (1996)

[30] Boshoff, H.P. — Analyses of coal product samples of producing south African collieries, Bulletin No. 107, CSIR Pretoria (1992)

[31] Vasil'ev, A.A. Dombrovskii, V.I. — Investigation of erosion of air heaters by ash of Ekibastuz coal *Teploenergetika*, 25, vol. 1, pp. 31 - 33 (1978)

[32]	von Bormann, F.	Research into improvement of the performance and operation of regenerative air heater: Commissioning of the test facilities, TRI ESKOM Report: TRR/P94/101 (1995)
[33]	Liebenberg, F.	Head of flow laboratory, ESKOM TRI private communication (1998)
[34]	Kline, S.J. McClintock, F.A.	Describing uncertainties in single-sample experiments, *Mechanical Engineering*, pp 3 - 8, Jan. (1953)
[35]	Operation instructions	*"Lambrecht Quecksilberbarometer"* (1980)
[36]	FDBR Handbuch	*Waerme- und Stroemungstechnik* (1982)
[37]	DIN Standard	DIN 24163, sheet 1 - 3
[38]	VDI-Wärmeatlas	Verein Deutscher Ingenieure, editor, 6th edition, VDI-Verlag, Duesseldorf (1991)